Competition between high-K states and rotational structures in ^{177}Ta

M. Dasgupta, G. D. Dracoulis, P. M. Walker,* A. P. Byrne, T. Kibédi, F. G. Kondev,† G. J. Lane,‡ and P. H. Regan*

Department of Nuclear Physics, Research School of Physical Sciences and Engineering, The Australian National University,
Canberra ACT 0200, Australia

High-spin states in ^{177}Ta have been studied using the ^{170}Er(^{11}B,4n) reaction. New intrinsic states have been observed corresponding to 3-, 5-, and 7-quasiparticle high-K structures. Rotational bands built on most of the 3- and 5-quasiparticle states and some transitions above the 7-quasiparticle states have been identified. Several isomers have been found, the longest lived being the $\frac{49}{2}^-$, 7-quasiparticle state with a meanlife of 192 μs. Configurations for the observed intrinsic states have been assigned on the basis of g_K values, alignments, and decay properties. While the properties of most of the bands are consistent with their proposed configurations, the behavior of some, including the one built on $K^\pi = \frac{21}{2}^-$ 3-quasiparticle isomer, is not well understood. Multiquasiparticle blocking calculations based on the Lipkin-Nogami method, are in good agreement with the excitation energies of the experimentally observed states and all the predicted states close to the yrast line up to spin $\frac{49}{2}$ have been observed experimentally. The calculations predict the existence of a 9-quasiparticle $\frac{67}{2}^-$ yrast trap at ~ 8.5 MeV.

PACS number(s): 21.10.Re, 21.10.Tg, 23.20.−g, 27.70.+q

I. INTRODUCTION

It is well known that the pairing correlations between nucleons in a nucleus are extremely important in the region of low angular momentum where they manifest themselves by reducing the nuclear moment of inertia with respect to the rigid-body estimates [1]. However, as the rotational frequency of the nucleus is increased, the resulting Coriolis and centrifugal forces tend to reduce the pairing correlations, an effect which has been extensively studied [2]. A decrease in the correlations is also expected for multiquasiparticle configurations because the unpaired nucleons block the single-particle states into which pairs of nucleons can scatter. These effects had not been studied extensively partly due to the lack of appropriate experimental data. Such data [3–9] are now becoming available around the mass 180 region, allowing the investigation [10] of pairing as a function of seniority.

Nuclei near $A \sim 180$ are particularly favorable candidates for studying the influence of many broken pairs of nucleons (at low rotational frequency) on pairing. In this region the proton and neutron Fermi levels are among orbitals with large values of Ω, the projection of angular momentum on the nuclear symmetry axis, so that high-K multiquasiparticle states compete favorably with collective rotational excitations to form the yrast line. Spectroscopic investigations have identified many such states [11–16], but experimental data for high seniority states had been fragmentary, mainly because their angular momenta are often close to the maximum attainable from the available reactions.

The nucleus ^{177}Ta can be favorably populated up to spins $\geqslant 20\hbar$ using the reaction ^{170}Er(^{11}B,4n) allowing access to the region where high-K multiquasiparticle states might exist [17]. Early [18–23] and more recent [24,25] studies of ^{177}Ta were reported by other groups, resulting in the identification of 1-quasiparticle bands and some of the 3-quasiparticle states and their associated bands. Our work, first reported in Ref. [4], is the only one which is sensitive to the identification of intrinsic states at higher spins due to the angular momentum input and the technique of time-correlated γ-ray spectroscopy employed in the measurements. It reveals the presence of one 1-quasiparticle, three 3-quasiparticle, five 5-quasiparticle and three 7-quasiparticle states in addition to the intrinsic states known from earlier investigations. Some of the new states are isomeric. Selected results, pertaining mainly to the yrast isomers, have been published earlier [4] together with some results for ^{176}Ta and a comparison with calculations of the multiquasiparticle states. The present paper addresses the complete level scheme involving intrinsic states and associated rotational bands, and compares the results with more recent calculations which supersede those of our earlier work.

II. EXPERIMENTAL METHOD

States in ^{177}Ta were populated by the reaction ^{170}Er(^{11}B,4n)^{177}Ta with a 55 MeV beam from the 14UD pelletron accelerator at the Australian National University. An isotopically enriched ^{170}Er target of thickness 5.5 mg cm^{-2} was used, which stopped most of the recoiling nuclei. A series of measurements was performed, focusing on different aspects of the spectroscopy, as discussed in the following subsections.

A. γ-γ coincidence measurements

A pulsed beam (~ 1 ns wide pulses, 1.7 μs apart) was used for this set of measurements. The γ rays were detected

*Present address: Department of Physics, University of Surrey, Guildford, UK.

†Present address: Physics Division, Argonne National Laboratory, Argonne, IL 60439.

‡Present address: Nuclear Science Division, Lawrence Berkeley National Laboratory, 1 Cyclotron Road, MS-88, Berkeley, CA 94720.

using the CAESAR array [26] containing six Compton-suppressed high-purity germanium (HPGe) detectors. An unsuppressed planar germanium detector (LEPS) was included to give enhanced efficiency and resolution for γ-ray transitions between ~ 15 and 100 keV. The energies of each two-fold coincidence (encompassing time differences of up to ± 0.856 μs) were recorded event-by-event, together with the time of each energy signal relative to the beam bunches, allowing unambiguous identification of γ-ray transitions preceding or following an isomer.

B. γ-ray singles measurement

Gamma rays were measured in singles mode under the experimental conditions described in Sec. II A. These data were used in part to determine relative intensities and populations of the different bands. The anisotropies were determined from the prompt-gated γ-ray spectra, encompassing time differences up to ± 40 ns with respect to the beam to minimize relaxation effects due to isomers.

C. Beam-γ measurements

The possible existence of isomers in the microsecond region was investigated using a chopped beam of 2 μs pulses, separated by 103 μs and the experimental setup described in Sec. II A. The energies of γ rays were recorded event-by-event, together with the time of each energy signal relative to the beam pulses. A fast veto was used to remove γ rays occurring in the 2 μs in-beam period, to increase the sensitivity to the γ rays following an isomer.

D. Conversion electron measurements

A separate experiment was performed to measure conversion coefficients, using a superconducting solenoidal spectrometer [27]. A relatively thin target of thickness 1.5 mg/cm^2 placed at 30° with respect to the beam was used to optimize the electron energy resolution. Since the presence of isomers with lifetimes in two distinctly different time regions (nanosecond and millisecond) had been established, the beam on/off periods were adjusted to cover two time regimes; 1 ns on (bunched), 900 ns off; and 80 μs on, 720 μs off. The spectrometer field was swept over a range of magnetic fields such that electrons of energies between 115 and 2145 keV for the former run, and 70 and 680 keV for the latter, were optimally transported to a cooled Si(Li) detector. During the latter measurement a veto was used to reject the prompt events. The γ rays were detected using a Compton-suppressed HPGe detector. Conversion electrons and γ rays were recorded in event-by-event mode with their times relative to the beam bursts.

III. ANALYSIS PROCEDURE

A. γ-γ coincidences

The data were sorted, following energy gain and time matching, into 4096×4096 channel matrices with the following constraints on the γ-γ coincidence relationship: (i) a requirement that two γ rays occur within ± 40 ns of each

other; (ii) a less stringent condition where the time relationship was relaxed to ± 150 ns in order to include low-energy γ rays which suffer from time walk in the detectors; (iii) a condition that two γ rays occur within ± 40 ns of each other and also *during* beam bursts; (iv) the complementary case where both γ rays are required to occur between beam bursts, thus selecting coincidence events below an isomer; (v) where the γ events are required to occur between beam bursts with the additional condition that they be separated in time between 80 and 300 ns; this matrix then allows for two event-projection types—(a) projection of those events that precede an isomer by gating on transitions that follow it; and (b) projections of those events that follow an isomer by gating on transitions that feed it; (vi) the same as the previous condition, with the required time difference between γ events being from 300 ns to 1.52 μs. Again, one can obtain two types of projections as detailed above. In this case the sensitivity to longer lived isomers is enhanced compared to sort (v). Background subtracted coincidence spectra were generated, for each individual γ-ray transition, from these matrices and were examined to construct the level scheme.

B. γ-γ time

In order to isolate the lifetimes of individual states, the coincidence data were also sorted into three-dimensional γ_1-γ_2-time matrices. For states depopulating by low-energy γ rays a separate matrix was constructed with any of the six HPGe detectors (γ_1) against the LEPS detector (γ_2). The time relationship between pairs of γ rays could be obtained from such matrices by taking background subtracted γ-ray gates on transitions preceding and following any state.

C. γ time

Two-dimensional matrices were generated of γ-ray energy vs their time of arrival with respect to the beam, using the data taken during the experiments described in Sec. II. Matrices were constructed corresponding to the different beam on/off periods: (a) 1 ns on, 900 ns off, (b) 2 μs on, 103 μs off, and (c) 80 μs on, 720 μs off; facilitating the measurement of the short-lived and the long-lived states. A separate γ-time matrix was constructed using the data recorded in the LEPS detector to determine the lifetimes of the states which are relatively short lived (meanlife < 1 μs), and decay by low-energy γ rays.

D. Conversion electrons

The data from the experiment discussed in Sec. II D were used to construct two-dimensional matrices of electron energy or γ-ray energy against the time of arrival with respect to the beam pulse. Prior to construction of the matrices, the electron events were subjected to momentum selection criteria [27] to eliminate background events arising mainly due to backscattering of electrons from the detector. Projections from the γ time and electron-time matrices were used to assemble electron and γ-ray spectra in specific time regions, selected to improve the sensitivity to specific decay paths, e.g., long-lived or short-lived isomer decay. Electron and
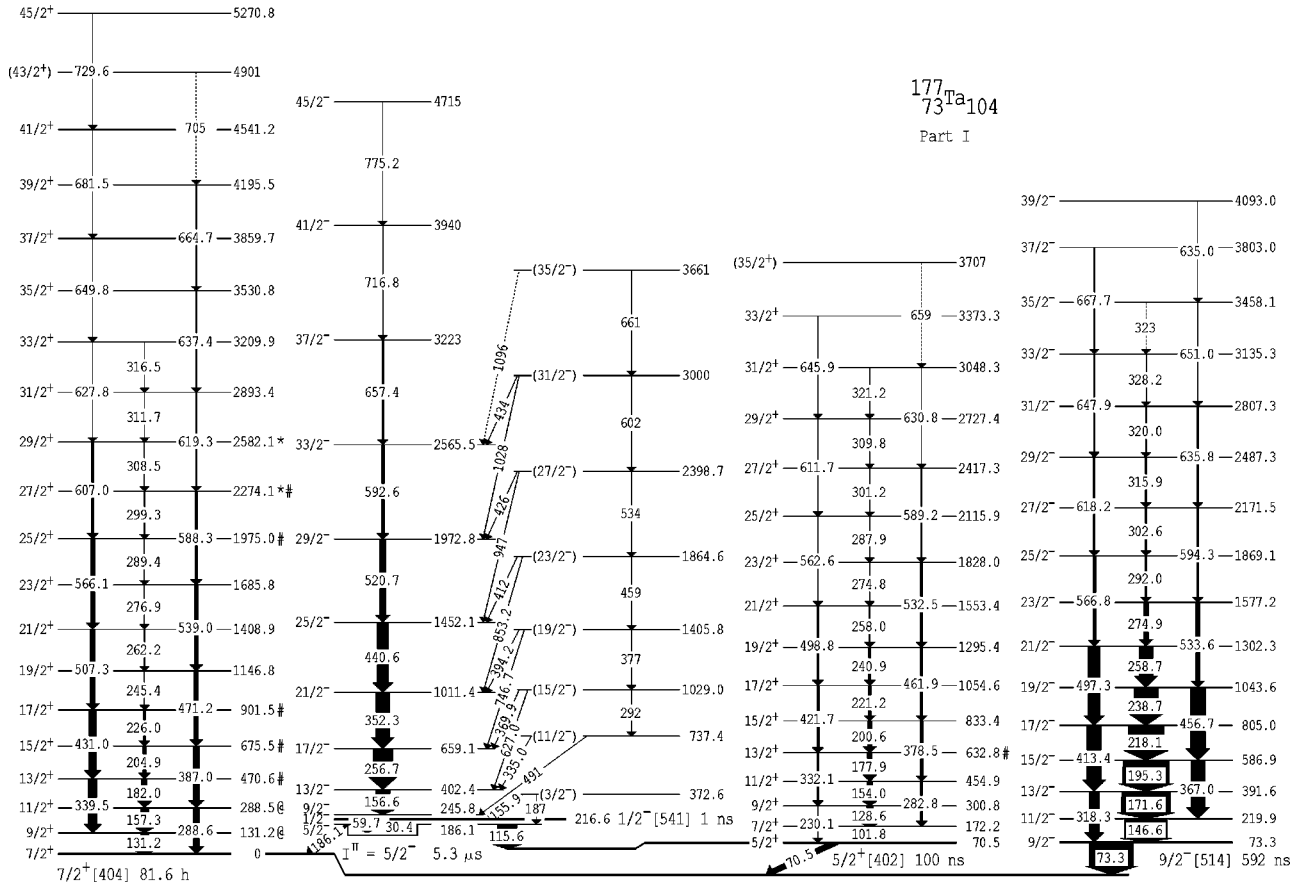
FIG. 1. Partial level scheme for ^{177}Ta showing the 1-quasiparticle bands. The arrow thicknesses are proportional to the singles γ-ray intensities. The symbols *, #, and @ on the side of the level indicate feeding from the $K^{\pi} = \frac{31}{2}^{+}$ isomer, the $K^{\pi} = \frac{17}{2}^{+}$ isomer (see Fig. 5) and the $K^{\pi} = (\frac{11}{2}^{-})$ band, respectively (see Fig. 2).

γ-ray intensities were then extracted and compared to determine the conversion coefficients.

IV. RESULTS

The present study confirms all the known 1-quasiparticle bands and agrees with the bandhead configurations assigned by previous works, hence they are adopted here. It is also convenient, at this stage, to use the configurations for the multiquasiparticle states, subsequently described and justified in Sec. V. The detailed level scheme for ^{177}Ta is presented in five parts in Figs. 1–5.

A. Previous work

The $\frac{7}{2}^{+}[404]$, $\frac{1}{2}^{-}[541]$, $\frac{5}{2}^{+}[402]$, and $\frac{9}{2}^{-}[514]$ intrinsic states associated with the excitation of one-quasiproton and their associated bands were known to $I^{\pi} = \frac{17}{2}^{+}$, $\frac{29}{2}^{-}$, $\frac{19}{2}^{+}$, $\frac{23}{2}^{-}$, respectively [18,19,21–23]. Archer *et al.* [25], in a work done parallel to the present one, extended them to $I^{\pi} = (\frac{45}{2}^{+})$, $\frac{53}{2}^{-}$, $(\frac{39}{2}^{+})$, $\frac{41}{2}^{-}$, respectively, and also reported a $K^{\pi} = (\frac{17}{2}^{+})$ 3-quasiparticle state at 1523 keV and its band members up to spins $(\frac{33}{2}^{+})$. The $K^{\pi} = \frac{21}{2}^{-}$ isomeric state [18–20] at 1355 keV and its rotational band up to $I^{\pi} = \frac{25}{2}^{-}$, and the $K^{\pi} = \frac{23}{2}^{+}$ and $\frac{25}{2}^{+}$ states [21] at excitation energies

of 1699 and 2098 keV, respectively, were known previously. A $K^{\pi} = \frac{25}{2}^{+}$ intrinsic state at 1834.9 keV was reported by Barnéoud *et al.* [21]. The level scheme deduced from the present work disagrees with this assignment, as discussed in Sec. V C 9. No 5- and 7-quasiparticle states had been identified prior to this work. (Selected results of this work discussing the decay of the 7-quasiparticle $K^{\pi} = \frac{49}{2}^{-}$ isomer have been published earlier [4].)

B. Level scheme

The present level scheme was constructed using a range of information; from the various time correlated γ-γ matrices (Sec. III A), by considering prompt coincidences with characteristic tantalum x rays, by elimination of other known transitions in neighboring nuclei and by using the results from earlier measurements [18–23,25] which were confirmed independently. All the new bands and intrinsic states identified in this work were found to be connected to known states and hence their association with ^{177}Ta as listed in Table I, is unambiguous. The table includes some γ-ray transitions which were found to be in coincidence with γ rays associated with ^{177}Ta but which could not be associated with band structures.
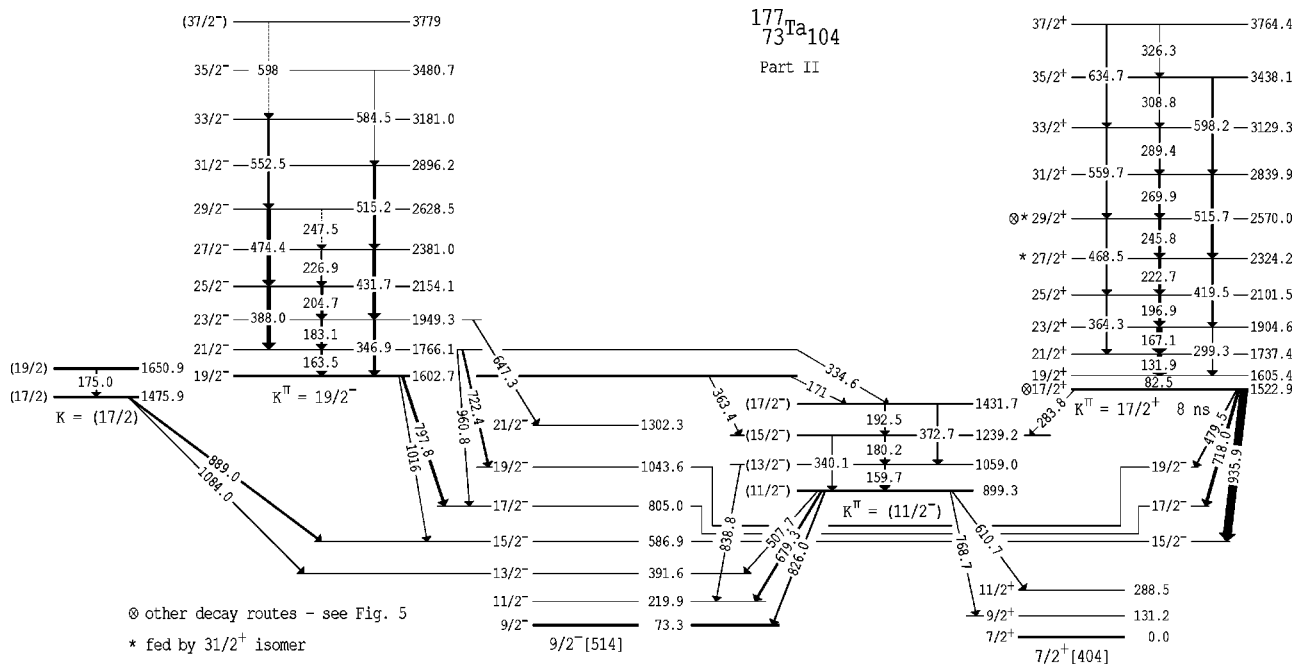
FIG. 2. Part II of the level scheme for ^{177}Ta showing the $K^{\pi}=(\frac{11}{2}^-)$ rotational sequence and the short-lived 3-quasiparticle bands which feed the $K^{\pi}=\frac{9}{2}^-$ band (see Fig. 1).
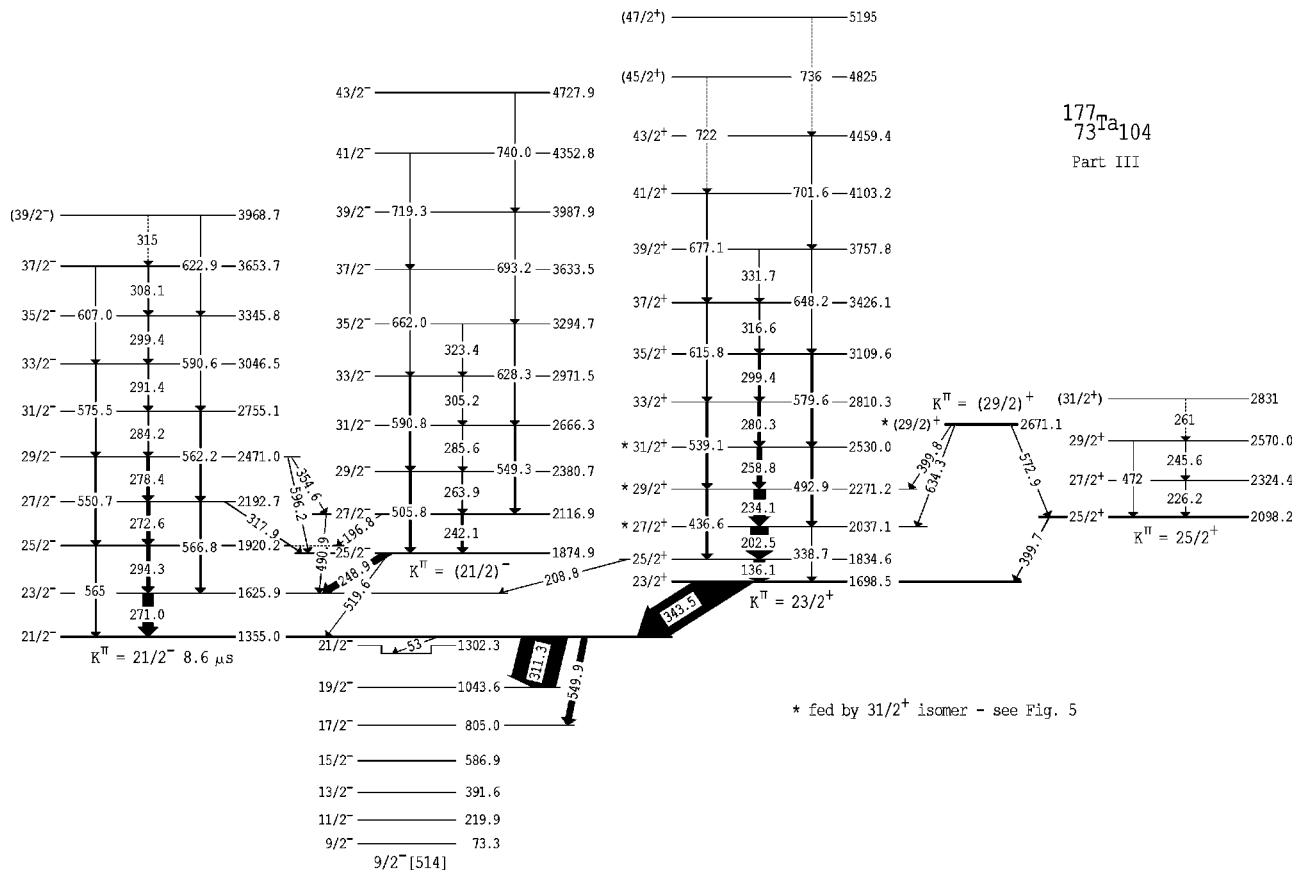
FIG. 3. Part III of the level scheme for ^{177}Ta showing the $K^{\pi}=\frac{21}{2}^-$ isomer at 1355.0 keV and other 3-quasiparticle bands and the $K^{\pi}=(\frac{29}{2})^+$ 5-quasiparticle state, that decay to it.
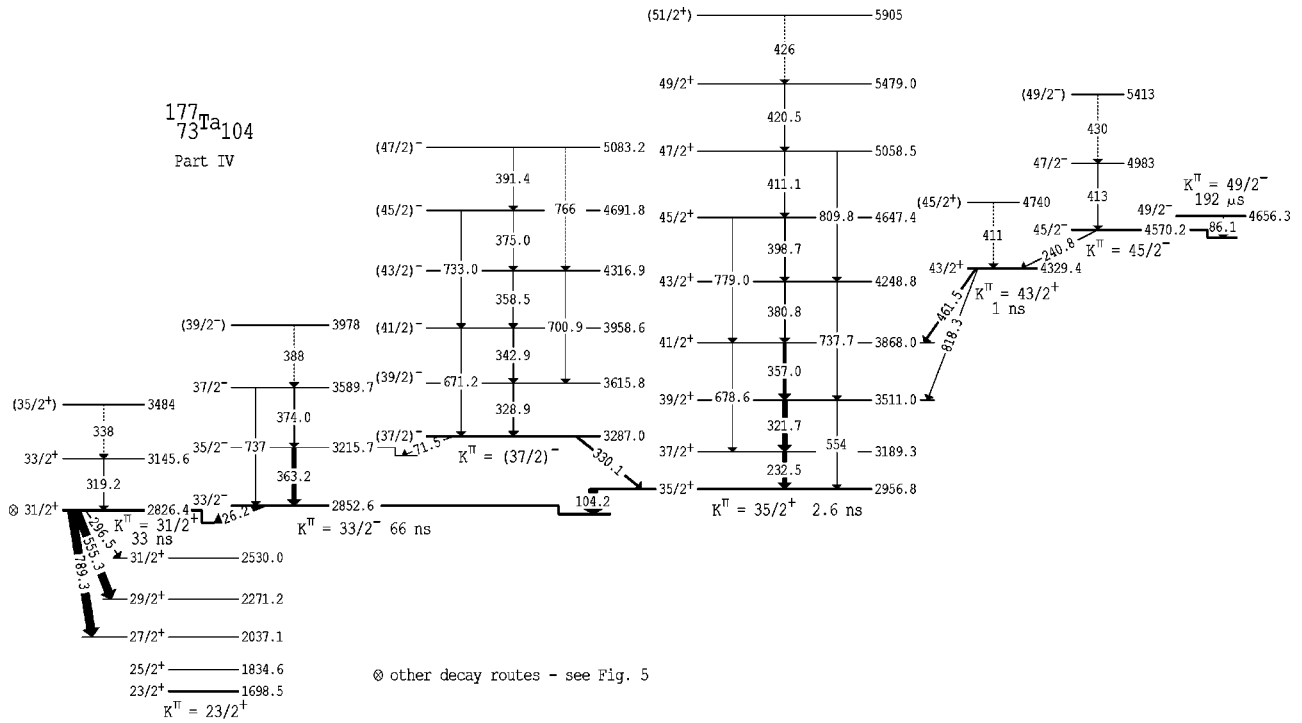
FIG. 4. Part IV of the level scheme for ^{177}Ta showing the 5- and 7-quasiparticle structures and bands.

1. 1-quasiparticle bands

The rotational bands built on 1-quasiparticle states are shown in Fig. 1. They are associated with the $g_{7/2}$, $h_{9/2}$, $d_{5/2}$, and $h_{11/2}$ proton orbitals and the corresponding band structures are labeled with the Nilsson configurations $\frac{7}{2}^+[404]$, $\frac{1}{2}^-[541]$, $\frac{5}{2}^+[402]$, and $\frac{9}{2}^-[514]$, respectively. Another possible 1-quasiparticle structure has been identified at 899 keV, and is labeled by $K^\pi=(\frac{11}{2}^-)$ in Fig. 2. The rotational sequence based on $\frac{7}{2}^+[404]$, $\frac{1}{2}^-[541]$, and

$\frac{5}{2}^+[402]$ states have been confirmed up to $I^\pi=\frac{45}{2}^+$, $\frac{45}{2}^-$, and $(\frac{35}{2}^+)$, respectively, and are in agreement with those recently reported in Ref. [25]. The $\frac{9}{2}^-[514]$ band has been observed up to $I^\pi=\frac{39}{2}^-$, but the assignment of rotational states above $I=\frac{33}{2}$ disagrees with that of Ref. [25], as will be discussed in Sec. V C 4.

Summed prompt (±40 ns) coincidence spectra associated with the $\frac{5}{2}^+[402]$, $\frac{1}{2}^-[541]$, and $\frac{7}{2}^+[404]$ bands are shown in Fig. 6. The high-spin members of each band can
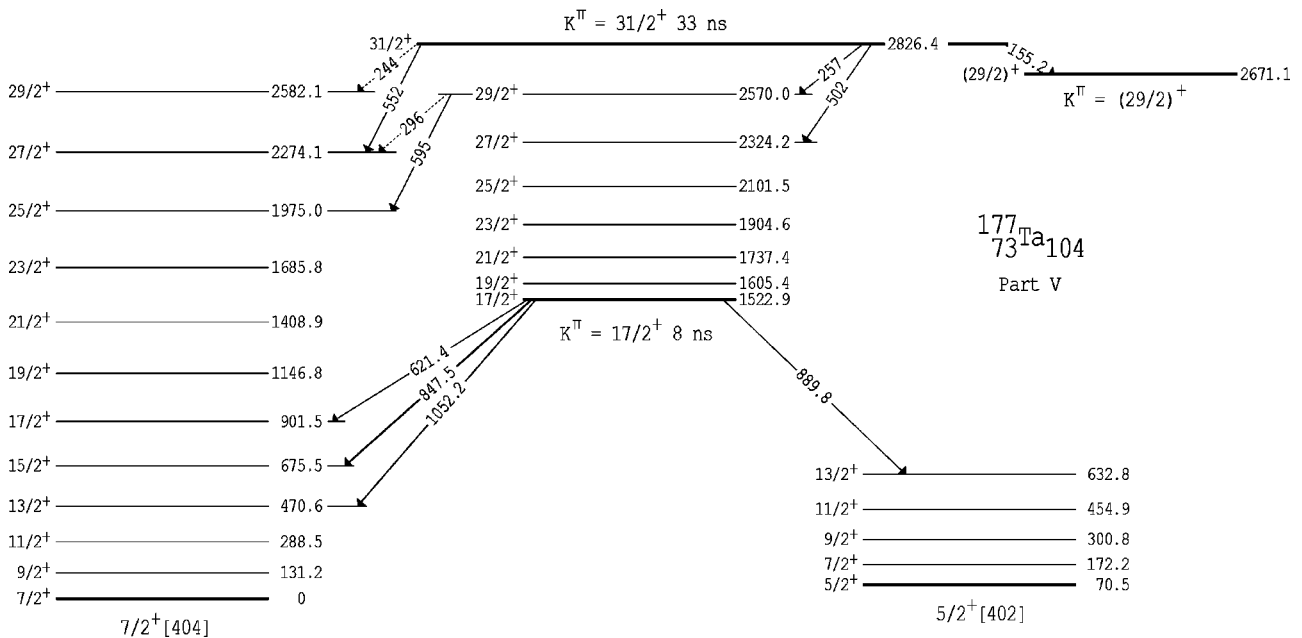
FIG. 5. Part V of the level scheme for ^{177}Ta showing the weak decay routes of the $K^\pi=\frac{31}{2}^+$ and $\frac{17}{2}^+$ isomers.

TABLE I. Energies, intensities, angular distributions, and placements of transitions assigned to ^{177}Ta. The intensities are indicative only.

E_γ	$I_\gamma{}^a$	A_2/A_0	E_i	E_f	K,J_i^π	K,J_f^π
26.2	132 (32)		2852.6	2826.4	$\frac{33}{2},\frac{33}{2}-$	$\frac{31}{2},\frac{31}{2}+$
30.4[b]			216.6	186.1	$\frac{1}{2},\frac{1}{2}-$	$\frac{1}{2},\frac{5}{2}-$
53	8 (3)[c]		1355.0	1302.3	$\frac{21}{2},\frac{21}{2}-$	$\frac{9}{2},\frac{21}{2}-$
59.7[b]			245.8	186.1	$\frac{1}{2},\frac{9}{2}-$	$\frac{1}{2},\frac{5}{2}-$
70.5	139 (26)		70.5	0	$\frac{5}{2},\frac{5}{2}+$	$\frac{7}{2},\frac{7}{2}+$
71.5	4 (3)[c]		3287.0	3215.7	$(\frac{37}{2}),(\frac{37}{2})-$	$\frac{33}{2},\frac{35}{2}-$
73.3	1013 (49)		73.3	0	$\frac{9}{2},\frac{9}{2}-$	$\frac{7}{2},\frac{7}{2}+$
82.5	30 (3)[c]		1605.4	1522.9	$\frac{17}{2},\frac{19}{2}+$	$\frac{17}{2},\frac{17}{2}+$
86.1	2 (1)[c]		4656.3	4570.2	$\frac{49}{2},\frac{49}{2}-$	$\frac{45}{2},\frac{45}{2}-$
101.8	67 (6)	0.10 (17)	172.2	70.5	$\frac{5}{2},\frac{7}{2}+$	$\frac{5}{2},\frac{5}{2}+$
104.2	211 (7)	−0.15 (6)	2956.8	2852.6	$\frac{35}{2},\frac{35}{2}+$	$\frac{33}{2},\frac{33}{2}-$
115.6	455 (20)		186.1	70.5	$\frac{1}{2},\frac{5}{2}-$	$\frac{5}{2},\frac{5}{2}+$
128.6	157 (13)[c]		300.8	172.2	$\frac{5}{2},\frac{9}{2}+$	$\frac{5}{2},\frac{7}{2}+$
131.2	196 (22)	} 0.09 (7)	131.2	0	$\frac{7}{2},\frac{9}{2}+$	$\frac{7}{2},\frac{7}{2}+$
131.9	100 (12)[c]		1737.4	1605.4	$\frac{17}{2},\frac{21}{2}+$	$\frac{17}{2},\frac{19}{2}+$
136.1	264 (17)		1834.6	1698.5	$\frac{23}{2},\frac{25}{2}+$	$\frac{23}{2},\frac{23}{2}+$
146.6	1000 (27)	−0.04 (5)	219.9	73.3	$\frac{9}{2},\frac{11}{2}-$	$\frac{9}{2},\frac{9}{2}-$
154.0	131 (19)[c]		454.9	300.8	$\frac{5}{2},\frac{11}{2}+$	$\frac{5}{2},\frac{9}{2}+$
155.2	9 (3)[c]		2826.4	2671.1	$\frac{31}{2},\frac{31}{2}+$	$(\frac{29}{2}),(\frac{29}{2}+)$
155.9[b]			372.6	216.6	$\frac{1}{2},(\frac{3}{2}-)$	$\frac{1}{2},\frac{1}{2}-$
156.6	333 (20)[c]	} 0.18 (5)	402.4	245.8	$\frac{1}{2},\frac{13}{2}-$	$\frac{1}{2},\frac{9}{2}-$
157.3	204 (40)[c]		288.5	131.2	$\frac{7}{2},\frac{11}{2}+$	$\frac{7}{2},\frac{9}{2}+$
159.7	39 (8)[c]	0.12 (14)	1059.0	899.3	$(\frac{11}{2}),(\frac{13}{2}-)$	$(\frac{11}{2}),(\frac{11}{2}-)$
163.5	46 (12)[c]	0.33 (29)	1766.1	1602.7	$\frac{19}{2},\frac{21}{2}-$	$\frac{19}{2},\frac{19}{2}-$
167.1	131 (19)[c]	0.10 (11)	1904.6	1737.4	$\frac{17}{2},\frac{23}{2}+$	$\frac{17}{2},\frac{21}{2}+$
171	9 (3)[c]		1602.7	1431.7	$\frac{19}{2},\frac{19}{2}-$	$(\frac{11}{2}),(\frac{17}{2}-)$
171.6	1129 (30)	−0.01 (5)	391.6	219.9	$\frac{9}{2},\frac{13}{2}-$	$\frac{9}{2},\frac{11}{2}-$
175.0	14 (6)		1650.9	1475.9	$(\frac{17}{2}),(\frac{19}{2})$	$(\frac{17}{2}),(\frac{17}{2})$
177.9	113 (13)	0.01 (13)	632.8	454.9	$\frac{5}{2},\frac{13}{2}+$	$\frac{5}{2},\frac{11}{2}+$
180.2	29 (6)[c]		1239.2	1059.0	$(\frac{11}{2}),(\frac{15}{2}-)$	$(\frac{11}{2}),(\frac{13}{2}-)$
182.0	130 (9)[c]		470.6	288.5	$\frac{7}{2},\frac{13}{2}+$	$\frac{7}{2},\frac{11}{2}+$
183.1	40 (14)[c]		1949.3	1766.1	$\frac{19}{2},\frac{23}{2}-$	$\frac{19}{2},\frac{21}{2}-$
186.1	68 (7)[c]		186.1	0	$\frac{1}{2},\frac{5}{2}-$	$\frac{7}{2},\frac{7}{2}+$
187	12 (3)[c]		372.6	186.1	$\frac{1}{2},(\frac{3}{2}-)$	$\frac{1}{2},\frac{5}{2}-$
192.5	15 (3)		1431.7	1239.2	$(\frac{11}{2}),(\frac{17}{2}-)$	$(\frac{11}{2}),(\frac{15}{2}-)$
195.3	1071 (21)	−0.03 (7)	586.9	391.6	$\frac{9}{2},\frac{15}{2}-$	$\frac{9}{2},\frac{13}{2}-$
196.8	9 (5)[c]	} −0.09(15)	2116.9	1920.2	$(\frac{21}{2}),\frac{27}{2}-$	$\frac{21}{2},\frac{25}{2}-$
196.9	71 (11)[c]		2101.5	1904.6	$\frac{17}{2},\frac{25}{2}+$	$\frac{17}{2},\frac{23}{2}+$
200.6	104 (13)	0.08 (39)	833.4	632.8	$\frac{5}{2},\frac{15}{2}+$	$\frac{5}{2},\frac{13}{2}+$
202.5	413 (15)	0.14 (9)	2037.1	1834.6	$\frac{23}{2},\frac{27}{2}+$	$\frac{23}{2},\frac{25}{2}+$
204.7	53 (11)[c]	} 0.13 (18)	2154.1	1949.3	$\frac{19}{2},\frac{25}{2}-$	$\frac{19}{2},\frac{23}{2}-$
204.9	76 (9)[c]		675.5	470.6	$\frac{7}{2},\frac{15}{2}+$	$\frac{7}{2},\frac{13}{2}+$
208.8	9 (2)[c]		1834.6	1625.9	$\frac{23}{2},\frac{25}{2}+$	$\frac{21}{2},\frac{23}{2}-$
218.1	831 (19)	−0.02 (4)	805.0	586.9	$\frac{9}{2},\frac{17}{2}-$	$\frac{9}{2},\frac{15}{2}-$
221.2	69 (9)[c]		1054.6	833.4	$\frac{5}{2},\frac{17}{2}+$	$\frac{5}{2},\frac{15}{2}+$
222.7	59 (9)[c]		2324.2	2101.5	$\frac{17}{2},\frac{27}{2}+$	$\frac{17}{2},\frac{25}{2}+$
226.0	58 (9)[c]		901.5	675.5	$\frac{7}{2},\frac{17}{2}+$	$\frac{7}{2},\frac{15}{2}+$
226.2	10 (3)[c]	} 0.42 (24)	2324.4	2098.2	$\frac{25}{2},\frac{27}{2}+$	$\frac{25}{2},\frac{25}{2}+$
226.9	25 (8)[c]		2381.0	2154.1	$\frac{19}{2},\frac{27}{2}-$	$\frac{19}{2},\frac{25}{2}-$

TABLE I. (*Continued*).

E_γ	$I_\gamma{}^a$	A_2/A_0	E_i	E_f	K,J_i^π	K,J_f^π
228				805.0		$\frac{9}{2},\frac{17}{2}-$
230.1	25 (4)^c		300.8	70.5	$\frac{5}{2},\frac{9}{2}+$	$\frac{5}{2},\frac{5}{2}+$
232.5	107 (9)	-0.20 (12)	3189.3	2956.8	$\frac{35}{2},\frac{37}{2}+$	$\frac{35}{2},\frac{35}{2}+$
234.1	276 (16)	0.14 (7)	2271.2	2037.1	$\frac{23}{2},\frac{29}{2}+$	$\frac{23}{2},\frac{27}{2}+$
238.7	567 (29)^c	-0.06 (6)	1043.6	805.0	$\frac{9}{2},\frac{19}{2}-$	$\frac{9}{2},\frac{17}{2}-$
240.8	24 (4)^c	}0.01 (10)	4570.2	4329.4	$\frac{45}{2},\frac{45}{2}-$	$\frac{43}{2},\frac{43}{2}+$
240.9	48 (9)^c		1295.4	1054.6	$\frac{5}{2},\frac{19}{2}+$	$\frac{5}{2},\frac{17}{2}+$
242.1	57 (10)^c	0.30 (21)	2116.9	1874.9	$(\frac{21}{2}),\frac{27}{2}-$	$(\frac{21}{2}),\frac{25}{2}-$
244			2826.4	2582.1	$\frac{31}{2},\frac{31}{2}+$	$\frac{7}{2},\frac{29}{2}+$
245.4	27 (4)^c		1146.8	901.5	$\frac{7}{2},\frac{19}{2}+$	$\frac{7}{2},\frac{17}{2}+$
245.6	6 (2)^c	}0.10 (11)	2570.0	2324.4	$\frac{25}{2},\frac{29}{2}+$	$\frac{25}{2},\frac{27}{2}+$
245.8	49 (7)^c		2570.0	2324.2	$\frac{17}{2},\frac{29}{2}+$	$\frac{17}{2},\frac{27}{2}+$
247.5			2628.5	2381.0	$\frac{19}{2},\frac{29}{2}-$	$\frac{19}{2},\frac{27}{2}-$
248.9	162 (27)^c	0.23 (10)	1874.9	1625.9	$(\frac{21}{2}),\frac{25}{2}-$	$\frac{21}{2},\frac{23}{2}-$
256.7	455 (11)	0.23 (4)	659.1	402.4	$\frac{1}{2},\frac{17}{2}-$	$\frac{1}{2},\frac{13}{2}-$
257	7 (2)^c		2826.4	2570.0	$\frac{31}{2},\frac{31}{2}+$	$\frac{17}{2},\frac{29}{2}+$
258.0	43 (8)^c		1553.4	1295.4	$\frac{5}{2},\frac{21}{2}+$	$\frac{5}{2},\frac{19}{2}+$
258.7	339 (17)^c	}-0.02 (7)	1302.3	1043.6	$\frac{9}{2},\frac{21}{2}-$	$\frac{9}{2},\frac{19}{2}-$
258.8	116 (18)^c		2530.0	2271.2	$\frac{23}{2},\frac{31}{2}+$	$\frac{23}{2},\frac{29}{2}+$
261			2831	2570.0	$\frac{25}{2},(\frac{31}{2}+)$	$\frac{25}{2},\frac{29}{2}+$
262.2	24 (4)^c		1408.9	1146.8	$\frac{7}{2},\frac{21}{2}+$	$\frac{7}{2},\frac{19}{2}+$
263.9	32 (5)^c	0.34 (39)	2380.7	2116.9	$(\frac{21}{2}),\frac{29}{2}-$	$(\frac{21}{2}),\frac{27}{2}-$
269.9	35 (7)^c		2839.9	2570.0	$\frac{17}{2},\frac{31}{2}+$	$\frac{17}{2},\frac{29}{2}+$
271.0	249 (30)	0.08 (4)	1625.9	1355.0	$\frac{21}{2},\frac{23}{2}-$	$\frac{21}{2},\frac{21}{2}-$
272.6	85 (18)^c	0.33 (13)	2192.7	1920.2	$\frac{21}{2},\frac{27}{2}-$	$\frac{21}{2},\frac{25}{2}-$
274.8	27 (9)^c	}-0.07 (5)	1828.0	1553.4	$\frac{5}{2},\frac{23}{2}+$	$\frac{5}{2},\frac{21}{2}+$
274.9	120 (15)^c		1577.2	1302.3	$\frac{9}{2},\frac{23}{2}-$	$\frac{9}{2},\frac{21}{2}-$
276.9	18 (4)^c		1685.8	1408.9	$\frac{7}{2},\frac{23}{2}+$	$\frac{7}{2},\frac{21}{2}+$
278.4	72 (15)^c		2471.0	2192.7	$\frac{21}{2},\frac{29}{2}-$	$\frac{21}{2},\frac{27}{2}-$
280.3	74 (11)^c	0.04 (5)	2810.3	2530.0	$\frac{23}{2},\frac{33}{2}+$	$\frac{23}{2},\frac{31}{2}+$
282.8	55 (7)		454.9	172.2	$\frac{5}{2},\frac{11}{2}+$	$\frac{5}{2},\frac{7}{2}+$
283.8	16 (4)^c		1522.9	1239.2	$\frac{17}{2},\frac{17}{2}+$	$(\frac{11}{2}),(\frac{15}{2}-)$
284.2	25 (9)^c		2755.1	2471.0	$\frac{21}{2},\frac{31}{2}-$	$\frac{21}{2},\frac{29}{2}-$
285.6	15 (4)^c		2666.3	2380.7	$(\frac{21}{2}),\frac{31}{2}-$	$(\frac{21}{2}),\frac{29}{2}-$
287.9	21 (4)^c		2115.9	1828.0	$\frac{5}{2},\frac{25}{2}+$	$\frac{5}{2},\frac{23}{2}+$
288.6	153 (30)^c	0.13 (5)	288.5	0	$\frac{7}{2},\frac{11}{2}+$	$\frac{7}{2},\frac{7}{2}+$
289.4	18 (8)^c		1975.0	1685.8	$\frac{7}{2},\frac{25}{2}+$	$\frac{7}{2},\frac{23}{2}+$
289.4	24 (5)^c		3129.3	2839.9	$\frac{17}{2},\frac{33}{2}+$	$\frac{17}{2},\frac{31}{2}+$
291.4	31 (10)^c		3046.5	2755.1	$\frac{21}{2},\frac{33}{2}-$	$\frac{21}{2},\frac{31}{2}-$
292.0	56 (6)^c		1869.1	1577.2	$\frac{9}{2},\frac{25}{2}-$	$\frac{9}{2},\frac{23}{2}-$
292	9 (3)^c		1029.0	737.4	$\frac{1}{2},(\frac{15}{2}-)$	$\frac{1}{2},(\frac{11}{2}-)$
294.3	88 (23)^c		1920.2	1625.9	$\frac{21}{2},\frac{25}{2}-$	$\frac{21}{2},\frac{23}{2}-$
296			2570.0	2274.1	$\frac{17}{2},\frac{29}{2}+$	$\frac{7}{2},\frac{27}{2}+$
296.5	23 (7)^c	0.32 (16)	2826.4	2530.0	$\frac{31}{2},\frac{31}{2}+$	$\frac{23}{2},\frac{31}{2}+$
299.3	11 (4)^c		2274.1	1975.0	$\frac{7}{2},\frac{27}{2}+$	$\frac{7}{2},\frac{25}{2}+$
299.3	26 (3)^c		1904.6	1605.4	$\frac{17}{2},\frac{23}{2}+$	$\frac{17}{2},\frac{19}{2}+$
299.4	28 (8)^c		3345.8	3046.5	$\frac{21}{2},\frac{35}{2}-$	$\frac{21}{2},\frac{33}{2}-$
299.4	44 (7)^c		3109.6	2810.3	$\frac{23}{2},\frac{35}{2}+$	$\frac{23}{2},\frac{33}{2}+$
301.2	18 (3)^c		2417.3	2115.9	$\frac{5}{2},\frac{27}{2}+$	$\frac{5}{2},\frac{25}{2}+$
302.6	40 (5)^c	-0.02 (10)	2171.5	1869.1	$\frac{9}{2},\frac{27}{2}-$	$\frac{9}{2},\frac{25}{2}-$

TABLE I. (*Continued*).

E_γ	$I_\gamma{}^a$	A_2/A_0	E_i	E_f	K,J_i^π	K,J_f^π
305.2	13 (3)[c]		2971.5	2666.3	$(\frac{21}{2}),\frac{33}{2}-$	$(\frac{21}{2}),\frac{31}{2}-$
308.1	30 (7)		3653.7	3345.8	$\frac{21}{2},\frac{37}{2}-$	$\frac{21}{2},\frac{35}{2}-$
308.5	13 (4)[c]		2582.1	2274.1	$\frac{7}{2},\frac{29}{2}+$	$\frac{7}{2},\frac{27}{2}+$
308.8	17 (3)[c]		3438.1	3129.3	$\frac{17}{2},\frac{35}{2}+$	$\frac{17}{2},\frac{33}{2}+$
309.8	14 (3)[c]		2727.4	2417.3	$\frac{5}{2},\frac{29}{2}+$	$\frac{5}{2},\frac{27}{2}+$
311.3	1042 (20)		1355.0	1043.6	$\frac{21}{2},\frac{21}{2}-$	$\frac{9}{2},\frac{19}{2}-$
311.7	9 (1)[c]		2893.4	2582.1	$\frac{7}{2},\frac{31}{2}+$	$\frac{7}{2},\frac{29}{2}+$
315			3968.7	3653.7	$\frac{21}{2},(\frac{39}{2}-)$	$\frac{21}{2},\frac{37}{2}-$
315.9	44 (6)[c]	−0.40 (20)	2487.3	2171.5	$\frac{9}{2},\frac{29}{2}-$	$\frac{9}{2},\frac{27}{2}-$
316.5	6 (1)[c]		3209.9	2893.4	$\frac{7}{2},\frac{33}{2}+$	$\frac{7}{2},\frac{31}{2}+$
316.6	25 (4)[c]		3426.1	3109.6	$\frac{23}{2},\frac{37}{2}+$	$\frac{23}{2},\frac{35}{2}+$
317.9	25 (5)[c]		2192.7	1874.9	$\frac{21}{2},\frac{27}{2}-$	$(\frac{21}{2}),\frac{25}{2}-$
318.3	245 (30)[c]	0.13 (14)	391.6	73.3	$\frac{9}{2},\frac{13}{2}-$	$\frac{9}{2},\frac{9}{2}-$
319.2	7 (3)		3145.6	2826.4	$\frac{31}{2},\frac{33}{2}+$	$\frac{31}{2},\frac{31}{2}+$
320.0	23 (6)[c]		2807.3	2487.3	$\frac{9}{2},\frac{31}{2}-$	$\frac{9}{2},\frac{29}{2}-$
321.2			3048.3	2727.4	$\frac{5}{2},\frac{31}{2}+$	$\frac{5}{2},\frac{29}{2}+$
321.7	112 (12)	−0.05 (21)	3511.0	3189.3	$\frac{35}{2},\frac{39}{2}+$	$\frac{35}{2},\frac{37}{2}+$
323			3458.1	3135.3	$\frac{9}{2},\frac{35}{2}-$	$\frac{9}{2},\frac{33}{2}-$
323.4	5 (2)[c]		3294.7	2971.5	$(\frac{21}{2}),\frac{35}{2}-$	$(\frac{21}{2}),\frac{33}{2}-$
326.3	7 (2)[c]		3764.4	3438.1	$\frac{17}{2},\frac{37}{2}+$	$\frac{17}{2},\frac{35}{2}+$
328.2	12 (3)[c]		3135.3	2807.3	$\frac{9}{2},\frac{33}{2}-$	$\frac{9}{2},\frac{31}{2}-$
328.9	32 (8)[c]		3615.8	3287.0	$(\frac{37}{2}),(\frac{39}{2})-$	$(\frac{37}{2}),(\frac{37}{2})-$
330.1	57 (11)[c]	0.20 (19)	3287.0	2956.8	$(\frac{37}{2}),(\frac{37}{2})-$	$\frac{35}{2},\frac{35}{2}+$
331.7	18 (2)[c]		3757.8	3426.1	$\frac{23}{2},\frac{39}{2}+$	$\frac{23}{2},\frac{37}{2}+$
332.1	45 (9)[c]		632.8	300.8	$\frac{5}{2},\frac{13}{2}+$	$\frac{5}{2},\frac{9}{2}+$
334.6	13 (3)[c]		1766.1	1431.7	$\frac{19}{2},\frac{21}{2}-$	$(\frac{11}{2}),(\frac{17}{2}-)$
335.0	10 (4)[c]		737.4	402.4	$\frac{1}{2},(\frac{11}{2}-)$	$\frac{1}{2},\frac{13}{2}-$
338			3484	3145.6	$\frac{31}{2},(\frac{35}{2}+)$	$\frac{31}{2},\frac{33}{2}+$
338.7	23 (7)[c]		2037.1	1698.5	$\frac{23}{2},\frac{27}{2}+$	$\frac{23}{2},\frac{23}{2}+$
339.5	209 (18)[c]	} 0.43 (10)	470.6	131.2	$\frac{7}{2},\frac{13}{2}+$	$\frac{7}{2},\frac{9}{2}+$
340.1	19 (5)		1239.2	899.3	$(\frac{11}{2}),(\frac{15}{2}-)$	$(\frac{11}{2}),(\frac{11}{2}-)$
342.9	28 (4)[c]		3958.6	3615.8	$(\frac{37}{2}),(\frac{41}{2})-$	$(\frac{37}{2}),(\frac{39}{2})-$
343.5	759 (20)	−0.25 (4)	1698.5	1355.0	$\frac{23}{2},\frac{23}{2}+$	$\frac{21}{2},\frac{21}{2}-$
346.9	60 (15)[c]		1949.3	1602.7	$\frac{19}{2},\frac{23}{2}-$	$\frac{19}{2},\frac{19}{2}-$
352.3	332 (8)	0.20 (4)	1011.4	659.1	$\frac{1}{2},\frac{21}{2}-$	$\frac{1}{2},\frac{17}{2}-$
354.6	9 (4)[c]		2471.0	2116.9	$\frac{21}{2},\frac{29}{2}-$	$(\frac{21}{2}),\frac{27}{2}-$
357.0	83 (11)	0.33 (7)	3868.0	3511.0	$\frac{35}{2},\frac{41}{2}+$	$\frac{35}{2},\frac{37}{2}+$
358.5	9 (3)[c]		4316.9	3958.6	$(\frac{37}{2}),(\frac{43}{2})-$	$(\frac{37}{2}),(\frac{41}{2})-$
363.2	104 (21)[c]	} 0.22 (5)	3215.7	2852.6	$\frac{33}{2},\frac{35}{2}-$	$\frac{33}{2},\frac{33}{2}-$
363.4	11 (3)[c]		1602.7	1239.2	$\frac{19}{2},\frac{19}{2}-$	$(\frac{11}{2}),(\frac{15}{2}-)$
364.3	30 (11)[c]		2101.5	1737.4	$\frac{17}{2},\frac{25}{2}+$	$\frac{17}{2},\frac{21}{2}+$
367.0	332 (40)[c]	0.26 (6)	586.9	219.9	$\frac{9}{2},\frac{15}{2}-$	$\frac{9}{2},\frac{11}{2}-$
369.9	8 (4)[c]		1029.0	659.1	$\frac{1}{2},(\frac{15}{2}-)$	$\frac{1}{2},\frac{17}{2}-$
372.7	25 (4)[c]		1431.7	1059.0	$(\frac{11}{2}),(\frac{17}{2}-)$	$(\frac{11}{2}),(\frac{13}{2}-)$
374.0	24 (6)[c]		3589.7	3215.7	$\frac{33}{2},\frac{37}{2}-$	$\frac{33}{2},\frac{35}{2}-$
375.0	8 (2)[c]		4691.8	4316.9	$(\frac{37}{2}),(\frac{45}{2})-$	$(\frac{37}{2}),(\frac{43}{2})-$
377	10 (4)[c]		1405.8	1029.0	$\frac{1}{2},(\frac{19}{2}-)$	$\frac{1}{2},(\frac{15}{2}-)$
378.5	60 (9)[c]		833.4	454.9	$\frac{5}{2},\frac{15}{2}+$	$\frac{5}{2},\frac{11}{2}+$

TABLE I. (*Continued*).

E_γ	$I_\gamma{}^{a}$	A_2/A_0	E_i	E_f	K,J_i^π	K,J_f^π
380.8	28 (5)[c]		4248.8	3868.0	$\frac{35}{2},\frac{43}{2}+$	$\frac{35}{2},\frac{41}{2}+$
387.0	160 (13)[c]	0.22 (5)	675.5	288.5	$\frac{7}{2},\frac{15}{2}+$	$\frac{7}{2},\frac{11}{2}+$
388.0	94 (15)[c]		2154.1	1766.1	$\frac{19}{2},\frac{25}{2}-$	$\frac{19}{2},\frac{21}{2}-$
388			3978	3589.7	$\frac{33}{2},(\frac{39}{2}-)$	$\frac{33}{2},\frac{37}{2}-$
391.4	7 (2)[c]		5083.2	4691.8	$(\frac{37}{2}),(\frac{47}{2})^-$	$(\frac{37}{2}),(\frac{45}{2})^-$
394.2	11 (4)[c]		1405.8	1011.4	$\frac{1}{2},(\frac{19}{2}-)$	$\frac{1}{2},\frac{21}{2}-$
398.7	14 (3)[c]		4647.4	4248.8	$\frac{35}{2},\frac{45}{2}+$	$\frac{35}{2},\frac{43}{2}+$
399.7	26 (13)[c]	}-0.59 (21)	2098.2	1698.5	$\frac{25}{2},\frac{25}{2}+$	$\frac{23}{2},\frac{23}{2}+$
399.8	17 (11)[c]		2671.1	2271.2	$(\frac{29}{2}),(\frac{29}{2}+)$	$\frac{23}{2},\frac{29}{2}+$
411			4740	4329.4	$\frac{43}{2},(\frac{45}{2}+)$	$\frac{43}{2},\frac{43}{2}+$
411.1	11 (2)[c]		5058.5	4647.4	$\frac{35}{2},\frac{47}{2}+$	$\frac{35}{2},\frac{45}{2}+$
412	9 (2)[c]		1864.6	1452.1	$\frac{1}{2},(\frac{23}{2}-)$	$\frac{1}{2},\frac{25}{2}-$
413			4983	4570.2	$\frac{45}{2},\frac{47}{2}-$	$\frac{45}{2},\frac{45}{2}-$
413.4	345 (34)	0.13 (5)	805.0	391.6	$\frac{9}{2},\frac{17}{2}-$	$\frac{9}{2},\frac{13}{2}-$
419.5	30 (6)[c]		2324.2	1904.6	$\frac{17}{2},\frac{27}{2}+$	$\frac{17}{2},\frac{23}{2}+$
420.5	7 (1)[c]		5479.0	5058.5	$\frac{35}{2},\frac{49}{2}+$	$\frac{35}{2},\frac{47}{2}+$
421.7	56 (11)[c]		1054.6	632.8	$\frac{5}{2},\frac{17}{2}+$	$\frac{5}{2},\frac{13}{2}+$
426	3 (1)[c]		2398.7	1972.8	$\frac{1}{2},(\frac{27}{2}-)$	$\frac{1}{2},\frac{29}{2}-$
426			5905	5479.0	$\frac{35}{2},(\frac{51}{2}+)$	$\frac{35}{2},\frac{49}{2}+$
430			5413	4983	$\frac{45}{2},(\frac{49}{2}-)$	$\frac{45}{2},\frac{47}{2}-$
431.0	187 (9)	0.14 (52)	901.5	470.6	$\frac{7}{2},\frac{17}{2}+$	$\frac{7}{2},\frac{13}{2}+$
431.7	84 (15)[c]		2381.0	1949.3	$\frac{19}{2},\frac{27}{2}-$	$\frac{19}{2},\frac{23}{2}-$
434	2 (1)[c]		3000	2565.5	$\frac{1}{2},(\frac{31}{2}-)$	$\frac{1}{2},\frac{33}{2}-$
436.6	64 (7)		2271.2	1834.6	$\frac{23}{2},\frac{29}{2}+$	$\frac{23}{2},\frac{25}{2}+$
440.6	267 (10)	0.19 (3)	1452.1	1011.4	$\frac{5}{2},\frac{25}{2}-$	$\frac{5}{2},\frac{21}{2}-$
456.7	351 (45)[c]	0.17 (6)	1043.6	586.9	$\frac{9}{2},\frac{19}{2}-$	$\frac{9}{2},\frac{15}{2}-$
459	10 (4)[c]		1864.6	1405.8	$\frac{1}{2},(\frac{23}{2}-)$	$\frac{1}{2},(\frac{19}{2}-)$
461.5	44 (6)[c]	}0.16 (6)	4329.4	3868.0	$\frac{43}{2},\frac{43}{2}+$	$\frac{35}{2},\frac{41}{2}+$
461.9	57 (10)[c]		1295.4	833.4	$\frac{5}{2},\frac{19}{2}+$	$\frac{5}{2},\frac{15}{2}+$
468.5	34 (7)[c]		2570.0	2101.5	$\frac{17}{2},\frac{29}{2}+$	$\frac{17}{2},\frac{25}{2}+$
471.2	107 (9)	0.27 (5)	1146.8	675.5	$\frac{7}{2},\frac{19}{2}+$	$\frac{7}{2},\frac{15}{2}+$
472	7 (3)[c]		2570.0	2098.2	$\frac{25}{2},\frac{29}{2}+$	$\frac{25}{2},\frac{25}{2}+$
474.4	81 (15)		2628.5	2154.1	$\frac{19}{2},\frac{29}{2}-$	$\frac{19}{2},\frac{25}{2}-$
479.5	35 (4)	-0.34 (48)	1522.9	1043.6	$\frac{17}{2},\frac{17}{2}+$	$\frac{9}{2},\frac{19}{2}-$
490.9	17 (5)		2116.9	1625.9	$(\frac{21}{2}),\frac{27}{2}-$	$\frac{21}{2},\frac{23}{2}-$
491	15 (3)[c]		737.4	245.8	$\frac{1}{2},(\frac{11}{2}-)$	$\frac{1}{2},\frac{9}{2}-$
492.9	58 (7)	0.31 (9)	2530.0	2037.1	$\frac{23}{2},\frac{31}{2}+$	$\frac{23}{2},\frac{27}{2}+$
497.3	270 (30)	0.35 (10)	1302.3	805.0	$\frac{9}{2},\frac{21}{2}-$	$\frac{9}{2},\frac{17}{2}-$
498.8	51 (11)[c]	0.41 (13)	1553.4	1054.6	$\frac{5}{2},\frac{21}{2}+$	$\frac{5}{2},\frac{17}{2}+$
502	10 (2)[c]		2826.4	2324.2	$\frac{31}{2},\frac{31}{2}+$	$\frac{17}{2},\frac{27}{2}+$
505.8	52 (9)[c]		2380.7	1874.9	$(\frac{21}{2}),\frac{29}{2}-$	$(\frac{21}{2}),\frac{25}{2}-$
507.3	116 (4)	}0.11 (7)	1408.9	901.5	$\frac{7}{2},\frac{21}{2}+$	$\frac{7}{2},\frac{17}{2}+$
507.7	25 (4)[c]		899.3	391.6	$(\frac{11}{2}),(\frac{11}{2}-)$	$\frac{9}{2},\frac{13}{2}-$
515.2	49 (20)[c]		2896.2	2381.0	$\frac{19}{2},\frac{31}{2}-$	$\frac{19}{2},\frac{27}{2}-$
515.7	50 (9)[c]		2839.9	2324.2	$\frac{17}{2},\frac{31}{2}+$	$\frac{17}{2},\frac{27}{2}+$
519.6	14 (6)[c]		1874.9	1355.0	$(\frac{21}{2}),\frac{25}{2}-$	$\frac{21}{2},\frac{21}{2}-$
520.7	141 (9)	0.28 (4)	1972.8	1452.1	$\frac{1}{2},\frac{29}{2}-$	$\frac{1}{2},\frac{25}{2}-$
528				586.9		$\frac{9}{2},\frac{15}{2}-$

TABLE I. (*Continued*).

E_γ	$I_\gamma{}^{a}$	A_2/A_0	E_i	E_f	K,J_i^π	K,J_f^π
532.5	45 (11)[c]		1828.0	1295.4	$\frac{5}{2},\frac{23}{2}^+$	$\frac{5}{2},\frac{19}{2}^+$
533.6	100 (20)[c]	}0.34 (7)	1577.2	1043.6	$\frac{9}{2},\frac{23}{2}^-$	$\frac{9}{2},\frac{19}{2}^-$
534	10 (3)[c]		2398.7	1864.6	$\frac{1}{2},(\frac{27}{2}^-)$	$\frac{1}{2},(\frac{23}{2}^-)$
539.0	98 (4)[c]	}0.46 (5)	1685.8	1146.8	$\frac{7}{2},\frac{23}{2}^+$	$\frac{7}{2},\frac{19}{2}^+$
539.1	55 (10)[c]		2810.3	2271.2	$\frac{23}{2},\frac{33}{2}^+$	$\frac{23}{2},\frac{29}{2}^+$
549.3	33 (7)[c]	}0.10 (8)	2666.3	2116.9	$(\frac{21}{2}),\frac{31}{2}^-$	$(\frac{21}{2}),\frac{27}{2}^-$
549.9	140 (17)[c]		1355.0	805.0	$\frac{21}{2},\frac{21}{2}^-$	$\frac{9}{2},\frac{17}{2}^-$
550.7	43 (9)[c]		2471.0	1920.2	$\frac{21}{2},\frac{29}{2}^-$	$\frac{21}{2},\frac{25}{2}^-$
552	5 (2)[c]		2826.4	2274.1	$\frac{31}{2},\frac{31}{2}^+$	$\frac{7}{2},\frac{27}{2}^+$
552.5	51 (10)[c]		3181.0	2628.5	$\frac{19}{2},\frac{33}{2}^-$	$\frac{19}{2},\frac{29}{2}^-$
554	3 (1)[c]		3511.0	2956.8	$\frac{35}{2},\frac{39}{2}^+$	$\frac{35}{2},\frac{35}{2}^+$
555.3	182 (30)	-0.20 (13)	2826.4	2271.2	$\frac{31}{2},\frac{31}{2}^+$	$\frac{23}{2},\frac{29}{2}^+$
559.7	27 (5)[c]	0.16 (11)	3129.3	2570.0	$\frac{17}{2},\frac{33}{2}^+$	$\frac{17}{2},\frac{29}{2}^+$
562.2	39 (8)[c]		2755.1	2192.7	$\frac{21}{2},\frac{31}{2}^-$	$\frac{21}{2},\frac{27}{2}^-$
562.6	36 (8)[c]		2115.9	1553.4	$\frac{5}{2},\frac{25}{2}^+$	$\frac{5}{2},\frac{21}{2}^+$
565	14 (5)[c]		1920.2	1355.0	$\frac{21}{2},\frac{25}{2}^-$	$\frac{21}{2},\frac{21}{2}^-$
566.1	102 (9)[c]		1975.0	1408.9	$\frac{7}{2},\frac{25}{2}^+$	$\frac{7}{2},\frac{21}{2}^+$
566.8	71 (8)[c]		1869.1	1302.3	$\frac{9}{2},\frac{25}{2}^-$	$\frac{9}{2},\frac{21}{2}^-$
566.8	34 (15)[c]		2192.7	1625.9	$\frac{21}{2},\frac{27}{2}^-$	$\frac{21}{2},\frac{23}{2}^-$
572.9	15 (6)[c]		2671.1	2098.2	$(\frac{29}{2}),(\frac{29}{2}^+)$	$\frac{25}{2},\frac{25}{2}^+$
575.5	34 (8)[c]		3046.5	2471.0	$\frac{21}{2},\frac{33}{2}^-$	$\frac{21}{2},\frac{29}{2}^-$
579.6	55 (8)[c]	0.21 (11)	3109.6	2530.0	$\frac{23}{2},\frac{35}{2}^+$	$\frac{23}{2},\frac{31}{2}^+$
584.5	12 (3)[c]		3480.7	2896.2	$\frac{19}{2},\frac{35}{2}^-$	$\frac{19}{2},\frac{31}{2}^-$
588.3	62 (4)[c]		2274.1	1685.8	$\frac{7}{2},\frac{27}{2}^+$	$\frac{7}{2},\frac{23}{2}^+$
589.2	25 (5)[c]		2417.3	1828.0	$\frac{5}{2},\frac{27}{2}^+$	$\frac{5}{2},\frac{23}{2}^+$
590.6	24 (8)[c]		3345.8	2755.1	$\frac{21}{2},\frac{35}{2}^-$	$\frac{21}{2},\frac{31}{2}^-$
590.8	39 (7)[c]		2971.5	2380.7	$(\frac{21}{2}),\frac{33}{2}^-$	$(\frac{21}{2}),\frac{29}{2}^-$
592.6	77 (7)[c]		2565.5	1972.8	$\frac{1}{2},\frac{33}{2}^-$	$\frac{1}{2},\frac{29}{2}^-$
594.3	44 (6)[c]		2171.5	1577.2	$\frac{9}{2},\frac{27}{2}^-$	$\frac{9}{2},\frac{23}{2}^-$
595	3 (1)[c]		2570.0	1975.0	$\frac{17}{2},\frac{29}{2}^+$	$\frac{7}{2},\frac{25}{2}^+$
596.2	14 (7)[c]		2471.0	1874.9	$\frac{21}{2},\frac{29}{2}^-$	$(\frac{21}{2}),\frac{25}{2}^-$
598			3779	3181.0	$\frac{19}{2},(\frac{37}{2}^-)$	$\frac{19}{2},\frac{33}{2}^-$
598.2	29 (7)[c]		3438.1	2839.9	$\frac{17}{2},\frac{35}{2}^+$	$\frac{17}{2},\frac{31}{2}^+$
602	6 (3)[c]		3000	2398.7	$\frac{1}{2},(\frac{31}{2}^-)$	$\frac{1}{2},(\frac{27}{2}^-)$
607.0	71 (9)[c]		2582.1	1975.0	$\frac{7}{2},\frac{29}{2}^+$	$\frac{7}{2},\frac{25}{2}^+$
607.0	8 (3)[c]		3653.7	3046.5	$\frac{21}{2},\frac{37}{2}^-$	$\frac{21}{2},\frac{33}{2}^-$
610.7	20 (5)[c]		899.3	288.5	$(\frac{11}{2}),(\frac{11}{2}^-)$	$\frac{7}{2},\frac{11}{2}^+$
611.7	30 (9)[c]		2727.4	2115.9	$\frac{5}{2},\frac{29}{2}^+$	$\frac{5}{2},\frac{25}{2}^+$
615.8	30 (7)[c]		3426.1	2810.3	$\frac{23}{2},\frac{37}{2}^+$	$\frac{23}{2},\frac{33}{2}^+$
618.2	43 (6)[c]		2487.3	1869.1	$\frac{9}{2},\frac{29}{2}^-$	$\frac{9}{2},\frac{25}{2}^-$
619.3	44 (9)[c]		2893.4	2274.1	$\frac{7}{2},\frac{31}{2}^+$	$\frac{7}{2},\frac{27}{2}^+$
621.4	18 (3)[c]		1522.9	901.5	$\frac{17}{2},\frac{17}{2}^+$	$\frac{7}{2},\frac{17}{2}^+$
622.9	8 (3)[c]		3968.7	3345.8	$\frac{21}{2},(\frac{39}{2}^-)$	$\frac{21}{2},\frac{35}{2}^-$
627.0	14 (5)[c]		1029.0	402.4	$\frac{1}{2},(\frac{15}{2}^-)$	$\frac{1}{2},\frac{13}{2}^-$
627.8	13 (3)[c]		3209.9	2582.1	$\frac{7}{2},\frac{33}{2}^+$	$\frac{7}{2},\frac{29}{2}^+$
628.3	14 (3)[c]		3294.7	2666.3	$(\frac{21}{2}),\frac{35}{2}^-$	$(\frac{21}{2}),\frac{31}{2}^-$
630.8	11 (4)[c]		3048.3	2417.3	$\frac{5}{2},\frac{31}{2}^+$	$\frac{5}{2},\frac{27}{2}^+$
634.3	14 (5)[c]		2671.1	2037.1	$(\frac{29}{2}),(\frac{29}{2}^+)$	$\frac{23}{2},\frac{27}{2}^+$
634.7	20 (8)	0.60(20)	3764.4	3129.3	$\frac{17}{2},\frac{37}{2}^+$	$\frac{17}{2},\frac{33}{2}^+$

TABLE I. (*Continued*).

E_γ	$I_\gamma{}^a$	A_2/A_0	E_i	E_f	K,J_i^π	K,J_f^π
635.0	10 (4)^c		4093.0	3458.1	$\frac{9}{2},\frac{39}{2}-$	$\frac{9}{2},\frac{35}{2}-$
635.8	34 (6)^c		2807.3	2171.5	$\frac{9}{2},\frac{31}{2}-$	$\frac{9}{2},\frac{27}{2}-$
637.4	18 (3)^c		3530.8	2893.4	$\frac{7}{2},\frac{35}{2}+$	$\frac{7}{2},\frac{31}{2}+$
645.9	10 (4)^c		3373.3	2727.4	$\frac{5}{2},\frac{33}{2}+$	$\frac{5}{2},\frac{29}{2}+$
647.3	23 (10)^c		1949.3	1302.3	$\frac{19}{2},\frac{23}{2}-$	$\frac{9}{2},\frac{21}{2}-$
647.9	87 (9)^c		3135.3	2487.3	$\frac{9}{2},\frac{33}{2}-$	$\frac{9}{2},\frac{29}{2}-$
648.2	27 (7)^c		3757.8	3109.6	$\frac{23}{2},\frac{39}{2}+$	$\frac{23}{2},\frac{35}{2}+$
649.8	9 (2)^c		3859.7	3209.9	$\frac{7}{2},\frac{37}{2}+$	$\frac{7}{2},\frac{33}{2}+$
651.0	17 (5)^c		3458.1	2807.3	$\frac{9}{2},\frac{35}{2}-$	$\frac{9}{2},\frac{31}{2}-$
657.4	44 (4)^c		3223	2565.5	$\frac{1}{2},\frac{37}{2}-$	$\frac{1}{2},\frac{33}{2}-$
659			3707	3048.3	$\frac{5}{2},(\frac{35}{2}+)$	$\frac{5}{2},\frac{31}{2}+$
661			3661	3000	$\frac{1}{2},(\frac{35}{2}-)$	$\frac{1}{2},(\frac{31}{2}-)$
662.0	10 (3)^c		3633.5	2971.5	$(\frac{21}{2}),\frac{37}{2}-$	$(\frac{21}{2}),\frac{33}{2}-$
664.7	13 (3)^c		4195.5	3530.8	$\frac{7}{2},\frac{39}{2}+$	$\frac{7}{2},\frac{35}{2}+$
667.7	14 (4)^c		3803.0	3135.3	$\frac{9}{2},\frac{37}{2}-$	$\frac{9}{2},\frac{33}{2}-$
671.2	12 (3)^c		3958.6	3287.0	$(\frac{37}{2}),(\frac{41}{2})-$	$(\frac{37}{2}),(\frac{37}{2})-$
677.1	30 (8)^c		4103.2	3426.1	$\frac{23}{2},\frac{41}{2}+$	$\frac{23}{2},\frac{37}{2}+$
678.6	6 (2)^c	$\left.\rule{0pt}{3ex}\right\}0.17\ (9)$	3868.0	3189.3	$\frac{35}{2},\frac{41}{2}+$	$\frac{35}{2},\frac{37}{2}+$
679.3	51 (8)^c		899.3	219.9	$(\frac{11}{2}),(\frac{11}{2}-)$	$\frac{9}{2},\frac{11}{2}-$
681.5	5 (2)^c		4541.2	3859.7	$\frac{7}{2},\frac{41}{2}+$	$\frac{7}{2},\frac{37}{2}+$
693.2	11 (3)^c		3987.9	3294.7	$(\frac{21}{2}),\frac{39}{2}-$	$(\frac{21}{2}),\frac{35}{2}-$
700.9	6 (2)^c		4316.9	3615.8	$(\frac{37}{2}),(\frac{43}{2})-$	$(\frac{37}{2}),(\frac{39}{2})-$
701.6	13 (2)^c		4459.4	3757.8	$\frac{23}{2},\frac{43}{2}+$	$\frac{23}{2},\frac{39}{2}+$
705			4901	4195.5	$\frac{7}{2},(\frac{43}{2}+)$	$\frac{7}{2},\frac{39}{2}+$
716.8	24 (5)^c		3940	3223	$\frac{1}{2},\frac{41}{2}-$	$\frac{1}{2},\frac{37}{2}-$
718.0	65 (4)^c		1522.9	805.0	$\frac{17}{2},\frac{17}{2}+$	$\frac{9}{2},\frac{17}{2}-$
719.3	4 (1)^c		4352.8	3633.5	$(\frac{21}{2}),\frac{41}{2}-$	$(\frac{21}{2}),(\frac{37}{2}-)$
722			4825	4103.2	$\frac{23}{2},(\frac{45}{2}+)$	$\frac{23}{2},\frac{41}{2}+$
722.4	38 (5)^c	$-0.29\ (25)$	1766.1	1043.6	$\frac{19}{2},\frac{21}{2}-$	$\frac{9}{2},\frac{19}{2}-$
729.6	3 (1)^c		5270.8	4541.2	$\frac{7}{2},\frac{45}{2}+$	$\frac{7}{2},\frac{41}{2}+$
733.0	5 (2)^c		4691.8	3958.6	$(\frac{37}{2}),(\frac{45}{2})-$	$(\frac{37}{2}),(\frac{41}{2})-$
736			5195	4459.4	$\frac{23}{2},(\frac{47}{2}+)$	$\frac{23}{2},\frac{43}{2}+$
737	7 (5)^c		3589.7	2852.6	$\frac{33}{2},\frac{37}{2}-$	$\frac{33}{2},\frac{33}{2}-$
737.7	8 (2)^c		4248.8	3511.0	$\frac{35}{2},\frac{43}{2}+$	$\frac{35}{2},\frac{39}{2}+$
740.0	2 (1)^c		4727.9	3987.9	$(\frac{21}{2}),\frac{43}{2}-$	$(\frac{21}{2}),\frac{39}{2}-$
746.7	13 (3)^c		1405.8	659.1	$\frac{1}{2},(\frac{19}{2}-)$	$\frac{1}{2},\frac{17}{2}-$
766			5083.2	4316.9	$(\frac{37}{2}),(\frac{47}{2})-$	$(\frac{37}{2}),(\frac{43}{2})-$
768.7	4 (1)^c		899.3	131.2	$(\frac{11}{2}),(\frac{11}{2}-)$	$\frac{7}{2},\frac{9}{2}+$
775.2	9 (3)^c		4715	3940	$\frac{1}{2},\frac{45}{2}-$	$\frac{1}{2},\frac{41}{2}-$
779.0	4 (1)^c		4647.4	3868.0	$\frac{35}{2},\frac{45}{2}+$	$\frac{35}{2},\frac{41}{2}+$
789.3	190 (6)	0.42 (13)	2826.4	2037.1	$\frac{31}{2},\frac{31}{2}+$	$\frac{23}{2},\frac{27}{2}+$
797.8	52 (4)	$-0.29\ (33)$	1602.7	805.0	$\frac{19}{2},\frac{19}{2}-$	$\frac{9}{2},\frac{17}{2}-$
809.8	4 (1)^c		5058.5	4248.8	$\frac{35}{2},\frac{47}{2}+$	$\frac{35}{2},\frac{43}{2}+$
818.3	6 (1)^c		4329.4	3511.0	$\frac{43}{2},\frac{43}{2}+$	$\frac{35}{2},\frac{39}{2}+$
826.0	35 (4)	$-0.15\ (16)$	899.3	73.3	$(\frac{11}{2}),(\frac{11}{2}-)$	$\frac{9}{2},\frac{9}{2}-$
838.8	7 (1)^c		1059.0	219.9	$(\frac{11}{2}),(\frac{13}{2}-)$	$\frac{9}{2},\frac{11}{2}-$
844				586.9		$\frac{9}{2},\frac{15}{2}-$
847.5	31 (7)^c		1522.9	675.5	$\frac{17}{2},\frac{17}{2}+$	$\frac{7}{2},\frac{15}{2}+$

TABLE I. (*Continued*).

E_γ	$I_\gamma{}^a$	A_2/A_0	E_i	E_f	K,J_i^π	K,J_f^π
853.2	16 (4)[c]		1864.6	1011.4	$\frac{1}{2},(\frac{23}{2}^-)$	$\frac{1}{2},\frac{21}{2}^-$
889.0	47 (7)[c]		1475.9	586.9	$(\frac{17}{2}),(\frac{17}{2})$	$\frac{9}{2},\frac{15}{2}^-$
889.8	13 (4)[c]		1522.9	632.8	$\frac{17}{2},\frac{17}{2}^+$	$\frac{5}{2},\frac{13}{2}^+$
895				1043.6		$\frac{9}{2},\frac{19}{2}^-$
935.9	183 (22)[c]	−0.24 (25)	1522.9	586.9	$\frac{17}{2},\frac{17}{2}^+$	$\frac{9}{2},\frac{15}{2}^-$
947	8 (3)[c]		2398.7	1452.1	$\frac{1}{2},(\frac{27}{2}^-)$	$\frac{1}{2},\frac{25}{2}^-$
960.8	14 (3)[c]		1766.1	805.0	$\frac{19}{2},\frac{21}{2}^-$	$\frac{9}{2},\frac{17}{2}^-$
1016	4 (1)[c]		1602.7	586.9	$\frac{19}{2},\frac{19}{2}^-$	$\frac{9}{2},\frac{15}{2}^-$
1028	6 (2)[c]		3000	1972.8	$\frac{1}{2},(\frac{31}{2}^-)$	$\frac{1}{2},\frac{29}{2}^-$
1052.2	21 (6)[c]		1522.9	470.6	$\frac{17}{2},\frac{17}{2}^+$	$\frac{7}{2},\frac{13}{2}^+$
1084.0	24 (7)[c]		1475.9	391.6	$(\frac{17}{2}),(\frac{17}{2})$	$\frac{9}{2},\frac{13}{2}^-$
1096			3661	2565.5	$\frac{1}{2},(\frac{35}{2}^-)$	$\frac{1}{2},\frac{33}{2}^-$

[a]Relative intensities determined from singles and coincidence spectra.
[b]Reference [37].
[c]Relative intensity extracted from prompt coincidence projection.

be clearly seen in the figure. Figure 7 shows a summed prompt coincidence spectrum associated with the $\frac{9}{2}^-[514]$ band. The intense γ rays in the figure are associated with the $\frac{9}{2}^-[514]$ band itself and the relatively weak γ rays belong to the 3-quasiparticle bands (see Fig. 2), most of which decay through the $\frac{9}{2}^-[514]$ band. Due to the long lifetime ($\tau_m = 8.6$ μs) of the $\frac{21}{2}^-$ 3-quasiparticle state, the γ rays preceding it do not appear in Fig. 7.

2. 3-quasiparticle bands

The 3-quasiparticle states and their associated bands are shown in Figs. 2, 3, and include the new $K=(\frac{17}{2})$ state at 1475.9 keV and $K^\pi=\frac{19}{2}^-$ state at 1602.7 keV (both in Fig. 2), and the band based on $I^\pi=\frac{25}{2}^-$ state at 1874.9 keV (Fig.
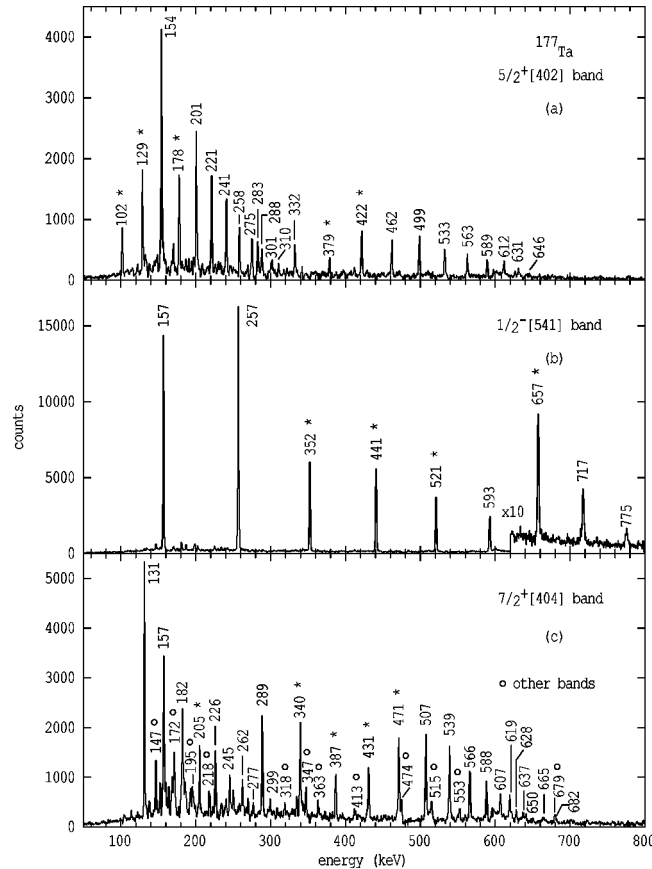
FIG. 6. Summed γ-ray coincidence spectra relating to the $K^\pi = \frac{5}{2}^+$, $\frac{1}{2}^-$ (favored sequence), and $\frac{7}{2}^+$ bands (cf. Fig. 1). The gating transitions are indicated by asterisks.
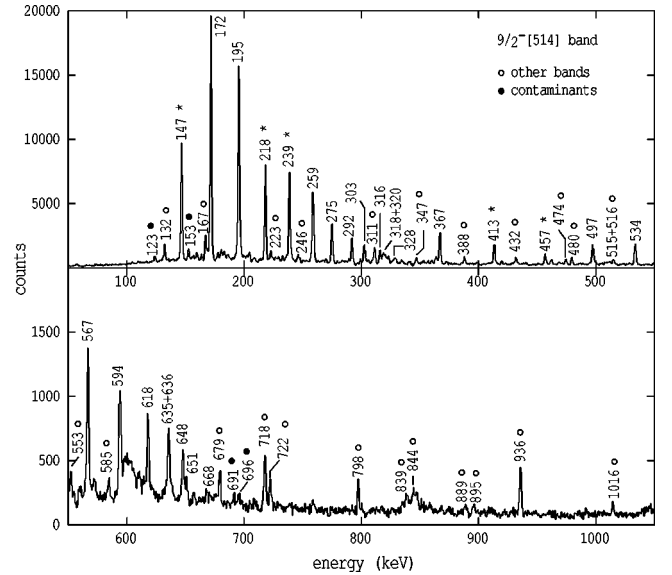
FIG. 7. Coincidence γ-ray spectrum constructed from gates on γ-rays, marked by asterisk, in the $\frac{9}{2}^-[514]$ band projecting all γ-rays in a ±40 ns time window. The spectrum shows the γ rays associated with the $\frac{9}{2}^-[514]$ band and with bands built on the $K^\pi=(\frac{11}{2}^-)$, $\frac{17}{2}^+$, and $\frac{19}{2}^-$ states (cf. Fig. 2) which decay through the $\frac{9}{2}^-[514]$ band.
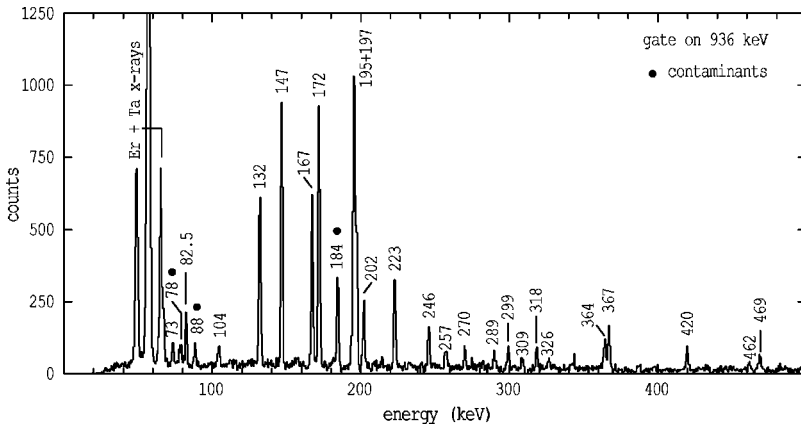
FIG. 8. Coincidence γ-ray spectrum relating to the $K^\pi = \frac{17}{2}^+$ band (see Fig. 2). The spectrum is generated by gating on the 935.9 keV transition which depopulates the $K^\pi = \frac{17}{2}^+$ level, and projecting all γ rays within a time interval of ± 150 ns.

3). This work also extends the rotational sequence built on the previously known states, the $K^\pi = \frac{21}{2}^-$, $\frac{23}{2}^+$, $\frac{25}{2}^+$ at 1355.0, 1698.5, and 2098.2 keV, respectively (all in Fig. 3).

The present measurement, confirms the $K^\pi = \frac{17}{2}^+$ bandhead at 1522.9 keV (Fig. 2) identified by Archer *et al.* [25] as $K^\pi = (\frac{17}{2}^+)$, but it disagrees with their assignment of the first member of the rotational band as being at 1656.2 keV. In the present work it is assigned to be at 1605.4 keV with a decay to the $K^\pi = \frac{17}{2}^+$ bandhead by a 82.5 keV transition. This transition is clearly visible in Fig. 8 which shows the coincidences with the 935.9 keV transition depopulating the bandhead. The out-of-band transitions (see Fig. 5) from the $I^\pi = \frac{29}{2}^+$ level at 2570 keV to the $K^\pi = \frac{7}{2}^+$ band and the decay of the $K^\pi = \frac{31}{2}^+$ isomer to the $I^\pi = \frac{27}{2}^+$ and $\frac{29}{2}^+$ members of the $K^\pi = \frac{17}{2}^+$ band further supports our energy and spin assignments. (The transition may have been missed in Ref. [25] because of their insensitivity to low-energy transitions.)

Most of the 3-quasiparticle states ultimately decay (Fig. 3) to the $\frac{21}{2}^-$ isomeric state at 1355 keV. Figure 9 shows the events that precede its decay. This spectrum is generated by gating on the 311.3 keV transition (which depopulates the isomer) and the 171.6, 195.3, and 218.1 keV transitions of the $\frac{9}{2}^-[514]$ band (which is fed by the isomer), with an appropriate time gate. The spectrum corresponds mainly to the portion of the level scheme in Fig. 3, though the γ rays preceding the $K^\pi = \frac{31}{2}^+$ isomer (Fig. 4), including the main decay route of the $K^\pi = \frac{49}{2}^-$ isomer, can also be seen clearly. The strongest γ rays are associated with the $K^\pi = \frac{23}{2}^+$ band above the 1698.5 keV level, which lies in the main decay route of the $K^\pi = \frac{31}{2}^+$ isomer.

3. 5- and 7-quasiparticle bands

The 5-quasiparticle, $K^\pi = (\frac{29}{2})^+$ state at 2671.1 keV (Fig. 3), $K^\pi = \frac{31}{2}^+$, $\frac{33}{2}^-$, and $\frac{35}{2}^+$ isomeric states at 2826.4, 2852.6, and 2956.8 keV, respectively (Fig. 4) and the $K^\pi = (\frac{37}{2})^-$ state at 3287.0 keV have been identified in this work. Also identified are the three 7-quasiparticle states at 4329.4, 4570.2, and 4656.3 keV labeled $K^\pi = \frac{43}{2}^+$, $\frac{45}{2}^-$, $\frac{49}{2}^-$, respectively, in Fig. 4. These states are weakly populated as they are close to the maximum input angular momentum brought in by the reaction.

Figure 10 shows transitions occurring between beam bursts, which de-excite the $K^\pi = \frac{49}{2}^-$ isomer. This out-of-beam coincidence spectrum is generated by gating on the 240.8 and 461.5 keV transitions below the isomer, with the additional condition that the coincident γ rays should occur within ± 40 ns of each other. This constraint reduces the intensity of the γ rays following the $K^\pi = \frac{33}{2}^-$ isomer in the spectrum (and incidentally reduces the efficiency below ~ 70 keV). The weak 502 and 935.9 keV γ rays in the spectrum are due to the decay branch of the $K^\pi = \frac{31}{2}^+$ isomer to the $K^\pi = \frac{17}{2}^+$ band (see Fig. 5) which subsequently decays mainly to the $\frac{9}{2}^-[514]$ band. The inset shows out-of-beam coincidences with the 104 keV γ-ray projecting events in the LEPS detector, with the time condition relaxed to ± 150 ns. It illustrates the presence of the 26 keV γ ray, which follows
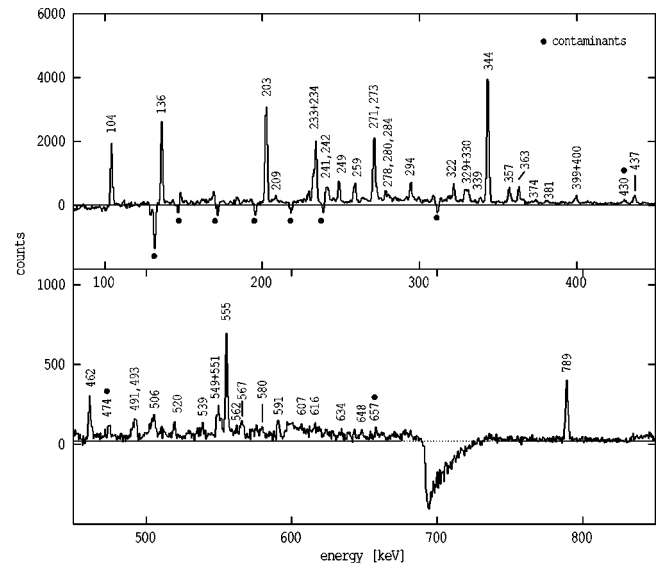
FIG. 9. Summed γ-ray coincidence spectrum obtained with delayed gating on the 172, 195, 218, and 311 keV transitions below the $K^\pi = \frac{21}{2}^-$ isomer, thus showing all the transitions preceding the isomer (see Fig. 3). To remove random contributions the corresponding delayed spectrum has been subtracted. The negative peaks in the upper panel are from contaminant transitions in ^{175}Ta and that in the lower panel is from the inelastic neutron excitation of the 691 keV 0^+ isomer in ^{72}Ge.
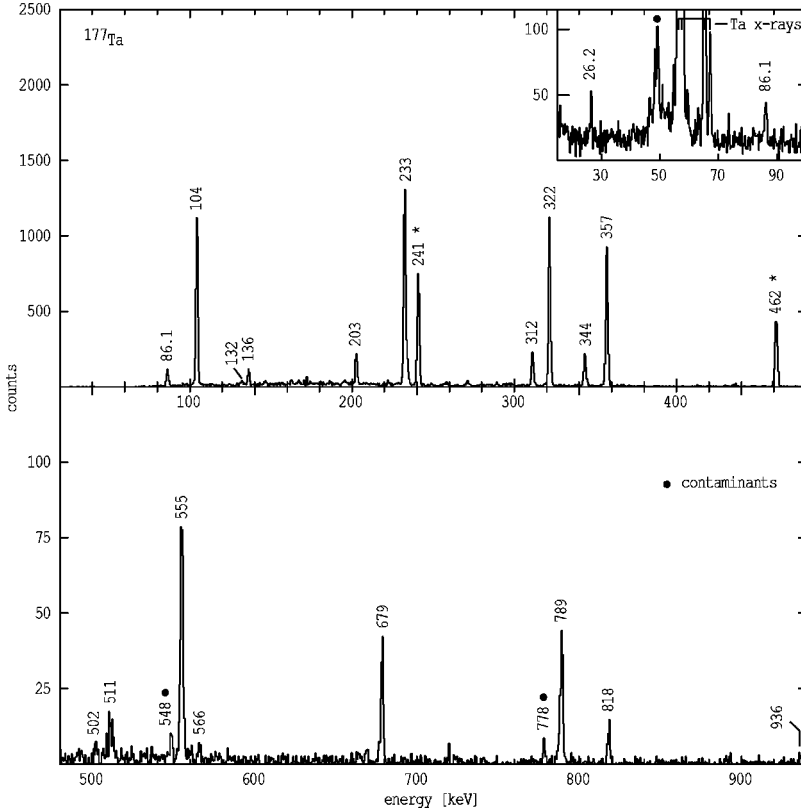
FIG. 10. Out-of-beam coincidence spectrum (± 40 ns), gated by 241 and 462 keV γ rays (marked by asterisk), showing the decay path of the $K^{\pi} = \frac{49}{2}^-$ isomer (see Fig. 4). The inset shows a detail of the x-ray region, gated by the 104.2 keV transition, with the time restriction relaxed to ± 150 ns. The 26.2 and 86.1 keV γ rays from the decay of $K^{\pi} = \frac{33}{2}^-$ and $\frac{49}{2}^-$ isomers, respectively, are clearly visible.

the decay of the $K^{\pi} = \frac{33}{2}^-$ isomer and plays a crucial role in determining the correct spins of the intrinsic states.

C. Transition intensities and angular distributions

The relative intensities of the γ-ray transitions given in Table I are normalized to the intensity of the 147 keV transition in the $\frac{9}{2}^-[514]$ band, which is arbitrarily taken to be 1000 units. Due to the complexity of the spectrum, many of the transition intensities are obtained from either across-isomer projections or from prompt-coincidence projections. While angular correlation effects in the former are expected to be minimal, they may significantly affect the intensities obtained from the latter. The intensities obtained solely from the prompt coincidence data are indicated in Table I and have not been corrected for angular correlation effects which are estimated to be $< 15\%$.

The prompt gated γ-ray spectra recorded in singles (see Sec. II B) at $\pm 48°$, $\pm 97°$, and $\pm 145°$ were analyzed to obtain the angular distribution information. Due to the limited number of angles in the array, only the A_0 and A_2 coefficients could be extracted, with the A_4 term set at zero. The fitted A_2 values are given in Table I and are discussed for the particular transitions in Sec. V C.

D. Electron conversion coefficients and multipolarities

The electron conversion coefficients are given in Table II. Total electron-conversion coefficients were obtained from the γ-γ coincidence spectra by determining the balance of the transition intensities feeding and depopulating a given state. The K-, L-, and M-conversion coefficients were deter-

mined from the conversion electron measurements as detailed in Sec. III D. Figure 11 shows the γ-ray and the corresponding conversion electron spectra optimized with the appropriate time gates to select transitions following the decay of the $K^{\pi} = \frac{49}{2}^-$ isomer (Fig. 4).

E. Level lifetimes

Time spectra for each individual transition generated from the γ-time and γ-γ-time matrices (see Secs. III B and III C) were used to determine the meanlives of the intrinsic states. The accuracy to which short lifetimes can be measured depends critically on the measurement of the time response as a function of the γ-ray energy for one detector in the case of γ-time measurements and for two detectors for the γ-γ-time measurements [28]. The response functions for the γ-time measurements were obtained by fitting the time spectra of prompt γ rays using a single Gaussian. For the γ-γ-time measurements, the response functions for pairs of transitions were obtained by fitting the time difference spectra for a number of pairs of prompt γ rays in a cascade whose energies lie in the neighborhood of the γ rays of interest. The positions and widths of the Gaussians obtained from the fitting procedure were parametrized and used for subsequent analyses. For very short lifetimes (< 5 ns), instead of using the universal fit parameters, response functions determined from prompt γ rays with energies close to the line of interest were used.

In determining the lifetimes from γ-time measurements only those lines which were free of contaminants were used, while in the case of γ-γ-time measurements, contaminants

TABLE II. Total (T), K-, L-, and M-electron conversion coefficients and assigned multipolarities.

E (keV)	Type	Experiment	Assigned multipolarity	Theoretical values
26.2	T	3(1)	$E1$	2.72
53	T	11(6)	$M1(E2)$	$M1$:5 $E2$:61
71.5	T	7(2)	$M1$	$M1$:12 $E1$:0.87 $E2$:15
86.1	L	4(1)	$E2$	$E2$:4.36 $M1$:0.919
	T	7.3(9)	$M1$ or $E2$	$M1$:7.01 $E2$:6.9
104.2	L	0.05(5)	$E1$	0.047
	M	0.03(5)	$E1$	0.011
	T	0.4(1)	$E1$	0.331
136.1	T	1.93(20)	$M1$	1.880
	L	0.35(12)	$M1$	0.246
155.2	T	2.0(6)	$M1$	$M1$:1.30 $E2$:0.7
195.3, 196.9	K	0.39(9)[a]	$M1/E2$	$M1$:0.561 $E2$:0.177
202.5	K	0.41(8)	$M1/E2$	$M1$:0.513 $E2$:0.163
208.8	T	0.05(2)	$E1$	0.055
218.1	K	0.48(7)	$M1$	0.418
	L	0.091(24)	$M1/E2$	$M1$:0.065 $E2$:0.070
232.5	T	0.45(4)	$M1$	0.421
232.5, 234.1	K	0.18(3)[b]	$M1/E2$	$M1$:0.348 $E2$:0.112
240.8	K	0.059(21)	$E1$	0.032
	T	0.043(4)	$E1$	0.038
248.9	T	0.38(3)	$M1$	0.349
271.0	K	0.25(6)	$M1$	0.277
296.5	K	0.024(14)	$E1$	0.019
311.3	K	0.17(2)	$M1$	0.159
	L	0.030(9)	$M1$	0.025
321.7	K	0.18(3)	$M1$	$M1$:0.145 $E2$:0.047
	L	0.031(8)	$M1$	$M1$:0.022 $E2$:0.016
343.5	K	0.016(6)	$E1$	0.014
352.3	K	0.028(3)	$E2$	0.037
357.0	K	0.120(17)	$M1$	0.110
363.2	K	0.08(2)	$M1$	0.105
399.7	K	0.11(3)	$M1$	$M1$:0.082 $E2$:0.027
413.4	K	0.023(10)	$E2$	0.025
456.7	K	0.014(9)	$E2$	0.019
461.5	K	0.051(7)	$M1$	0.056
	L	0.007(2)	$M1$	0.0085
507.7	K	0.02(1)	$M1$	$M1$:0.044 $E2$:0.015
549.9	K	0.018(11)	$E2$	0.013
555.3	K	0.036(11)	$M1$	0.035
	K	0.038(2)	$M1$	0.035
679.0	K	<0.006	$E1$ or $E2$	$E1$:0.0031 $E2$:0.0079
718.0	K	<0.002	$E1$	$E1$:0.0027 $E2$:0.007
789.3	K	<0.005(2)	$E1$ or $E2$	$E1$:0.002 $E2$:0.006
	K	0.006(1)	$E2$	0.0057
797.8	K	0.013(3)	$M1$	0.014
935.9	K	<0.002	$E1$	$E1$:0.0017 $E2$:0.0041

[a]Approximately 84% 195.3 keV and 16% 196.9 keV.
[b]Approximately 69% 232.5 keV and 31% 234.1 keV.

usually do not pose a problem. Wherever possible, several γ-ray transitions or pairs of transitions were used to obtain independent measurements of the meanlives. For overlapping transitions which are partially resolved in the LEPS detector, separate time spectra were obtained by unfolding.

The meanlives of the intrinsic states range from several ns to a few hundred μs and are summarized in Table III.

The meanlives of the 1-quasiparticle $\frac{5}{2}^+$[402], $\frac{9}{2}^-$[514] bandheads and the $I^\pi = \frac{5}{2}^-$ state of the $\frac{1}{2}^-$[541] band are in agreement with those in the literature [23]. Of the nine
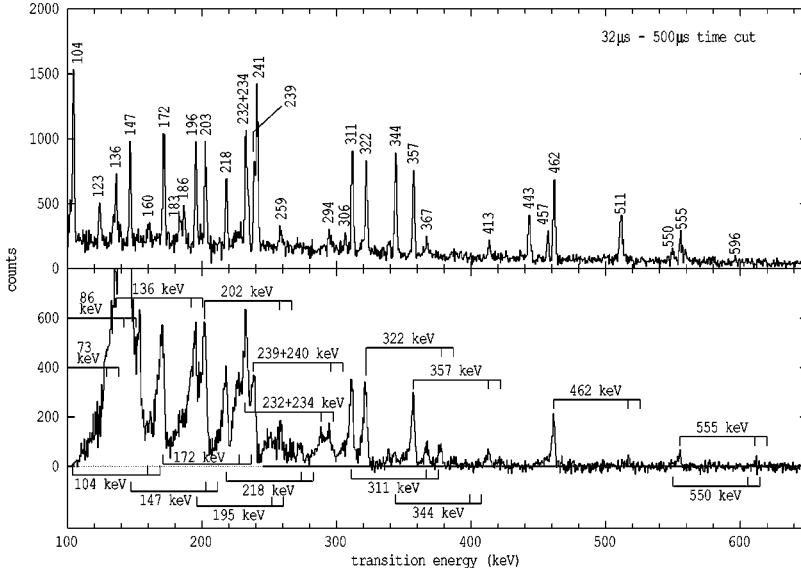
FIG. 11. Associated out-of-beam γ-ray and conversion electron spectra corresponding to a time cut of 32–500 μs, with a longer time spectrum (500– 850 μs) subtracted to preferentially select transitions from the decay of the $K^{\pi} = \frac{49}{2}^{-}$, 192 μs isomer.

3-quasiparticle states, only two have significant meanlives. The lifetime of the newly identified $K^{\pi} = \frac{17}{2}^{+}$ bandhead was measured using both the γ-time method and the γ-γ-time method, yielding a value of 8 ± 2 ns. The meanlife of the $K^{\pi} = \frac{21}{2}^{-}$ state, measured by analyzing the γ-time spectra for a number of lines following the isomer, was found to be 8.6 ± 0.3 μs which is close, but not equal, to the previously reported [20] value of 7.24 ± 0.29 μs.

Since the extraction of the meanlives of the $K^{\pi} = \frac{31}{2}^{+}$ and $K^{\pi} = \frac{33}{2}^{-}$ 5-quasiparticle states (Fig. 4), determined to be 33 ± 6 ns and 66 ± 5 ns, respectively, involved fitting complex decay curves, it requires some comment. The $K^{\pi} = \frac{33}{2}^{-}$ state at 2852.6 keV is mainly fed by 104.2 and 363.2 keV transitions and decays solely by the 26.2 keV γ ray to the $K^{\pi} = \frac{31}{2}^{+}$ state at 2826.4 keV, which subsequently decays to the $K^{\pi} = \frac{23}{2}^{+}$ state by 555.3 and 789.3 keV γ rays as shown in Fig. 4. The γ-γ-time data involving the 26.2 keV γ-ray transition could not be used due to insufficient statistics. Hence the meanlives of the $K^{\pi} = \frac{31}{2}^{+}$ and $\frac{33}{2}^{-}$ states were determined in two steps. The time spectrum of the 26.2 keV γ ray was analyzed first to obtain a measure of the meanlife of the $K^{\pi} = \frac{33}{2}^{-}$ state, and then the combined decay curve (from $K^{\pi} = \frac{33}{2}^{-}$ and $\frac{31}{2}^{+}$ states) was analyzed to obtain

the meanlife of the $\frac{31}{2}^{+}$ state and to determine better the meanlife of the $\frac{33}{2}^{-}$ state.

The 26.2 keV γ ray is expected to suffer from time walk even in the LEPS detector and hence the time spectra of other γ rays close in energy to 26.2 keV, namely 19.2, 27.5, and 31.8 keV, were analyzed to determine the spectrum shape and the time zero position and thus the appropriate response function. The analysis of the time spectrum for the 26.2 keV gate, shown in the upper panel of Fig. 12, yielded a meanlife of 85 ± 25 ns for the $K^{\pi} = \frac{33}{2}^{-}$ state at 2852.6 keV. Despite the large uncertainties, it was extremely useful in limiting the allowable range of meanlife for the $K^{\pi} = \frac{33}{2}^{-}$ state in the analysis of the combined decay curve.

The combined decay curves were generated by (i) the γ-time method using the 555.3 and 789.3 keV transitions and (ii) the γ-γ-time method using the {104.2} {555.3, 789.3, 436.6} keV and {363.2} {555.3, 789.3, 436.6} keV pairs where the notation denotes that the 104.2 keV (or 363.2 keV) transition is used as the start and either the 555.3 or 789.3 or 436.6 keV transitions are used as stop (LEPS detector used for the 104.2 keV). The time spectrum obtained from the pairs {363.2}{436.6, 555.3, 789.3} keV is shown in Fig. 12 along with the fit using meanlife values of 33 ± 6 ns for the $K^{\pi} = \frac{31}{2}^{+}$ state and 66 ± 5 ns for the $K^{\pi} = \frac{33}{2}^{-}$ level. These values were obtained by taking a weighted average of all the different measurements. The meanlife of the $K^{\pi} = \frac{33}{2}^{-}$ state is consistent with the value (85 ± 25 ns) obtained from the analysis of the time spectra for the 26.2 keV γ ray. In our previous publication [4], the meanlives were quoted to be 60 and 25 ns for the $K^{\pi} = \frac{31}{2}^{+}$ and $\frac{33}{2}^{-}$ states, respectively, whereas the present more complete analysis shows that a reversal of those lifetimes explains the data better.

The meanlife of the $K^{\pi} = \frac{35}{2}^{+}$ state at 2956.8 keV was determined to be 2.4 ± 0.5 ns from the analysis of the time spectrum of the 104.2 keV transition in the LEPS detector, and 3 ± 1 ns using the γ-ray pairs {104.2}{232.5, 321.7, 357.0, 461.5} keV in the γ-γ-time method, leading to a weighted average of 2.6 ± 0.5 ns. Due to insufficient statistics, only limits could be placed on the lifetimes of the K^{π}

TABLE III. Measured meanlives of states in ^{177}Ta.

E (keV)	K^{π}	τ_m	E (keV)	K^{π}	τ_m
70.5	$\frac{5}{2}^{+}$	100 (3) ns	2098.2	$\frac{25}{2}^{+}$	<4 ns
73.3	$\frac{9}{2}^{-}$	592 (10) ns	2671.1	$(\frac{29}{2})^{+}$	<4 ns
186.1	$\frac{5}{2}^{-a}$	5.3 (2) μs	2826.4	$\frac{31}{2}^{+}$	33 (6) ns
899.3	$(\frac{11}{2}^{-})$	<2 ns	2852.6	$\frac{33}{2}^{-}$	66 (5) ns
1355.0	$\frac{21}{2}^{-}$	8.6 (3) μs	2956.8	$\frac{35}{2}^{+}$	2.6 (5) ns
1476.0	$(\frac{17}{2})$	<2 ns	3287.0	$(\frac{37}{2})^{-}$	<2 ns
1522.9	$\frac{17}{2}^{+}$	8 (2) ns	4329.4	$\frac{43}{2}^{+}$	1.0 (3) ns
1602.8	$\frac{19}{2}^{-}$	<2 ns	4570.2	$\frac{45}{2}^{-}$	<1 ns
1698.5	$\frac{23}{2}^{+}$	<1.5 ns	4656.3	$\frac{49}{2}^{-}$	192 (6) μs

$^{a}I^{\pi} = \frac{5}{2}^{-}$ state of the $K^{\pi} = \frac{1}{2}^{-}$ band.
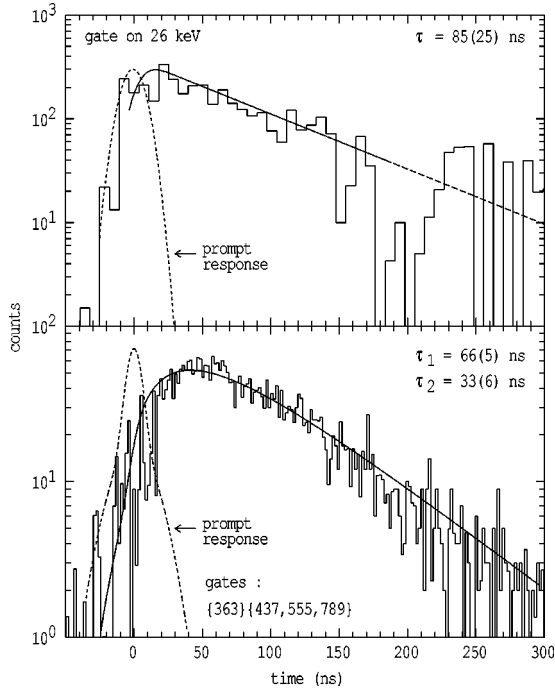
FIG. 12. The upper panel shows the time spectrum of the 26.2 keV transition which depopulates the $K^\pi = \frac{33}{2}^-$ isomer at 2852.6 keV (see Fig. 4). Prompt response curves are indicated. Data beyond 190 ns were not used in the fit due to distortions present in the spectra for very low-energy lines. The lower panel shows the spectrum obtained from gates on the 363.2 keV transition (start), which feeds the $\frac{33}{2}^-$ isomer and any of the 555.3, 789.3, or 436.6 keV γ rays (stop) depopulating the $\frac{31}{2}^+$ isomer. This decay curve therefore depends on the meanlives of both the $K^\pi = \frac{31}{2}^+$ and $\frac{33}{2}^-$ isomers (both in Fig. 4).

$=(\frac{29}{2})^+$ (at 2671.1 keV) and $(\frac{37}{2})^-$ (at 3287.0 keV) 5-quasiparticle states.

The meanlife of the $K^\pi = \frac{43}{2}^+$ 7-quasiparticle state at 4329.4 keV was measured to be 1.0 ± 0.3 ns by the γ-time method using the 461.5 keV transition observed in the LEPS detector. The time spectrum for the decay of the longest-lived isomer in ^{177}Ta, the $K^\pi = \frac{49}{2}^-$ 7-quasiparticle state at 4656.3 keV, obtained by combining gates on the 461, 357, and 104 keV transitions (see Fig. 4), is shown in the lower panel of Fig. 13 along with a fit with a meanlife of 192 ± 6 μs. The upper panel of the figure shows the decay curve for the 1.4 ± 0.1 ms isomer in ^{176}Ta [4], measured during the same experiment, for comparison.

V. QUASIPARTICLE CONFIGURATION ASSIGNMENTS

Many new multiquasiparticle states and their rotational structures have been identified in this work. Configuration assignments have been made by taking into account the observed properties such as $g_K - g_R$ values and alignments, as detailed below. For convenience each band has been labeled by a K quantum number, assumed to be equal to the spin of the bandhead, although it is to be understood that cases of significant alignment also imply mixed K.
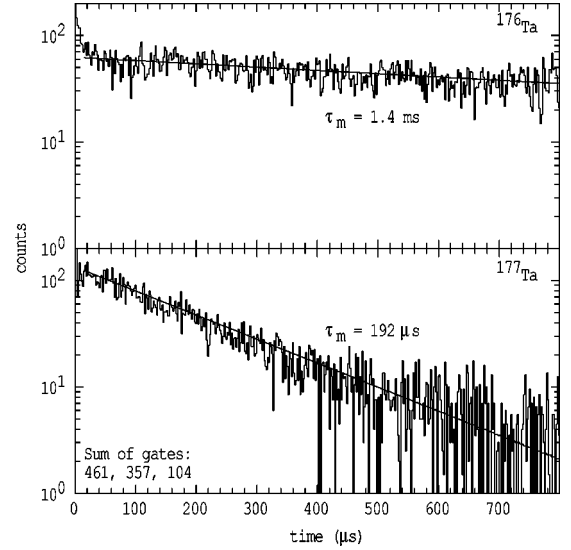
FIG. 13. Time spectra with gates on transitions following the 20^- isomer in ^{176}Ta (upper panel) and the $\frac{49}{2}^-$ isomer in ^{177}Ta (lower panel). The solid lines are fits with lifetimes as indicated.

A. $g_K - g_R$ values

The γ-ray branching ratios were deduced from the intensities of the $\Delta I = 1$ and $\Delta I = 2$ in-band transitions, deduced mainly from coincidence data. $B(M1)/B(E2)$ and $g_K - g_R$ values were obtained using the rotational model expressions [3]. The $(g_K - g_R)/Q_0$ values have been calculated with the assumption that K is equal to the bandhead spin and using a value of $Q_0 = 7.27$ eb, an estimate obtained by taking the average of the quadrupole moments of neighboring Hf nuclei [31,32]. Since the branching ratios yield only the magnitude of the quadrupole-dipole mixing ratio, the sign of δ has been obtained from the measured anisotropies. A positive sign was determined for all the bands where there were adequate statistics. The values for $B(M1)/B(E2)$, $g_K - g_R$ and δ are presented in Table IV.

The experimental g_K values, given in Table V, were calculated assuming $g_R = 0.29 \pm 0.03$, which was obtained [6] from the measured [33] magnetic moment of the $\frac{7}{2}^+[404]$ ground state in ^{177}Ta and the value of $g_K - g_R = 0.46 \pm 0.02$, deduced from the experimental branching ratios in the band. They are compared in Table V with the predictions using additivity for the suggested configurations, for Nilsson model wave functions with deformation parameters $\epsilon_2 = 0.248$, $\epsilon_4 = 0.041$ obtained by averaging the calculated parameters [29] for ^{176}Hf and ^{178}W, modified oscillator parameters κ and μ as given in Ref. [30] and $g_s = 0.7$ g_s^{free}, where g_s^{free} is the gyromagnetic ratio for free proton and neutron intrinsic spin.

The results for configurations involving $i_{13/2}$ neutrons are not expected to agree with these simple estimates as the calculations assume a pure configuration, whereas $i_{13/2}$ neutrons can involve strong Coriolis K mixing. In such cases, the g_K values have been calculated using the geometric model of Dönau [34] which gives

$$K g_K = \sum_j g_{\Omega_j} \Omega_j - \frac{K}{\sqrt{(I^2 - K^2)}} \sum_j (g_{\Omega_j} - g_R) i_j, \quad (1)$$

TABLE IV. Experimental branching and mixing ratios, $B(M1)/B(E2)$ and $g_K - g_R$ values.

I^π ($\hbar$)	$E_\gamma(\Delta I=1)$ (keV)	$E_\gamma(\Delta I=2)$ (keV)	λ[a]	$B(M1)/B(E2)$ ($\mu_N^2/e^2\mathrm{b}^2$)	$\lvert g_K - g_R\rvert$[b]	$\lvert\delta\rvert$[c]
$7/2^+[404]$, $E=0$						
$\frac{11}{2}^+$	157.3	288.6	0.8(1)	0.35(5)	0.41(3)	0.48(4)
$\frac{13}{2}^+$	182.0	339.5	1.6(2)	0.27(3)	0.45(3)	0.43(3)
$\frac{15}{2}^+$	204.9	387.0	2.1(4)	0.29(6)	0.50(6)	0.37(4)
$\frac{17}{2}^+$	226.0	431.0	3.2(4)	0.25(2)	0.50(3)	0.37(2)
$\frac{19}{2}^+$	245.4	471.2	4.0(16)	0.25(10)	0.51(11)	0.34(8)
$\frac{21}{2}^+$	262.2	507.3	4.8(11)	0.25(6)	0.52(6)	0.33(4)
$5/2^+[402]$, $E=70.5$ keV						
$\frac{9}{2}^+$	128.6	230.1	0.16(5)	1.3(4)	$1.21^{+(15)}_{-(20)}$	0.16(2)
$\frac{11}{2}^+$	154.0	282.8	0.42(7)	0.8(1)	1.15(9)	0.17(1)
$\frac{13}{2}^+$	177.9	332.1	0.40(8)	1.2(2)	$1.52^{+(14)}_{-(17)}$	0.12(1)
$\frac{15}{2}^+$	200.6	378.5	0.58(6)	1.2(1)	1.54(8)	0.12(1)
$\frac{17}{2}^+$	221.2	421.7	0.8(2)	1.0(3)	1.5(2)	0.12(1)
$\frac{19}{2}^+$	240.9	461.9	1.2(3)	0.8(2)	1.4(1)	0.13(1)
$\frac{21}{2}^+$	258.0	498.8	1.2(7)	1.1(7)	$1.56^{+(43)}_{-(58)}$	0.11(3)
$\frac{23}{2}^+$	274.8	532.5	1.7(5)	0.8(2)	1.4(2)	0.12(2)
$9/2^-[514]$, $E=73.3$ keV						
$\frac{13}{2}^-$	171.6	318.3	0.22(3)	1.9(3)	0.68(6)	0.26(2)
$\frac{15}{2}^-$	195.3	367.0	0.31(5)	1.8(3)	0.85(6)	0.21(2)
$\frac{17}{2}^-$	218.1	413.4	0.42(6)	1.9(3)	0.95(7)	0.18(1)
$\frac{19}{2}^-$	238.7	456.7	0.62(8)	1.6(2)	0.93(6)	0.18(1)
$\frac{21}{2}^-$	258.7	497.3	0.8(1)	1.6(3)	0.96(8)	0.17(1)
$\frac{23}{2}^-$	274.9	533.6	0.85(8)	1.7(2)	1.03(7)	0.16(1)
$\frac{25}{2}^-$	292.0	566.8	1.3(3)	1.3(3)	0.9(1)	0.17(2)
$\frac{27}{2}^-$	302.6	594.3	1.1(2)	1.7(3)	1.06(9)	0.14(1)
$\frac{29}{2}^-$	315.9	618.2	1.1(3)	1.8(5)	$1.12^{+(14)}_{-(16)}$	0.13(2)
$\frac{31}{2}^-$	320.0	635.8	1.5(6)	1.5(6)	1.0(2)	0.14(3)
$K^\pi=(11/2^-)$, $E=899.3$ keV						
$(\frac{15}{2}^-)$	180.2	340.1	0.6(2)	0.7(3)	$0.32^{+(7)}_{-(8)}$	0.5(1)
$K^\pi=17/2^+$, $E=1522.9$ keV						
$\frac{23}{2}^+$	167.1	299.3	0.21(5)	1.6(4)	0.34(4)	0.29(3)
$\frac{25}{2}^+$	196.9	364.3	0.41(7)	1.3(2)	0.36(3)	0.30(3)
$\frac{27}{2}^+$	222.7	419.5	0.51(9)	1.5(3)	0.42(4)	0.27(2)
$\frac{29}{2}^+$	245.8	468.5	0.7(2)	1.4(3)	0.42(5)	0.27(2)
$\frac{31}{2}^+$	269.9	515.7	1.5(5)	0.8(3)	0.34(6)	0.35(7)
$\frac{33}{2}^+$	289.4	559.7	1.1(3)	1.4(4)	0.46(7)	0.26(4)
$K^\pi=19/2^-$, $E=1602.7$ keV						
$\frac{23}{2}^-$	183.1	346.9	1.5(3)	$0.01^{+(10)\mathrm{d}}$	$0.02^{+(4)\mathrm{d}}$	$6.2_{-(43)}$[d]
$\frac{25}{2}^-$	204.7	388.0	1.8(6)	0.2(1)	0.10(4)	1.1(5)
$\frac{27}{2}^-$	226.9	431.7	3.3(9)	0.09(7)	$0.08^{+(4)}_{-(3)}$	1.4(8)
$K^\pi=21/2^-$, $E=1355.0$ keV						
$\frac{25}{2}^-$	294.3	565	0.16(8)	9(5)	$0.45^{+(10)}_{-(16)}$	0.35(9)
$\frac{27}{2}^-$	272.6	566.8	0.4(1)	4.8(14)	$0.45^{+(6)}_{-(7)}$	0.31(4)
$\frac{29}{2}^-$	278.4	550.7	0.6(1)	2.5(6)	0.37(5)	0.35(4)
$\frac{31}{2}^-$	284.2	562.2	1.5(5)	1.0(4)	0.26(5)	0.5(1)
$\frac{33}{2}^-$	291.4	575.5	1.1(4)	1.5(6)	$0.34^{+(6)}_{-(7)}$	0.35(7)
$\frac{35}{2}^-$	299.4	590.6	0.9(3)	1.8(6)	$0.40^{+(6)}_{-(7)}$	0.29(5)
$K^\pi=(21/2)^-$, $E=1874.9$ keV						
$\frac{29}{2}^-$	263.9	505.8	1.6(7)	0.5(3)	$0.18^{+(5)}_{-(6)}$	0.7(2)

TABLE IV. (*Continued*).

I^π ($\hbar$)	$E_\gamma(\Delta I=1)$ (keV)	$E_\gamma(\Delta I=2)$ (keV)	λ[a]	$B(M1)/B(E2)$ ($\mu_N^2/e^2 b^2$)	$|g_K-g_R|$[b]	$|\delta|$[c]
$\frac{31}{2}^-$	285.6	549.3	2.2(12)	0.5(4)	0.17(7)	0.7(4)
$\frac{33}{2}^-$	305.2	590.8	3.0(13)	0.4(3)	0.17(6)	0.7(3)
$K^\pi=23/2^+, E=1698.5$ keV						
$\frac{27}{2}^+$	202.5	338.7	0.06(2)	5.3(19)	$0.31^{+(5)}_{-(6)}$	0.33(6)
$\frac{29}{2}^+$	234.1	436.6	0.23(6)	3.3(9)	$0.33^{+(4)}_{-(5)}$	0.33(5)
$\frac{31}{2}^+$	258.8	492.9	0.5(1)	2.0(4)	0.30(3)	0.38(4)
$\frac{33}{2}^+$	280.3	539.1	0.8(3)	1.5(5)	$0.28^{+(4)}_{-(5)}$	0.41(7)
$\frac{35}{2}^+$	299.4	579.6	1.3(3)	1.1(3)	0.26(3)	0.45(6)
$\frac{37}{2}^+$	316.6	615.8	1.1(3)	1.6(5)	$0.33^{+(4)}_{-(5)}$	0.35(5)
$K^\pi=25/2^+, E=2098.2$ keV						
$\frac{29}{2}^+$	245.6	472	1.2(4)	0.5(3)	0.11(4)	1.0(4)
$K^\pi=33/2^-, E=2852.6$ keV						
$\frac{37}{2}^-$	374.0	737	0.3(3)	8(17)	$0.22^{+(9)}_{-(26)}$	0.6(4)
$K^\pi=35/2^+, E=2956.8$ keV						
$\frac{39}{2}^+$	321.7	554	0.02(1)	60(37)	$0.57^{+(11)}_{-(21)}$	0.19(5)
$\frac{41}{2}^+$	357.0	678.6	0.08(1)	28(4)	0.53(3)	0.22(1)
$\frac{43}{2}^+$	380.8	737.7	0.3(2)	7(7)	$0.32^{+(9)}_{-(18)}$	0.4(2)
$K^\pi=(37/2)^-, E=3287.0$ keV						
$(\frac{41}{2})^-$	342.9	671.2	0.5(2)	2.3(23)	0.10(5)	1.1(7)
$(\frac{43}{2})^-$	358.5	700.9	0.6(2)	3.1(19)	$0.17^{+(4)}_{-(5)}$	0.7(2)

[a]Branching ratios $\lambda = I_\gamma(I \to I-2)/I_\gamma(I \to I-1)$.
[b]Assuming pure K and $Q_0 = 7.27$ e b.
[c]Values calculated using rotational model.
[d]Other limits could not be calculated as δ^2 is negative when the upper limit of the branching ratio is used.

where i_j is the alignment of the jth nucleon. The range of calculated g_K values are given in the last column of Table V and they will be discussed in relation to the individual configurations in Sec. V C.

B. Alignments

The degree of rotational alignment $i(\omega)$ is a measure of the quasiparticle contribution to the total angular momentum of the rotating nucleus and is defined as

$$i(\omega) = I_x(\omega) - I_{ref}(\omega), \qquad (2)$$

where $I_x(\omega) = \{I(I+1) - K^2\}^{1/2}$ is the component of the total angular momentum of the band on the axis of rotation and $I_{ref}(\omega) = (\mathcal{I}_0\omega + \mathcal{I}_1\omega^3)$ is the total aligned angular momentum of a reference configuration [35]. The alignment is configuration dependent and primarily determined by the number of quasiparticles in the strongly Coriolis mixed orbitals, e.g., $i_{13/2}$ and $h_{9/2}$. The alignments for multiquasiparticle bands are expected to be equal to the sum of the constituent 1-quasiparticle components, although strict additivity breaks down due to pairing differences. The values $\mathcal{I}_0 = 35$ MeV$^{-1}\hbar^2$ and $\mathcal{I}_1 = 70$ MeV$^{-3}\hbar^4$, chosen to give an approximately constant aligned angular momentum for the
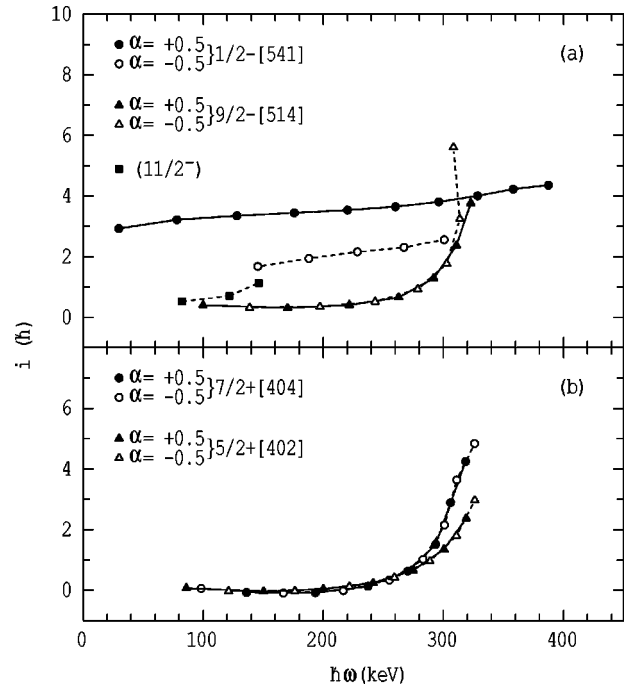
FIG. 14. Alignments as a function of rotational frequency for the 1-quasiparticle bands (Fig. 1) as indicated, with reference parameters $\mathcal{I}_0 = 35$ MeV$^{-1}\hbar^2$ and $\mathcal{I}_1 = 70$ MeV$^{-3}\hbar^4$.

$\frac{1}{2}^-[541]$ band, have been used in calculating the experimental alignments, which are shown in Figs. 14–16 for the different bands in ^{177}Ta. These are discussed in relation to individual bands in the following subsections.

C. Characterization of bands

The individual intrinsic states and their rotational structures are discussed in this section. The bands based on the 1355.0 keV level with $K^\pi = \frac{21}{2}^-$ and the 1874.9 keV level with $K^\pi = (\frac{21}{2})^-$ mix, and are discussed separately in Sec. VI.

1. $\frac{7}{2}^+[404]$ band (Figs. 1 and 5)

The $K^\pi = \frac{7}{2}^+$ band has been extended to $I^\pi = \frac{45}{2}^+$. The previous assignment of a $\frac{7}{2}^+[404]$ Nilsson configuration is consistent with the experimental g_K value of 0.75(4) which is in reasonable agreement with the theoretical estimate of 0.62. This band lies in the decay route of the $K^\pi = \frac{17}{2}^+$ and $K^\pi = \frac{31}{2}^+$ isomeric states (Fig. 5).

2. $\frac{1}{2}^+[541]$ band (Fig. 1)

The $\alpha = +\frac{1}{2}$ decoupled sequence, assigned to this configuration, was observed up to $I^\pi = \frac{45}{2}^-$. The $\frac{1}{2}^-$ and $\frac{3}{2}^-$ levels and the $\frac{9}{2}^- \rightarrow \frac{5}{2}^-$ transition, proposed by earlier works [36,37] have been included in the level scheme. The rotational band members of the $\alpha = -\frac{1}{2}$ sequence were identified up to $(\frac{35}{2}^-)$, and both the $\Delta I = 1$ and $\Delta I = 2$ crossover transitions to the $\alpha = +\frac{1}{2}$ sequence have been observed up to $I^\pi = (\frac{31}{2}^-)$. In-band transitions are weak for this sequence with a preference for out-of-band decays to the $\alpha = +\frac{1}{2}$ sequence. The large alignment of $\sim 3.5\hbar$ units for the $\alpha = +\frac{1}{2}$ sequence is consistent with its $h_{9/2}$ proton configuration. The meanlife of the $I^\pi = \frac{5}{2}^-$ state, the lowest state in the $\frac{1}{2}^-[541]$ band, is measured to be 5.3 ± 0.2 μs in the present work, which agrees well with the previously compiled value [23] of 5.2 ± 0.3 μs.

3. $\frac{5}{2}^+[402]$ band (Fig. 1)

The $K^\pi = \frac{5}{2}^+$ band was observed up to $I^\pi = \frac{33}{2}^+$ and tentatively up to $\frac{35}{2}^+$ and the results of the present work agree well with those of Ref. [25], except for the $\frac{31}{2}^+ \rightarrow \frac{29}{2}^+$ transition energy which was assigned as 324 keV in Ref. [25], compared with our assignment of 321 keV. This band, being furthest from the yrast line among the 1-quasiparticle bands, is weakly populated compared to the others. The experimental g_K value of 1.67(6) is consistent with the configuration assignment. The meanlife of the bandhead is determined to be 100 ± 3 ns and agrees well with the previously compiled value of 105 ± 7 ns [23].

4. $\frac{9}{2}^-[514]$ band (Fig. 1)

This band is observed up to $\frac{39}{2}^-$, where it seems to be approaching a band crossing. The assignment of the higher members of the band ($I^\pi > \frac{31}{2}^-$) differ from those of Ref. [25]. The present work assigns the $\frac{35}{2}^- \rightarrow \frac{31}{2}^-$, $\frac{37}{2}^- \rightarrow \frac{33}{2}^-$ transitions as 651.0 and 667.7 keV, respectively (these are

weak but clearly seen in Fig. 7), while in Ref. [25] the equivalent transitions are given as 666 and 677 keV, respectively. In their publication [25] the spectrum with a 316 keV gate shows a γ ray at 677 keV but the 666 keV line is not visible. However, the dipole transition between the $I^\pi = \frac{31}{2}^-$ and $\frac{33}{2}^-$ levels is clearly visible in that spectrum and one would therefore expect to see the 666 keV line with comparable intensity. The absence of the 666 keV line in the 316 keV gate indicates that it unlikely to be in the band. The present work shows that while a 315.9 keV transition is present in the $\frac{9}{2}^-$ band, there is also a 316.6 keV transition in the $\frac{23}{2}^+$ band (see Figs. 1 and 3) which could account for the 677 keV line in the coincidence spectrum in Ref. [25].

Being near yrast, this band is populated very strongly and all observed 3-quasiparticle states decay through it (see Figs. 2, 3). The value of $g_K = 1.20(4)$ agrees well with the theoretical prediction of 1.30 for the $\frac{9}{2}^-[514]$ configuration. The bandhead meanlife was measured to be 592 ± 10 ns which agrees with the previously compiled value [23] of 534 ± 72 ns, within the experimental uncertainty.

5. $I^\pi = (\frac{11}{2}^-)$ state at 899 keV (Fig. 2)

A possible intrinsic state situated at 899 keV (Fig. 2) and its first three rotational members have been identified. The upper limit for the meanlife of this state is 1 ns. The bandhead decays to the $\frac{9}{2}^-[514]$ and the $\frac{7}{2}^+[404]$ bands and the $(\frac{13}{2}^-)$ level decays to the $\frac{11}{2}^-$ member of the $\frac{9}{2}^-[514]$ band. The positive A_2 coefficient for the 679 keV transition, from the $(\frac{11}{2}^-)$ level at 899 keV to the $\frac{11}{2}^-$ member of the $\frac{9}{2}^-[514]$ band, suggests spins of $\frac{9}{2}$, $\frac{11}{2}$, $\frac{13}{2}$, or $\frac{15}{2}$. The $\frac{9}{2}$ assignment is ruled out due to various decay branches to the $K^\pi = \frac{9}{2}^-$ band and transitions from the $K^\pi = \frac{19}{2}^+$ band (see Fig. 2). The existence of the 826 keV transition from the $(\frac{11}{2}^-)$ level to the $K^\pi = \frac{9}{2}^-$ bandhead rules out the $\frac{15}{2}$ assignment, leaving spins of either $\frac{11}{2}$ or $\frac{13}{2}$. A value of $A_2 = -0.15(16)$ for the 826 keV transition suggests that the spin is likely to be $\frac{11}{2}$ and the presence of the 769 keV transition to the $\frac{9}{2}^+$ level of the $\frac{7}{2}^+[404]$ band argues against a $\frac{13}{2}^-$ alternative. The fact that higher members of the band are not populated could also be an indication of the lower spin value. In view of these arguments, the spin of the 899 keV level has been assigned tentatively as $(\frac{11}{2})$, although the $\frac{13}{2}$ possibility cannot be ruled out completely. The $(\frac{15}{2}^-)$ and $(\frac{17}{2}^-)$ members of the band are fed by 363.4 and 334.6 keV transitions from the $\frac{19}{2}^-$ and $\frac{21}{2}^-$ members of the $K^\pi = \frac{19}{2}^-$ band. Since the meanlife of the $K^\pi = \frac{19}{2}^-$ bandhead is <2 ns, these transitions are likely to be $E2$ rather than $M2$ in nature, leading to a negative parity for the band.

This state is too low to be a 3-quasiparticle state, and could be the $\frac{11}{2}^-[505]$ intrinsic state, however, among neighboring nuclei that intrinsic state has been identified at 1304 keV in $^{183}_{75}$Re [38] and at 647 keV in $^{185}_{77}$Ir [39] and therefore one would expect it to be at energies higher than 1300 keV in ^{177}Ta. Further, while the low alignment of

TABLE V. Experimental and calculated g_K values for configurations in ^{177}Ta.

$K^{\pi a}$	Main configurations[b]	g_K Expt.[c]	Calc.[d]	Calc.[e]
$\frac{7}{2}^+$	$\pi^1 \frac{7}{2}^+[404]$	0.75(4)	0.62	
$\frac{5}{2}^+$	$\pi^1 \frac{5}{2}^+[402]$	1.67(6)	1.56	
$\frac{9}{2}^-$	$\pi^1 \frac{9}{2}^-[514]$	1.20(4)	1.30	
$(\frac{11}{2}^-)$	$\pi^1 \frac{11}{2}^-[505]$	0.61(9)	1.27	
$(\frac{17}{2})$	$\nu^2[\frac{1}{2}^-,\frac{7}{2}^-]\otimes\pi^1[\frac{9}{2}^-]_{17/2^-}$		0.84	
$\frac{17}{2}^+$	$\pi^3[\frac{7}{2}^+,\frac{9}{2}^-,\frac{1}{2}^-]^f$	0.63(4)–0.75(7)	0.99	0.79–0.88
	$\nu^2[\frac{1}{2}^-,\frac{7}{2}^+]\otimes\pi^1[\frac{9}{2}^-]$		0.62	0.80–0.72
$\frac{19}{2}^-$	$\nu^2[\frac{7}{2}^+,\frac{7}{2}^-]\otimes\pi^1[\frac{5}{2}^+]$	0.38(4)	0.42	0.63–0.56
	$\nu^2[\frac{5}{2}^+,\frac{7}{2}^-]\otimes\pi^1[\frac{7}{2}^+]$		0.26	0.48–0.45
$\frac{21}{2}^-$	$\pi^3[\frac{5}{2}^+,\frac{7}{2}^+,\frac{9}{2}^-]^g$	0.64(3)^g	1.13	
	$\nu^2[\frac{7}{2}^+,\frac{7}{2}^-]\otimes\pi^1[\frac{7}{2}^+]$		0.21	0.37–0.34
	$\nu^2[\frac{7}{2}^-,\frac{5}{2}^-]\otimes\pi^1[\frac{9}{2}^-]$		0.56	
	$\nu^2[\frac{9}{2}^+,\frac{7}{2}^-]\otimes\pi^1[\frac{5}{2}^+]$		0.36	0.51–0.48
$\frac{23}{2}^+$	$\nu^2[\frac{7}{2}^+,\frac{7}{2}^-]\otimes\pi^1[\frac{9}{2}^-]$	0.58(4)	0.51	0.64–0.63
	$\nu^2[\frac{5}{2}^-,\frac{9}{2}^+]\otimes\pi^1[\frac{9}{2}^-]$		0.33	0.56–0.48
$\frac{23}{2}^-$	$\nu^2[\frac{7}{2}^-,\frac{9}{2}^+]\otimes\pi^1[\frac{7}{2}^+]$		0.18	0.34–0.31
$\frac{25}{2}^+$	$\nu^2[\frac{7}{2}^-,\frac{9}{2}^+]\otimes\pi^1[\frac{9}{2}^-]$	0.40(5)	0.46	0.56
$(\frac{29}{2})^+$	$\nu^2[\frac{5}{2}^-,\frac{7}{2}^-]\otimes\pi^3[\frac{7}{2}^+,\frac{9}{2}^-,\frac{1}{2}^-]$		0.58	
$\frac{31}{2}^+$	$\nu^4[\frac{1}{2}^-,\frac{5}{2}^-,\frac{7}{2}^-,\frac{9}{2}^+]\otimes\pi^1[\frac{9}{2}^-]$		0.33	
	$\nu^2[\frac{1}{2}^-,\frac{9}{2}^+]\otimes\pi^3[\frac{5}{2}^+,\frac{7}{2}^+,\frac{9}{2}^-]$		0.72	
	$\nu^4[\frac{1}{2}^-,\frac{7}{2}^+,\frac{7}{2}^-,\frac{9}{2}^+]\otimes\pi^1[\frac{7}{2}^+]$		0.10	
$\frac{33}{2}^-$	$\nu^2[\frac{5}{2}^-,\frac{7}{2}^-]\otimes\pi^3[\frac{7}{2}^+,\frac{9}{2}^-,\frac{5}{2}^+]$	0.51^{+9}_{-26}	0.75	
$\frac{35}{2}^+$	$\nu^2[\frac{7}{2}^+,\frac{7}{2}^-]\otimes\pi^3[\frac{7}{2}^+,\frac{9}{2}^-,\frac{5}{2}^+]$	0.82(4)	0.69	0.77
	$\nu^4[\frac{5}{2}^-,\frac{7}{2}^+,\frac{7}{2}^-,\frac{9}{2}^+]\otimes\pi^1[\frac{7}{2}^+]$		0.01	0.30–0.17
	$\nu^2[\frac{5}{2}^-,\frac{9}{2}^+]\otimes\pi^3[\frac{5}{2}^+,\frac{7}{2}^+,\frac{9}{2}^-]$		0.57	0.74–0.68
$(\frac{37}{2})^-$	$\nu^4[\frac{5}{2}^-,\frac{7}{2}^+,\frac{7}{2}^-,\frac{9}{2}^+]\otimes\pi^1[\frac{9}{2}^-]$	0.43(4)	0.21	0.34
	$\nu^2[\frac{7}{2}^-,\frac{9}{2}^+]\otimes\pi^3[\frac{5}{2}^+,\frac{7}{2}^+,\frac{9}{2}^-]$		0.64	0.65
	$\nu^2[\frac{7}{2}^-,\frac{9}{2}^+]\otimes\pi^3[\frac{5}{2}^+,\frac{7}{2}^+,\frac{9}{2}^-]$		0.54	0.66
$\frac{43}{2}^+$	$\nu^4[\frac{1}{2}^-,\frac{5}{2}^-,\frac{7}{2}^-,\frac{9}{2}^+]\otimes\pi^3[\frac{7}{2}^+,\frac{9}{2}^-,\frac{5}{2}^+]$		0.52	
	$\nu^4[\frac{5}{2}^+,\frac{5}{2}^-,\frac{7}{2}^-,\frac{9}{2}^+]\otimes\pi^3[\frac{7}{2}^+,\frac{9}{2}^-,\frac{1}{2}^-]$		0.31	
$\frac{45}{2}^-$	$\nu^4[\frac{1}{2}^-,\frac{7}{2}^+,\frac{7}{2}^-,\frac{9}{2}^+]\otimes\pi^3[\frac{7}{2}^+,\frac{9}{2}^-,\frac{5}{2}^+]$		0.50	
$\frac{49}{2}^-$	$\nu^4[\frac{5}{2}^-,\frac{7}{2}^+,\frac{7}{2}^-,\frac{9}{2}^+]\otimes\pi^3[\frac{7}{2}^+,\frac{9}{2}^-,\frac{5}{2}^+]$		0.41	

[a]Parentheses imply that the spin or parity is undetermined experimentally.

[b]Configurations: *neutrons* (ν): $\frac{1}{2}^-[521]$; $\frac{7}{2}^+[633]$; $\frac{5}{2}^-[512]$; $\frac{7}{2}^-[514]$; $\frac{9}{2}^+[624]$; $\frac{5}{2}^+[642]$. *protons* (π): $\frac{9}{2}^-[514]$; $\frac{7}{2}^+[404]$; $\frac{5}{2}^+[402]$; $\frac{1}{2}^-[541]$.

[c]Experimental weighted average values. $g_R=0.29(3)$, $Q_0=7.27$ e b are assumed. K mixing has not been taken into account.

[d]Calculated values using Nilsson model wave functions, with parameters as described in the text. K mixing has not been taken into account.

[e]Calculations using the geometric model of Dönau as given by Eq. (1).

[f]Preferred configuration, see Sec. V C 7.

[g]Band mixes with $\nu^2\pi$ configuration, see Sec. VI C.

~ 0.7 for this band is consistent with an $\frac{11}{2}^-[505]$ assignment, the experimental value of $g_K=0.61(9)$ does not agree with the calculated value of 1.27. Another possibility is that the level is formed by a quadrupole vibration (2^+) coupled to the $\frac{9}{2}^-[514]$ configuration. States formed by quadrupole vibrations on $\frac{9}{2}^-[514]$, $\frac{5}{2}^+[402]$, and $\frac{7}{2}^+[404]$ configurations are known to exist in ^{177}Lu, ^{183}Ta, and ^{187}Re at 1306 [23], 857 [40], and 845 keV [41], respectively.

6. $K^{\pi}=(\frac{17}{2})$ state at 1476 keV (Fig. 2)

A level at 1476 keV which decays to the $K^{\pi}=\frac{9}{2}^{-}$ band has been identified, and possibly the next higher member of the band, but no others. The 1476 keV state seems to be fed by several weak branches. The intensity ratio of 2:1 for the 889.0 to the 1084.0 keV depopulating transitions makes it unlikely that transitions are $E1$ in nature, for which the expected ratio is around 1:2. This argues against $\frac{15}{2}^{+}$ or $\frac{13}{2}^{+}$ for the bandhead. The absence of a significant lifetime and the presence of the 1084 keV transition to the $\frac{13}{2}^{-}$ state, makes $\frac{17}{2}^{+}$ unfavorable. Further, there is no low-energy $\frac{15}{2}^{-}$ state which can be constructed from the available Nilsson orbitals, leaving the possibility of $\frac{13}{2}^{-}$ or $\frac{17}{2}^{-}$. If the state is $K=\frac{13}{2}$, then a $\frac{13}{2}^{-} \rightarrow \frac{11}{2}^{-}$ transition is expected to compete favorably with the 889 keV transition. In the absence of this transition, the state is assigned a tentative spin of $I=(\frac{17}{2})$. It is likely that the intrinsic state is associated with the 3-quasiparticle Nilsson configuration of $[\nu^{2}\{\frac{1}{2}^{-}[521], \frac{7}{2}^{-}[514]\} \otimes \pi^{1}\{\frac{9}{2}^{-}[514]\}]_{17/2^{-}}$ and is not populated strongly since its band cannot compete favorably with the neighboring $K^{\pi}=\frac{17}{2}^{+}$ and $\frac{19}{2}^{-}$ 3-quasiparticle bands (see Secs. V C 7 and V C 8), both of which have high alignments.

7. $K^{\pi}=\frac{17}{2}^{+}$ band at 1522.9 keV (Figs. 2 and 5)

A rotational band, extending up to $I^{\pi}=\frac{37}{2}^{+}$, based on a $K^{\pi}=\frac{17}{2}^{+}$ state at 1522.9 keV has been identified. This state was also identified in Ref. [25], but as discussed in Sec. IV B 2, their assignment of the $I^{\pi}=\frac{19}{2}^{+}$ state is incorrect. The bandhead has a meanlife of 8 ± 2 ns and decays to the $\frac{5}{2}^{+}$, $\frac{7}{2}^{+}$, $\frac{9}{2}^{-}$, and $(\frac{11}{2}^{-})$ bands, with the decay to the $K^{\pi}=\frac{9}{2}^{-}$ band being the strongest. $E1$ multipolarity is assigned to the 718.0 and 935.9 keV depopulating transitions to the $K^{\pi}=\frac{9}{2}^{-}$ band from the conversion coefficients (Table II). The 479.5 and 935.9 keV transitions have a negative A_{2} coefficient. On the basis of the above observations, a spin and parity of $K^{\pi}=\frac{17}{2}^{+}$ has been assigned to the bandhead. The relative intensities of the depopulating transitions are consistent with the spin and parity assignment. As shown in Fig. 5, there is chance near degeneracy of the $\frac{29}{2}^{+}$ level and $\frac{31}{2}^{+}$ levels of this band with those of the $K^{\pi}=\frac{7}{2}^{+}$ band and $K^{\pi}=\frac{31}{2}^{+}$ isomer, respectively. This gives rise to mixing and results in out-of-band transitions from the $\frac{17}{2}^{+}$ band to the $\frac{7}{2}^{+}$ band, and decay branches from the $K^{\pi}=\frac{31}{2}^{+}$ isomer. Though there is some evidence for the corresponding out-of-band transition ($E_{\gamma}=481$ keV) from the $\frac{29}{2}^{+}$ level of the $K^{\pi}=\frac{7}{2}^{+}$ band to the $\frac{25}{2}^{+}$ level of the $\frac{17}{2}^{+}$ band, low statistics prevents it from being conclusive. The presence of these transitions, induced by mixing, lends further support to the spin and parity of the $I^{\pi}=\frac{27}{2}^{+}$ and $\frac{29}{2}^{+}$ rotational states, and hence of the bandhead.

The high alignment of the band, shown in Fig. 15(a), indicates the presence of a particle in an aligned orbital. The likely Nilsson configurations for the bandhead are $\pi^{3}\{\frac{7}{2}^{+}[404], \frac{9}{2}^{-}[514], \frac{1}{2}^{-}[541]\}$ or $\nu^{2}\{\frac{1}{2}^{-}[521], \frac{7}{2}^{+}[633]\}\otimes\pi^{1}\{\frac{9}{2}^{-}[514]\}$. The g_{K} estimates using a simple Nilsson model give 0.99 and 0.62 for these two configura-
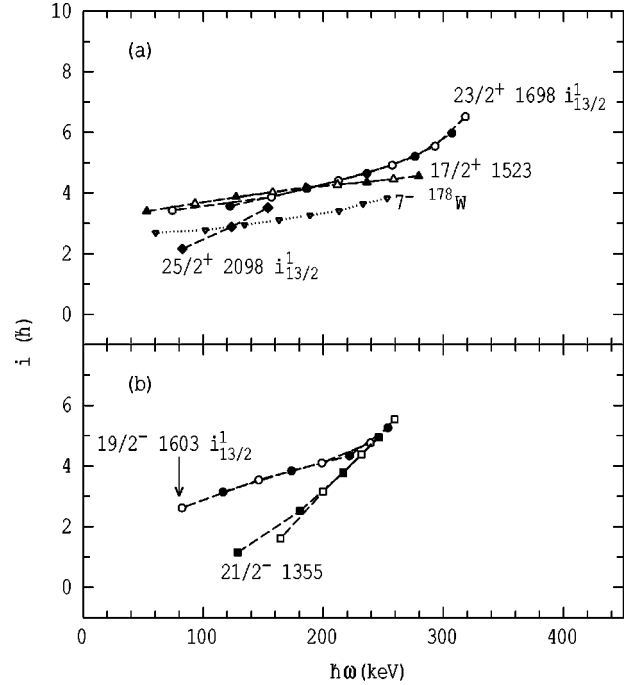
FIG. 15. As for Fig. 14 but for the 3-quasiparticle bands in ^{177}Ta (see Fig. 20 for the band on the 1874.9 keV state). The curves are labeled by the K values and excitation energy of the bandheads, and the number of $i_{13/2}$ neutrons present in the configuration. The alignment for the $K^{\pi}=7^{-}$ band in ^{178}W is shown for comparison with the $K^{\pi}=\frac{23}{2}^{+}$ band in ^{177}Ta.

tions, respectively, and the experimental $g_{K}=0.61(4)$ favors the latter. However, as shown in Fig. 17, the predicted g_{K} values for both configurations change when the experimental alignments are taken into account (see Sec. V A). The experimental values are not exactly reproduced by either of the
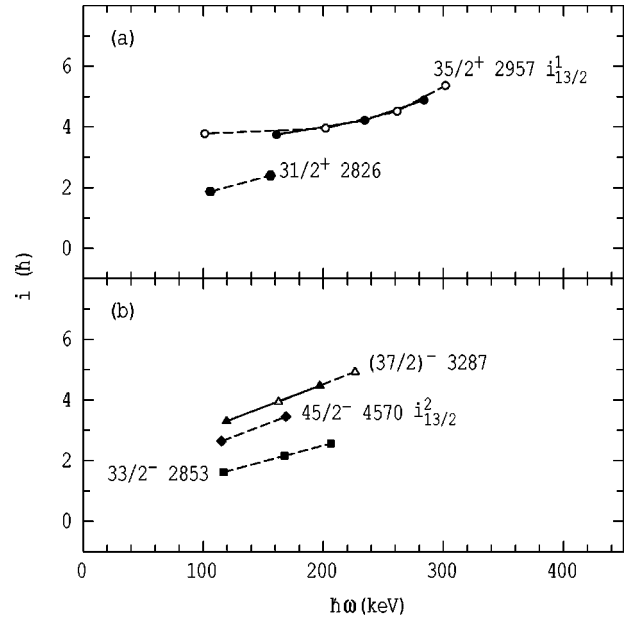
FIG. 16. Same as Fig. 14 but for the 5- and 7-quasiparticle structures in ^{177}Ta.
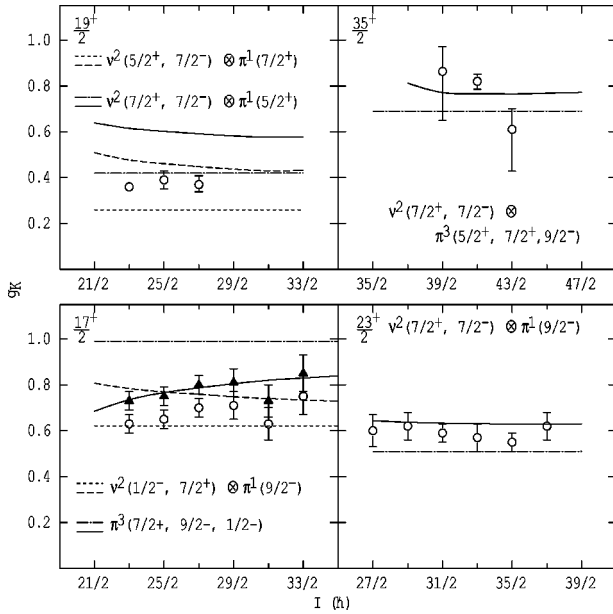
FIG. 17. Experimental g_K values as a function of spin, compared with the predictions of the Nilsson model (dash-dotted line) and the geometric model of Dönau [34] (solid line) for the indicated configurations. For the $K^\pi = \frac{17}{2}^+$ and $\frac{19}{2}^+$ states, also shown are the calculated g_K values for an alternative $\nu^2\pi$ configuration, using the Nilsson model (short-dashed line) and Dönau formalism (long-dashed line). The filled triangles in the $K^\pi = \frac{17}{2}^+$ panel show the experimental g_K values if $g_R = 0.39$, instead of 0.29, is used.

FIG. 18. Excitation energies versus $J(J+1)$ with an arbitrary rigid-rotor reference subtracted for the indicated bands. The experimental levels are shown by the filled symbols, and the results of band-mixing calculations (see Sec. VI C) are shown by the short-dashed lines and the solid lines, which are the loci of the unperturbed and perturbed levels, respectively. The calculations did not include the $K^\pi = \frac{19}{2}^-$ band.

predictions, but an increase in the g_R value of 0.1 (i.e., $g_R = 0.39$) makes the experimental points coincide with the predictions for π^3 configuration. Such an increase could occur as a result of reduced proton pairing in the 3-quasiproton configuration due to blocking effects. The slow rise in g_K as seen experimentally is also in accord with the π^3 structure. Thus, even though the identification of the structure is ambiguous, the experimental evidence would seem to favor the π^3 configuration. The calculations of Kondev *et al.* [6] which examined the energies of the two configurations for a range of tantalum nuclei show that the π^3 configuration is energetically favored for ^{177}Ta, thus lending further support for that configuration.

8. $K^\pi = \frac{19}{2}^-$ level at 1602.7 keV (Fig. 2)

A $\frac{19}{2}^-$ state and its rotational band extending up to $\frac{35}{2}^-$ and tentatively up to $\frac{37}{2}^-$, has been identified. The bandhead, and the lower members of the band decay to the $K^\pi = \frac{9}{2}^-$ and the $(\frac{11}{2}^-)$ bands. The 797.8 keV transition from the bandhead to the $\frac{17}{2}^-$ member of the $K^\pi = \frac{9}{2}^-$ band is determined to be $M1$ in character from the measured conversion coefficient (Table II), and has a negative A_2 coefficient, indicating that the spin of the level is either $\frac{15}{2}^-$ or $\frac{19}{2}^-$. The $\frac{15}{2}^-$ possibility is unlikely given the reasonably strong population of the band. Consistent with this is the observation that the intensity of the 1016 keV depopulating transition to a $\frac{15}{2}^-$ state of the $K^\pi = \frac{9}{2}^-$ band is much less than that of the 797.8 keV transition indicating that 1016 keV is not an $M1$ but probably an $E2$ transition. Since the excited band members

have significant out-of-band decay branches, the possibility of an unobserved lower level being the bandhead cannot be ruled out. However, the lower spin states which can be constructed from the available orbitals are expected to be energetically unfavored compared with a $\frac{19}{2}^-$ intrinsic state, therefore the $\frac{19}{2}^-$ level has been assumed to be the bandhead.

The high alignment of the band, shown in Fig. 15(b), is only consistent with the configurations: $\nu^2\{\frac{7}{2}^+[633], \frac{7}{2}^-[514]\} \otimes \pi^1\{\frac{5}{2}^+[402]\}$ or $\nu^2\{\frac{5}{2}^+[642], \frac{7}{2}^-[514]\} \otimes \pi^1\{\frac{7}{2}^+[404]\}$ with g_K values of 0.42 and 0.26, respectively, which with the inclusion of alignment effects give values of 0.61–0.59 and 0.48–0.45 over the spin range of $\frac{23}{2}$ to $\frac{27}{2}$. The experimental g_K value of 0.38(4) does not match with the expectations of either of the configurations (Fig. 17), although it appears to favor the latter which is, however, expected to be energetically unfavored.

The reason for this discrepancy could be due to mixing, most likely with the band based on the $\frac{21}{2}^-$ state at 1355.0 keV, as could be inferred from Fig. 18. Such mixing could change the in-band properties of both the bands as indeed is seen in the case of $\frac{21}{2}^-$ band (see Sec. VI C), which shows an unexpectedly rapid increase in alignment [Fig. 15(b)]. There is also a chance near degeneracy of the $\frac{19}{2}^-$ and $\frac{9}{2}^-$ bands at spin $\frac{35}{2}$, leading to mixing of the two bands at higher spins as is apparent from Fig. 18. No out-of-band transitions from either of the bands were identified.

9. $K^\pi = \frac{23}{2}^+$ state at 1698.5 keV (Fig. 3)

This state and its rotational levels up to the $\frac{31}{2}^+$ state were known from previous work [21]. However, in the present study the 1834.6 keV level is assigned as the $\frac{25}{2}^+$ member of the band, contrary to the previous assignment [21] of it being a $K^\pi = \frac{25}{2}^+$ intrinsic state with the higher levels being the rotational band built on it. Observation of the 338.7 keV $E2$ transition connecting the $\frac{27}{2}^+$ to $\frac{23}{2}^+$ level, and the $g_K - g_R$ values deduced from the intensities of the transitions depopulating the $I^\pi = \frac{27}{2}^+$ state supports our assignment. The rotational sequence extends up to $I^\pi = \frac{43}{2}^+$ and tentatively up to $(\frac{47}{2}^+)$. The band head de-excites by a 343.5 keV transition to the $K^\pi = \frac{21}{2}^-$ state at 1355 keV. The 343.5 keV transition is assigned $E1$ character from the measured electron conversion coefficient (Table II). A value of $A_2 = -0.25(4)$ for the 343.5 keV transition, combined with the $E1$ nature, fixes the spin and parity of the level as $\frac{23}{2}^+$. The $I^\pi = \frac{25}{2}^+$ rotational member has a strong in-band transition and it also decays to the $K^\pi = \frac{23}{2}^-$ state at 1625.9 keV by a 208.8 keV transition. The $E1$ nature of this transition deduced from the total conversion coefficient (Table II) further supports the spin and parity assignment. This band is on the main decay route of the $K^\pi = \frac{31}{2}^+$ isomer, the $(\frac{29}{2})^+$ level and the $K^\pi = \frac{25}{2}^+$ band (Fig. 3).

The band alignment shown in Fig. 15(a) is consistent with the presence of an $i_{13/2}$ neutron. The likely Nilsson configurations are listed in Table V. The experimental g_K value of 0.58(4) value favors the $\nu^2\{\frac{7}{2}^+[633], \frac{7}{2}^-[514]\} \otimes \pi^1\{\frac{9}{2}^-[514]\}$ configuration, and agrees very well with the expectations when alignment effects are included (see Fig. 17). The first transition in the band has a low energy caused probably by strong Coriolis mixing with members of the $K^\pi = \frac{25}{2}^+$ band obtained by replacing the $\frac{7}{2}^+[633]$ neutron by a $\frac{9}{2}^+[624]$ neutron, which will lower all states except the $\frac{23}{2}^+$ bandhead. The compressed first rotational transition is also observed [9,42] in ^{178}W for the $K^\pi = 7^-$ band, which is related to the present $\frac{23}{2}^+$ band by the removal of the $\frac{9}{2}^-[514]$ proton. The frequency dependence of the alignment of the $K^\pi = 7^-$ band and the $\frac{23}{2}^+$ band is almost identical [see Fig. 15(a)], the difference of about $1\hbar$ in magnitude being attributable to the additional $\frac{9}{2}^-[514]$ proton. This observation lends further support to the configuration assignment.

10. $K^\pi = \frac{25}{2}^+$ level at 2098.2 keV (Fig. 3)

This level was previously identified by Barnéoud *et al.* [21] as a $K^\pi = (\frac{25}{2}^-)$ state, based on the large negative angular distribution coefficient for the 399.7 keV depopulating transition and an assumption of it being $E1$, although the possibility of $M1$ nature was not discounted. However, in the present work the 399.7 keV transition has been assigned $M1$ character, based on the measured conversion coefficients given in Table II. The measured angular distribution coefficient is $A_2 = -0.59(21)$, but this is a combined value for the 399.7 keV transition and the 399.8 keV transition from the 2671.1 keV to the 2271.2 keV level (Fig. 3) which is probably a $J \rightarrow J$ transition. The total angular distribution coeffi-

cient being negative indicates that the spin of the 2098.2 keV level is likely to be either $\frac{21}{2}$ or $\frac{25}{2}$. The existence of a 572.9 keV transition from the $K^\pi = (\frac{29}{2})^+$ state at 2671.1 keV rules out the $\frac{21}{2}$ assignment, leading to the $\frac{25}{2}^+$ assignment. A band based on this state, extending up to $I^\pi = \frac{29}{2}^+$ and tentatively up to $I^\pi = \frac{31}{2}^+$ has been identified. The only likely Nilsson configuration is $\nu^2\{\frac{7}{2}^-[514], \frac{9}{2}^+[624]\} \otimes \pi^1\{\frac{9}{2}^-[514]\}$. The Nilsson estimate of the g_K value is 0.46 which changes to 0.56 with the inclusion of alignment effects. The experimental value of 0.39(16) compares well with the theoretical estimates and the band alignment of $i \sim 3\hbar$, shown in Fig. 15(a), is consistent with the presence of an $i_{13/2}$ neutron in the assignment.

11. $K^\pi = (\frac{29}{2})^+$ state at 2671.1 keV (Fig. 3)

This state is mainly fed by the $K^\pi = \frac{31}{2}^+$ isomer (see Fig. 5) and decays to the $K^\pi = \frac{25}{2}^+$ and $\frac{23}{2}^+$ bands as shown in Fig. 3. The associated band structure was not identified. The 155.2 keV transition from the $\frac{31}{2}^+$ isomer to the $(\frac{29}{2})^+$ level (Fig. 5), is assigned a $M1/E2$ character from the total conversion coefficient given in Table II, hence the assignment of positive parity. The existence of various depopulating transitions, restricts the spin to be either $\frac{29}{2}$ or $\frac{27}{2}$; the mixed $M1/E2$ character of 155.2 keV transition makes it unlikely to be the latter, leading to a tentative assignment of $(\frac{29}{2})^+$. The bandhead is likely to be a 5-quasiparticle structure as it lies close to the other 5-quasiparticle bandheads and is much higher than the 3-quasiparticle bandheads. The Nilsson configuration $\nu^2\{\frac{5}{2}^-[512], \frac{7}{2}^-[514]\} \otimes \pi^3\{\frac{7}{2}^+[404], \frac{9}{2}^-[514], \frac{1}{2}^-[541]\}$ is a possible candidate, but in the absence of an associated band, it is not possible to confirm it.

12. $K^\pi = \frac{31}{2}^+$ state at 2826.4 keV (Fig. 4)

This isomeric state has several decay routes, with the strongest being to the $K^\pi = \frac{23}{2}^+$ band members. The other branches go to the $(\frac{29}{2})^+$ intrinsic state, and to the members of the $\frac{7}{2}^+[404]$ and the $\frac{17}{2}^+$ bands, as shown in Fig. 5. The measured conversion coefficients for the 555.3 and 789.3 keV depopulating transitions to the $\frac{29}{2}^+$ and $\frac{27}{2}^+$ levels of the $K^\pi = \frac{23}{2}^+$ band, given in Table II, clearly show these transitions to be of $M1$ and $E2$ character, respectively, leading to an unambiguous assignment of the spin and parity of the state. The meanlife of this state is determined to be 33 ± 6 ns as detailed in Sec. IV E.

The alignment obtained from the tentative band members is $\sim 2.5\hbar$. Out of the possible Nilsson configurations given in Table V, the low alignment favors the first or the second, the third being discounted due to the presence of two aligned particles. The first configuration is expected to be energetically favored, but a firm assignment is precluded in the absence of information about other in-band properties.

13. $K^\pi = \frac{33}{2}^-$ state at 2852.6 keV (Fig. 4)

This state has a meanlife of 66 ± 5 ns and decays to the $K^\pi = \frac{31}{2}^+$ level by a 26.2 keV transition, which from the total

conversion coefficient must be of $E1$ character. Out of the possible spins of $\frac{31}{2}^-$ or $\frac{33}{2}^-$, the former is unlikely as the band built on this level is populated more strongly than the one built on the neighboring $K^\pi = \frac{31}{2}^+$ level (2826.4 keV). Further, if the spin is assumed to be $\frac{31}{2}^-$, it implies $K^\pi = \frac{35}{2}^+$ for the state at 2956.8 keV (Fig. 4; see Sec. V C 14), which would then be expected to have a decay route to the $K^\pi = \frac{31}{2}^+$ level at 2826.4 keV. Such a transition is absent. Combined, these observations lead to an assignment of $K^\pi = \frac{33}{2}^-$ for this state. The alignment obtained from the fragment of the rotational band identified is low, indicating an absence of aligned particles. The Nilsson configuration is likely to be $\nu^2\{\frac{5}{2}^-[512], \quad \frac{7}{2}^-[514]\} \otimes \pi^3\{\frac{7}{2}^+[404], \frac{9}{2}^-[514], \frac{5}{2}^+[402]\}$. The g_K value for this configuration is calculated to be 0.75, which is to be compared with the experimental value of 0.51^{+9}_{-26}. All the other possible configurations resulting in $K^\pi = \frac{33}{2}^-$ or $K^\pi = \frac{31}{2}^-$ have two $i_{13/2}$ neutrons and are not consistent with the observed alignment.

14. $K^\pi = \frac{35}{2}^+$ state at 2956.8 keV (Fig. 4)

The rotational band based on this new state extends up to $I^\pi = \frac{49}{2}^+$ and tentatively to $\frac{51}{2}^+$. The bandhead has a meanlife of 2.6 ± 5 ns and decays to the $K^\pi = \frac{33}{2}^-$ state by an 104.2 keV transition. This transition is assigned $E1$ character from the measured conversion coefficients (Table II) and has a negative A_2, giving spins of $\frac{31}{2}^+$ or $\frac{35}{2}^+$ for the state; the higher spin being favored by the relatively strong population of the band.

The high alignment of the band (Fig. 16), and a compressed spacing between the bandhead and the first rotational level, both indicate the presence of Coriolis interactions and hence the presence of $i_{13/2}$ neutrons. The possible 5-quasiparticle Nilsson configurations for the state are listed in Table V. The experimental g_K value of 0.82(4) derived from the lower members of the band favors the first configuration $\nu^2\{\frac{7}{2}^+[633], \quad \frac{7}{2}^-[514]\} \otimes \pi^3\{\frac{7}{2}^+[404], \quad \frac{9}{2}^-[514], \frac{5}{2}^+[402]\}$, and agrees well with the g_K value calculated including the alignment effects as illustrated in Fig. 17. The lowering of the $I^\pi = \frac{37}{2}^+$ level is likely to be caused by mixing with an (unobserved) $\frac{37}{2}^+$ intrinsic state, obtained by replacing the $\frac{7}{2}^+[633]$ neutron with a $\frac{9}{2}^+[624]$ neutron. (Such a mixing may also be responsible for the lower g_K value obtained from the higher spin members of the band as shown in Fig. 17.) This situation is similar to that of the $K^\pi = \frac{23}{2}^+$ band and indeed the frequency dependence and the magnitude of the alignment of both bands is very similar [Figs. 15(a) and 16(a)].

15. $K^\pi = (\frac{37}{2})^-$ state at 3287.0 keV (Fig. 4)

This level decays by a 71.5 keV transition to the $I^\pi = \frac{35}{2}^-$ level of the $K^\pi = \frac{33}{2}^-$ band and by a 330.1 keV transition to the $K^\pi = \frac{35}{2}^+$ state (Fig. 4). The 71.5 keV transition is assigned $M1$ character from the total conversion coefficient obtained from intensity balance; the $E1/M2$ possibility is ruled out by the absence of a significant bandhead lifetime. Spins of $\frac{33}{2}^-$, $\frac{35}{2}^-$, or $\frac{37}{2}^-$ are possible, but $\frac{33}{2}^-$ and $\frac{35}{2}^-$ are

unlikely on account of the weak but significant population of this band relative to the $K^\pi = \frac{35}{2}^+$ band.

The band extends up to $I^\pi = (\frac{47}{2})^-$ and has a high alignment of $i \sim 4\hbar$. The two likely Nilsson configurations are given in Table V. The experimental g_K value of 0.43(4) favors the $\nu^4\{\frac{5}{2}^-[512], \quad \frac{7}{2}^+[633], \quad \frac{7}{2}^-[514], \quad \frac{9}{2}^+[624]\} \otimes \pi^1\{\frac{9}{2}^-[514]\}$ configuration.

16. $K^\pi = \frac{43}{2}^+$ state at 4329.4 keV (Fig. 4)

A level which decays to the $\frac{39}{2}^+$ and $\frac{41}{2}^+$ members of the $K^\pi = \frac{35}{2}^+$ band has been identified but only a tentative identification of the first member of its rotational band was possible. The 461.5 keV depopulating transition to the $\frac{41}{2}^+$ state has been assigned $M1$ character from the conversion coefficient given in Table II, but its A_2 coefficient cannot be measured directly since there is another transition at 461.9 keV which occurs in the $\frac{5}{2}^+[402]$ band. A value of $A_2 = -0.18(18)$ for the 461.5 keV transition has been deduced from the known relative intensities of the 461.9 and 461.5 keV transitions, combined with the knowledge of the average of the A_2 coefficients for the other $E2$ transitions in the $\frac{5}{2}^+[402]$ band. Spins of $\frac{39}{2}^+$, $\frac{41}{2}^+$, or $\frac{43}{2}^+$ are thus possible but a $\frac{41}{2}^+$ value would require a quadrupole admixture which can be excluded by the conversion coefficient. A spin of $\frac{39}{2}^+$ for the bandhead is also unlikely given the population, thus leading to an assignment of $K^\pi = \frac{43}{2}^+$. This is consistent with the 818.3 keV branch to the $\frac{39}{2}^+$ level of the $K^\pi = \frac{35}{2}^+$ band being relatively weak, due to its implied quadrupole character. The meanlife of the state has been measured to be 1.0 ± 0.3 ns.

This state has been assigned the 7-quasiparticle Nilsson configuration of $\nu^4\{\frac{1}{2}^-[521], \quad \frac{5}{2}^-[512], \quad \frac{7}{2}^-[514], \frac{9}{2}^+[624]\} \otimes \pi^3\{\frac{7}{2}^+[404], \frac{9}{2}^-[514], \frac{5}{2}^+[402]\}$. It is unlikely to be the second configuration given in Table V which is energetically unfavored.

17. $K^\pi = \frac{45}{2}^-$ state at 4570.2 keV (Fig. 4)

This state decays to the $K^\pi = \frac{43}{2}^+$ state by a 240.8 keV transition which has been assigned $E1$ character from the measured conversion coefficients (Table II). The value of $A_2 = 0.01(20)$ deduced for the 240.8 keV transition, after taking account of another 240.9 keV $M1$ transition in the $\frac{5}{2}^+[402]$ band, indicates that it is unlikely to be a $J \to J$ transition. Spins of $\frac{41}{2}^-$ or $\frac{45}{2}^-$ are possible, the higher spin being favored by weak but observable population of the first few rotational members of the band. Furthermore, the Nilsson configuration corresponding to the $\frac{41}{2}^-$ state is expected to be higher in energy than the $\frac{45}{2}^-$ level. The Nilsson configuration assigned to this state is $\nu^4\{\frac{1}{2}^-[521], \frac{7}{2}^+[633], \frac{7}{2}^-[514], \frac{9}{2}^+[624]\} \otimes \pi^3\{\frac{7}{2}^+[404], \frac{9}{2}^-[514], \frac{5}{2}^+[402]\}$ and is consistent with the observed alignment (Fig. 16).

18. $K^\pi = \frac{49}{2}^-$ state at 4656.3 keV (Fig. 4)

The isomeric state with a meanlife of 192 ± 6 μs identified in this work, decays to the $\frac{45}{2}^-$ state by an 86.1 keV

transition, whose measured L conversion and the total conversion coefficient characterize it as $E2$ (Table II). The level spin value could be $\frac{41}{2}^-$ or $\frac{49}{2}^-$ but the absence of a γ-ray transition ($E_\gamma = 327$ keV) to the $\frac{43}{2}^+$ intrinsic state, despite the inhibited nature of the 86.1 keV transition (which leads to the extremely long meanlife), is only consistent with the $\frac{49}{2}^-$ possibility. The 7-quasiparticle configuration $\nu^4\{\frac{5}{2}^-[512], \frac{7}{2}^+[633], \frac{7}{2}^-[514], \frac{9}{2}^+[624]\} \otimes \pi^3\{\frac{7}{2}^+[404], \frac{9}{2}^-[514], \frac{5}{2}^+[402]\}$ is assigned to this state. The relatively strong population of the state and its subsequent decay path through a sequence of high-K isomers is consistent with its high-K value and its yrast nature. At this stage the long lifetime has precluded identification of transitions above the bandhead (a 257 keV γ ray is a candidate), although from the other bands one could anticipate population of states up to $\sim \frac{51}{2}$.

VI. THE BANDS BASED ON STATES AT 1355.0 AND 1874.9 keV

A chance near degeneracy at $I^\pi = \frac{25}{2}^-$ for these two bands (see Fig. 3) gives rise to mixing and therefore out-of-band transitions. The spin assignments are discussed first, followed by band-mixing calculations performed to understand their structure.

A. $K^\pi = \frac{21}{2}^-$ state at 1355.0 keV (Fig. 3)

The $K^\pi = \frac{21}{2}^-$ isomeric state was known from previous work [23] and has been the subject of some investigation [20,21] due to the K-forbidden nature of its decay. The conversion coefficients given in Table II confirm $M1$ and $E2$ multipolarities for the 311.3 and 549.9 keV transitions, respectively. The rotational sequence based on this level extends up to $\frac{37}{2}^-$ and possibly up to $\frac{39}{2}^-$.

B. The band based on the 1874.9 keV level (Fig. 3)

This level and its associated rotational band extending up to $\frac{43}{2}^-$ are new. The 248.9 keV transition from the 1874.9 keV to the $\frac{23}{2}^-$ level of the $K^\pi = \frac{21}{2}^-$ band, has been assigned $M1$ multipolarity from its total conversion coefficient (see Table II). This, combined with the existence of the crossover transitions to and from the $K^\pi = \frac{21}{2}^-$ band at 1355 keV, fixes the spin and parity of the 1875 keV level as $\frac{25}{2}^-$. Since the lower band members have significant out of band decay, the possibility of an unobserved $\frac{23}{2}^-$ or $\frac{21}{2}^-$ level being the bandhead cannot be ruled out.

C. Band-mixing calculations

The experimental level energies of the two bands (with an arbitrary rigid rotor reference removed) versus $I(I+1)$ are shown in Fig. 18 by the filled symbols, along with those of the nearby $\frac{9}{2}^-[514]$ band (at 73.3 keV, Fig. 1) and $K^\pi = \frac{19}{2}^-$ band (at 1602.7 keV, Fig. 2). In the figure perturbations are evident in the energy levels of the $K^\pi = \frac{21}{2}^-$ band at spin $\frac{25}{2}$, and in the $K^\pi = \frac{9}{2}^-$ band at higher spins, with the latter possibly due to mixing with the $K^\pi = \frac{19}{2}^-$ band. A band-mixing analysis including states from the $K^\pi = \frac{9}{2}^-$

band, the rotation-aligned band (s band), the $K^\pi = \frac{21}{2}^-$ band and the band based on the 1874.9 keV level was carried out to reproduce the experimental energy levels around $I^\pi = \frac{25}{2}^-$. The rotational states were calculated by assuming spin-independent interactions and moments of inertia which defined the unperturbed bands. The perturbed levels, shown in Fig. 18 by the solid lines, reproduce well the experimental levels and also the perturbation of the $\frac{25}{2}^-$ and $\frac{27}{2}^-$ levels of the $\frac{21}{2}^-$ band and the band beginning at 1874.9 keV. The branching ratios for these two bands were then calculated assuming different $g_K - g_R$ values depending on the assumptions about their configurations as detailed in the next two sections.

1. Structure of the $K^\pi = \frac{21}{2}^-$ band at 1355.0 keV

There are four possible Nilsson configurations for this structure:

(i) $\pi^3\{\frac{9}{2}^-[514], \frac{7}{2}^+[404], \frac{5}{2}^+[402]\}$,

(ii) $\nu^2\{\frac{7}{2}^-[514], \frac{5}{2}^-[512]\} \otimes \pi^1\{\frac{9}{2}^-[514]\}$,

(iii) $\nu^2\{\frac{7}{2}^-[514], \frac{7}{2}^+[633]\} \otimes \pi^1\{\frac{7}{2}^+[404]\}$,

(iv) $\nu^2\{\frac{7}{2}^-[514], \frac{9}{2}^+[624]\} \otimes \pi^1\{\frac{5}{2}^+[402]\}$.

Similar three-quasiparticle $\frac{21}{2}^-$ isomers and bands based on them are known in ^{175}Ta, where the $\frac{21}{2}^-$ band has a π^3 structure, and in ^{179}Ta where the structure is proposed to be a mixture of configurations (i), (ii), and (iv). In Ref. [7] the evolution of these configurations was studied for a series of tantalum isotopes and it was seen that while configuration (i) is favored in ^{175}Ta, all four configurations listed above are predicted to be close (energetically) in ^{177}Ta. Indeed, in a previous work [21] the $\frac{21}{2}^-$ state in ^{177}Ta was thought to be an admixture of configurations (i) and (ii).

The experimental branching ratios yield a value of $g_K - g_R \sim 0.45$ at low spins and ~ 0.36 at higher spins, neither of which match well with expectations for any of the above four configurations (Table V), though they are closest to that of configuration (ii), which however does not have an aligned particle. As shown in Fig. 15(b), the band starts with a low alignment of $\sim 1\hbar$ which rises rapidly to $\sim 6\hbar$. A gain in alignment would be expected if mixing with configurations with an aligned particle occur, but such a rapid gain is difficult to explain. The band-mixing analysis that follows, reproduces the branching intensities at the lower spins, but does not resolve the problem of explaining the $g_K - g_R$ values and the alignment.

The calculations were performed with two different $g_K - g_R$ values for the $K^\pi = \frac{21}{2}^-$ band, the first assuming $g_K - g_R = 0.8$ consistent with π^3 configuration and the second taking $g_K - g_R = 0.34$. The latter is an empirical value obtained from the branching of the $I^\pi = \frac{33}{2}^-$ level where mixing with other bands is not expected (see Fig. 18). This approach was preferred rather than the assumption of a value corresponding to one of the above four $\nu^2\pi$ configurations. In both calculations, the band beginning at 1874.9 keV was assumed to have $K^\pi = \frac{21}{2}^-$ with $g_K - g_R = 0.17$, obtained from the experimental branching ratios from its $I^\pi = \frac{33}{2}^-$ level. The experimental and calculated dipole intensity for the in-band and out-of-band transitions for the two bands are
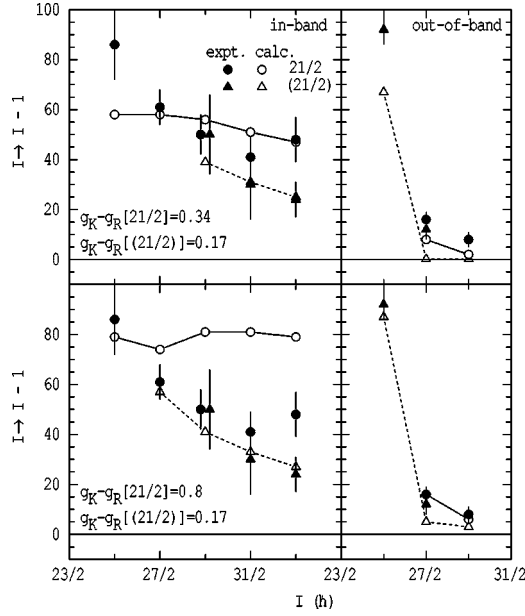
FIG. 19. Experimental and calculated dipole intensities for in-band (left panels) and out-of-band transitions (right panels) for the $K^\pi = \frac{21}{2}^-$ band at 1355.0 keV and the band above the 1874.9 keV state $[K^\pi = (\frac{21}{2})^-]$. The experimental values are shown by filled symbols and the calculated intensities assuming different $g_K - g_R$ values, as indicated, are shown by hollow symbols.

FIG. 20. Alignments as a function of rotational frequency with reference parameters $\mathcal{I}_0 = 35$ MeV$^{-1}\hbar^2$ and $\mathcal{I}_1 = 70$ MeV$^{-3}\hbar^4$ for the 1874.9 keV band assuming different values of K as indicated. The alignments of selected bands in neighboring nuclei are shown for comparison.

plotted in Fig. 19. While the calculation assuming $g_K - g_R = 0.8$ (lower panels) agrees with the experimental values up to spin $\frac{27}{2}$, it disagrees at higher spin values where a value of $g_K - g_R = 0.34$ explains the data better, indicating a change in structure of the $\frac{21}{2}^-$ band from a π^3 configuration at lower spins to a $\nu^2\pi$ configuration at higher spins.

The structure of the band at higher spins, however, remains an enigma since as indicated previously, the calculations, while successful in reproducing the branchings of the lower spin members, do not explain the experimental alignment or the $g_K - g_R$ values. The situation is made more complex since mixing of configuration (i) with all the others, i.e., (ii)–(iv) is likely in ^{177}Ta [7]. The large gain in alignment could arise from Coriolis mixing between configuration (iv) and the band based on the $\frac{19}{2}^-$ state (as could be implied by the loci of the two bands in Fig. 18), the latter obtained by replacing the $\frac{7}{2}^+[633]$ neutron by a $\frac{9}{2}^+[624]$ neutron. A quantitative comparison may be possible with a more complex band-mixing calculation, including the $K^\pi = \frac{19}{2}^-$ band, but has not been pursued as yet due to the inherent ambiguities.

2. The 1874.9 keV state and its band

If the $\frac{25}{2}^-$ level at 1874.9 keV is assumed to be the bandhead then the only likely configuration is $\nu^2\{\frac{7}{2}^+[633], \frac{9}{2}^+[624]\} \otimes \pi^1\{\frac{9}{2}^-[514]\}$. The experimental in-band γ-ray branching ratio for the $\frac{29}{2}$ state, assuming $K = \frac{25}{2}$, yields an imaginary value for the mixing ratio δ, indicating either too high a K value or K mixing. The experimental g_K value determined from the higher spin members is 0.35^{+6} (the

other limit being indeterminate as δ^2 is negative), compared with the theoretical Nilsson estimate of $g_K = 0.31$. The experimental alignment calculated assuming $K = \frac{25}{2}$ is compared in Fig. 20(a) with the alignment of the $K^\pi = \frac{25}{2}^-$ band [8] in ^{181}Re, which has the same configuration as that proposed. The low alignment of the band in ^{177}Ta combined with its different frequency dependence compared with that of the ^{181}Re band, argues against identification of the 1874.9 keV state as a $\frac{25}{2}^-$ bandhead. Furthermore, the experimental level is much lower (~ 400 keV) in energy than the predictions of the multiquasiparticle calculations for the $\frac{25}{2}^-$ intrinsic state (see Table VII and Sec. VII B).

The alternatives are that the bandhead is a lower lying but unobserved $\frac{23}{2}^-$ or $\frac{21}{2}^-$ level. The configurations consistent with the relatively high alignment of the band are

(i) $K^\pi = \frac{23}{2}^-$: $\nu^2\{\frac{7}{2}^-[514], \frac{9}{2}^+[624]\} \otimes \pi^1\{\frac{7}{2}^+[404]\}$,

(ii) $K^\pi = \frac{21}{2}^-$: $\nu^2\{\frac{7}{2}^-[514], \frac{9}{2}^+[624]\} \otimes \pi^1\{\frac{5}{2}^+[402]\}$,

(iii) $K^\pi = \frac{21}{2}^-$: $\nu^2\{\frac{7}{2}^-[514], \frac{7}{2}^+[633]\} \otimes \pi^1\{\frac{7}{2}^+[404]\}$.

The first two involve the $\nu^2\{\frac{7}{2}^-[514], \frac{9}{2}^+[624]\}$ combination, which also occurs in neighboring ^{179}Ta and ^{181}Re nuclei [7,8]. The third configuration involving the $\nu^2\{\frac{7}{2}^-[514], \frac{7}{2}^+[633]\}$ pair occurs in the $K^\pi = \frac{23}{2}^+$ and $K^\pi = 7^-$ band [9,42] in ^{178}W. The alignments for these bands is plotted in Figs. 20(b) and 20(c) along with the alignment for

TABLE VI. K-forbidden decays in ^{177}Ta.

E_γ (keV)	Mult.	I_γ (rel.)	α_T	$T_\gamma{}^{\text{a}}$ (s)	ν	$f_\nu{}^{\text{b}}$
$K^\pi=\frac{17}{2}{}^+, E=1522.9$ keV; $\tau_m=8(2)$ ns						
479.5	$E1$	10(1)	0.008	5.5×10^{-8}	3	31[b]
718.0	$E1$	15(2)	0.003	3.7×10^{-8}	3	40[b]
718.0	$M2$	15(2)	0.003	3.7×10^{-8}	3	40[b]
935.9	$E1$	42(3)	0.002	1.3×10^{-8}	3	37[b]
621.4	$M1$	5(1)	0.031	1.1×10^{-7}	4	33
847.2	$M1$	8(1)	0.014	6.9×10^{-8}	4	37
1052.3	$E2$	6(2)	0.004	9.2×10^{-8}	3	23
889.8	$E2$	3(1)	0.006	1.8×10^{-7}	4	10
283.5	$E1$	10(3)	0.026	5.5×10^{-8}	2	170[b]
$K^\pi=\frac{21}{2}{}^-, E=1355.0$ keV; $\tau_m=8.6(3)$ μs						
53	$M1$	0.3(1)	5	1.1×10^{-3}	5	23
311.3	$M1$	39(4)	0.190	8.4×10^{-6}	5	26
549.9	$E2$	5(1)	0.016	6.6×10^{-5}	4	24
$K^\pi=\frac{31}{2}{}^+, E=2826.4$ keV; $\tau_m=33(6)$ ns						
296.5	$M1$	7(1)	0.217	4.2×10^{-7}	3	79
555.3	$M1$	60(5)	0.041	4.9×10^{-8}	3	72
789.3	$E2$	57(5)	0.007	5.1×10^{-8}	2	41
256.5	$M1$	2.4(6)	0.322	1.2×10^{-6}	6	10
502.2	$E2$	3.3(5)	0.020	9.8×10^{-7}	5	5
552.2	$E2$	2.0(5)	0.016	1.5×10^{-6}	10	3
$K^\pi=\frac{43}{2}{}^+, E=4329.4$ keV; $\tau_m=1.0(3)$ ns						
461.5	$M1$	12(1)	0.067	7.8×10^{-10}	3	15
818.3	$E2$	0.7(1)	0.007	1.3×10^{-8}	2	23

${}^{\text{a}}T_\gamma=T_{\exp}\Sigma_i I_{\gamma i}(1+\alpha_{ti})/I_\gamma$.
${}^{\text{b}}$For $E1$ transitions the T_W value was multiplied by 10^3 before calculating f_ν.

the band in question assuming either $K=\frac{23}{2}$ or $K=\frac{21}{2}$ as appropriate. Whether the band has a configuration involving the $\nu^2\{\frac{7}{2}{}^-, \frac{9}{2}{}^+\}$ component is ambiguous, since its alignment does not match with that of the $K^\pi=\frac{23}{2}{}^-$ band [7] of ^{179}Ta with a configuration the same as (i), but is close to that of the $K^\pi=\frac{21}{2}{}^-$ band [8] of ^{181}Re which has the same configuration as (ii). The band however closely follows the trends of those involving the $\nu^2\{\frac{7}{2}{}^-[514], \frac{7}{2}{}^+[633]\}$ pair. Its alignment matches that of the 7^- band [9] in ^{178}W and the $K^\pi=\frac{23}{2}{}^+$ band in ^{177}Ta, the difference of $\sim 1\hbar$ compared to the latter being due to the addition of the $\frac{9}{2}{}^-[514]$ proton. The experimental g_K-g_R of 0.17 (or 0.13) assuming $K=\frac{21}{2}$ (or $\frac{23}{2}$) is closer to that of configuration (ii) (see Table V), once the alignment effects are included. Thus the band alignment favors configuration (iii), while the g_K-g_R favors configuration (ii), although configuration (i) cannot be ruled out experimentally. However, configuration (iii) is energetically favored according to the multiquasiparticle calculations given in Table VII, and predicted to lie ~ 365 and 436 keV below configurations (i) and (ii), respectively.

The possibility of the bandhead being an unobserved $\frac{21}{2}{}^-$ level was investigated utilizing the phenomenological band-mixing calculations using two sets of calculations; one assuming the bandhead to be a $K^\pi=\frac{21}{2}{}^-$ state at 1494 keV with $g_K-g_R=0.17$ for the band and the second assuming the

bandhead to be a $K^\pi=\frac{25}{2}{}^-$ state at 1874 keV (the possibility discussed in the previous section) with $g_K-g_R=0$; the g_K-g_R value in each case was obtained from the $I^\pi=\frac{33}{2}{}^-$ level of the band. A value of $K^\pi=\frac{21}{2}{}^-$ and $g_K-g_R=0.8$ (π^3 configuration) was used for the band at 1355 keV. The experimental branching ratios are compared to the two sets of calculations in Fig. 21. Experiment corresponds closely with the calculations assuming $K^\pi=\frac{25}{2}{}^-$ as the bandhead. If the bandhead is $K^\pi=\frac{21}{2}{}^-$ (or $K^\pi=\frac{23}{2}{}^-$ at 1673 keV) then the $\frac{27}{2}{}^-\to\frac{23}{2}{}^-$ $E2$ transition would be expected to be visible according to the calculations (Fig. 21 bottom panel), as would the out-of-band transition from the $\frac{23}{2}{}^-$ level to the $K^\pi=\frac{21}{2}{}^-$ bandhead. These transitions were not identified experimentally, though the possibility could not be ruled out completely due to complexity of the γ-ray spectrum.

In summary, the assignment of $K^\pi=\frac{25}{2}{}^-$ as the bandhead is supported by the observed branchings in the region of the $\frac{25}{2}{}^-$ state where there are perturbations, but the low alignment of the band and the results of the multiquasiparticle calculations which predict this state to be much higher argue against it. The scenario of an unobserved $K^\pi=\frac{21}{2}{}^-$ or $\frac{23}{2}{}^-$ state being the bandhead is still possible from the analysis of the branching ratios, and the band alignment and the g_K-g_R values could support either of the assignments. In the absence of any further information, this band has been asso-

TABLE VII. Calculated and experimental energies of multiquasiparticle states in ^{177}Ta.

K^π	Configuration[a]	Δ_n (keV)	Δ_p (keV)	E_{qp} (keV)	E_{res}[b] (keV)	E_{cal} (keV)	E_{expt} (keV)
$\frac{7}{2}^+$	$\pi^1[\frac{7}{2}^+]$	742	866	0		0	0
$\frac{5}{2}^+$	$\pi^1[\frac{5}{2}^+]$	742	860	63		63	70
$\frac{9}{2}^-$	$\pi^1[\frac{9}{2}^-]$	742	861	66		66	73
$\frac{1}{2}^-$	$\pi^1[\mathbf{\frac{1}{2}}^-]$	742	865	208		208	217
$\frac{11}{2}^-$	$\pi^1[\frac{11}{2}^-]$	742	908	1540		1540	(899)
$\frac{13}{2}^+$	$\nu^2[\frac{1}{2}^-,\frac{5}{2}^-]\otimes\pi^1[\frac{7}{2}^+]$	540	866	1655	-133	1522	
$\frac{13}{2}^-$	$\pi^3[\frac{1}{2}^-,\frac{5}{2}^+,\frac{7}{2}^+]$	742	598	1731	-212	1519	
$\frac{15}{2}^+$	$\nu^2[\frac{1}{2}^-,\frac{7}{2}^-]\otimes\pi^1[\frac{7}{2}^+]$	531	866	1417	-16	1401	
$\frac{17}{2}^+$	$\nu^2[\frac{5}{2}^-,\frac{7}{2}^-]\otimes\pi^1[\frac{5}{2}^+]$	533	860	1544	-65	1479	
$\frac{17}{2}^+$	$\pi^3[\frac{1}{2}^-,\frac{7}{2}^+,\frac{9}{2}^-]$	742	598	1736	-120	1616	1523
$\frac{19}{2}^+$	$\nu^2[\frac{5}{2}^-,\frac{7}{2}^-]\otimes\pi^1[\frac{7}{2}^+]$	533	866	1481	-128	1353	
$\frac{19}{2}^-$	$\nu^2[\mathbf{\frac{7}{2}}^+,\frac{7}{2}^-]\otimes\pi^1[\frac{5}{2}^+]$	538	860	1682	-75	1607	1603
$\frac{19}{2}^-$	$\nu^2[\mathbf{\frac{5}{2}}^+,\frac{7}{2}^-]\otimes\pi^1[\frac{7}{2}^+]$	551	866	1938	-155	1783	
$\frac{21}{2}^-$	$\pi^3[\frac{5}{2}^+,\frac{7}{2}^+,\frac{9}{2}^-]$	742	597	1536	-132	1404	1355
$\frac{21}{2}^-$	$\nu^2[\frac{5}{2}^-,\frac{7}{2}^-]\otimes\pi^1[\frac{9}{2}^-]$	533	861	1547	-99	1448	
$\frac{21}{2}^-$	$\nu^2[\mathbf{\frac{7}{2}}^+,\frac{7}{2}^-]\otimes\pi^1[\frac{7}{2}^+]$	538	866	1619	-152	1467	< 1875
$\frac{21}{2}^-$	$\nu^2[\frac{7}{2}^-,\mathbf{\frac{9}{2}}^+]\otimes\pi^1[\frac{5}{2}^+]$	550	860	2042	-138	1903	
$\frac{23}{2}^+$	$\nu^2[\mathbf{\frac{7}{2}}^+,\frac{7}{2}^-]\otimes\pi^1[\frac{9}{2}^-]$	538	861	1685	-99	1586	1699
$\frac{23}{2}^-$	$\nu^2[\frac{7}{2}^-,\mathbf{\frac{9}{2}}^+]\otimes\pi^1[\frac{7}{2}^+]$	550	866	1979	-147	1832	
$\frac{25}{2}^+$	$\nu^2[\frac{7}{2}^-,\mathbf{\frac{9}{2}}^+]\otimes\pi^1[\frac{9}{2}^-]$	550	861	2045	-99	1946	2098
$\frac{25}{2}^-$	$\nu^2[\mathbf{\frac{9}{2}}^+,\mathbf{\frac{7}{2}}^+]\otimes\pi^1[\frac{9}{2}^-]$	552	861	2201	$+71$	2272	
$\frac{27}{2}^-$	$\nu^2[\frac{1}{2}^-,\frac{5}{2}^-]\otimes\pi^3[\frac{5}{2}^+,\frac{7}{2}^+,\frac{9}{2}^-]$	540	597	3191	-266	2925	
$\frac{29}{2}^+$	$\nu^2[\frac{5}{2}^-,\frac{7}{2}^-]\otimes\pi^3[\frac{1}{2}^-,\frac{7}{2}^+,\frac{9}{2}^-]$	533	598	3218	-269	2949	(2671)
$\frac{31}{2}^+$	$\nu^4[\frac{1}{2}^-,\frac{5}{2}^-,\frac{7}{2}^-,\mathbf{\frac{9}{2}}^+]\otimes\pi^1[\frac{9}{2}^-]$	399	861	3206	-107	3099	2826
$\frac{33}{2}^-$	$\nu^2[\frac{5}{2}^-,\frac{7}{2}^-]\otimes\pi^3[\frac{5}{2}^+,\frac{7}{2}^+,\frac{9}{2}^-]$	533	597	3017	-305	2712	2853
$\frac{35}{2}^+$	$\nu^2[\mathbf{\frac{7}{2}}^+,\frac{7}{2}^-]\otimes\pi^3[\frac{5}{2}^+,\frac{7}{2}^+,\frac{9}{2}^-]$	538	597	3155	-322	2833	2957
$\frac{37}{2}^+$	$\nu^2[\frac{7}{2}^-,\mathbf{\frac{9}{2}}^+]\otimes\pi^3[\frac{5}{2}^+,\frac{7}{2}^+,\frac{9}{2}^-]$	550	597	3515	-380	3135	
$\frac{37}{2}^-$	$\nu^4[\frac{5}{2}^-,\mathbf{\frac{7}{2}}^+,\frac{7}{2}^-,\mathbf{\frac{9}{2}}^+]\otimes\pi^1[\frac{9}{2}^-]$	400	861	3414	173	3587	(3287)
$\frac{37}{2}^-$	$\nu^2[\mathbf{\frac{7}{2}}^+,\mathbf{\frac{9}{2}}^+]\otimes\pi^3[\frac{5}{2}^+,\frac{7}{2}^+,\frac{9}{2}^-]$	552	597	3671	-159	3512	
$\frac{39}{2}^-$	$\nu^2[\frac{7}{2}^-,\mathbf{\frac{9}{2}}^+]\otimes\pi^3[\frac{7}{2}^-,\frac{7}{2}^+,\frac{9}{2}^-]$	550	673	4457	-282	4175	
$\frac{41}{2}^-$	$\nu^2[\mathbf{\frac{7}{2}}^+,\frac{7}{2}^-]\otimes\pi^3[\frac{7}{2}^+,\frac{9}{2}^-,\frac{11}{2}^-]$	538	635	4837	-287	4550	
$\frac{43}{2}^+$	$\nu^4[\frac{1}{2}^-,\frac{5}{2}^-,\frac{7}{2}^-,\mathbf{\frac{9}{2}}^+]\otimes\pi^3[\frac{5}{2}^+,\frac{7}{2}^+,\frac{9}{2}^-]$	399	597	4677	-382	4295	4329
$\frac{45}{2}^-$	$\nu^4[\frac{1}{2}^-,\mathbf{\frac{7}{2}}^+,\frac{7}{2}^-,\mathbf{\frac{9}{2}}^+]\otimes\pi^3[\frac{5}{2}^+,\frac{7}{2}^+,\frac{9}{2}^-]$	400	597	4813	-345	4468	4570
$\frac{47}{2}^-$	$\nu^4[\mathbf{\frac{5}{2}}^+,\frac{5}{2}^-,\frac{7}{2}^-,\mathbf{\frac{9}{2}}^+]\otimes\pi^3[\frac{5}{2}^+,\frac{7}{2}^+,\frac{9}{2}^-]$	408	597	5219	-93	5126	
$\frac{49}{2}^-$	$\nu^4[\frac{5}{2}^-,\mathbf{\frac{7}{2}}^+,\frac{7}{2}^-,\mathbf{\frac{9}{2}}^+]\otimes\pi^3[\frac{5}{2}^+,\frac{7}{2}^+,\frac{9}{2}^-]$	400	597	4884	-132	4752	4656
$\frac{51}{2}^+$	$\nu^4[\frac{5}{2}^-,\mathbf{\frac{7}{2}}^+,\frac{7}{2}^-,\mathbf{\frac{9}{2}}^+]\otimes\pi^3[\frac{7}{2}^-,\frac{7}{2}^+,\frac{9}{2}^-]$	436	673	5827	-129	5698	
$\frac{53}{2}^-$	$\nu^4[\frac{1}{2}^-,\mathbf{\frac{7}{2}}^+,\frac{7}{2}^-,\mathbf{\frac{9}{2}}^+]\otimes\pi^5[\frac{7}{2}^-,\frac{7}{2}^+,\frac{9}{2}^-,\frac{5}{2}^+,\frac{1}{2}^-]$	400	454	6959	-327	6632	
$\frac{55}{2}^+$	$\nu^4[\frac{5}{2}^-,\mathbf{\frac{7}{2}}^+,\frac{7}{2}^-,\mathbf{\frac{9}{2}}^+]\otimes\pi^3[\frac{7}{2}^+,\frac{9}{2}^-,\frac{11}{2}^-]$	400	635	6566	-93	6473	
$\frac{57}{2}^-$	$\nu^4[\frac{5}{2}^-,\mathbf{\frac{7}{2}}^+,\frac{7}{2}^-,\mathbf{\frac{9}{2}}^+]\otimes\pi^5[\frac{7}{2}^-,\frac{7}{2}^+,\frac{9}{2}^-,\frac{5}{2}^+,\frac{1}{2}^-]$	400	454	7030	-185	6845	
$\frac{59}{2}^-$	$\nu^4[\mathbf{\frac{5}{2}}^+,\mathbf{\frac{7}{2}}^+,\frac{7}{2}^-,\mathbf{\frac{9}{2}}^+]\otimes\pi^5[\frac{1}{2}^+,\frac{7}{2}^+,\frac{9}{2}^-,\frac{5}{2}^+,\frac{3}{2}^-]$	400	441	6959	-327	6632	
$\frac{61}{2}^+$	$\nu^4[\frac{5}{2}^-,\mathbf{\frac{7}{2}}^+,\frac{7}{2}^-,\mathbf{\frac{9}{2}}^+]\otimes\pi^5[\frac{1}{2}^+,\frac{7}{2}^+,\frac{9}{2}^-,\frac{5}{2}^+,\frac{11}{2}^-]$	400	457	8179	-324	7855	
$\frac{63}{2}^+$	$\nu^4[\frac{5}{2}^-,\mathbf{\frac{7}{2}}^+,\frac{7}{2}^-,\mathbf{\frac{9}{2}}^+]\otimes\pi^5[\frac{7}{2}^-,\frac{7}{2}^+,\frac{9}{2}^-,\frac{1}{2}^-,\frac{11}{2}^-]$	400	454	8718	-196	8522	
$\frac{63}{2}^-$	$\nu^4[\frac{1}{2}^-,\mathbf{\frac{7}{2}}^+,\frac{7}{2}^-,\mathbf{\frac{9}{2}}^+]\otimes\pi^5[\frac{7}{2}^-,\frac{7}{2}^+,\frac{9}{2}^-,\frac{5}{2}^+,\frac{11}{2}^-]$	400	457	8434	$+277$	8711	

TABLE VII. (*Continued*).

K^π	Configuration[a]	Δ_n (keV)	Δ_p (keV)	E_{qp} (keV)	E_{res}[b] (keV)	E_{cal} (keV)	E_{expt} (keV)
$\frac{65}{2}+$	$\nu^4[\frac{5}{2}-,\mathbf{\frac{7}{2}+},\frac{7}{2}-,\mathbf{\frac{9}{2}+}]\otimes\pi^5[\frac{7}{2}-,\frac{7}{2}+,\frac{9}{2}+,\frac{3}{2}-,\frac{11}{2}-]$	400	463	9203	-384	8819	
$\frac{65}{2}-$	$\nu^4[\mathbf{\frac{5}{2}+},\frac{5}{2}-,\frac{7}{2}-,\mathbf{\frac{9}{2}+}]\otimes\pi^5[\frac{7}{2}-,\frac{7}{2}+,\frac{9}{2}+,\frac{5}{2}-,\frac{11}{2}-]$	408	457	8840	$+168$	9008	
$\frac{67}{2}-$	$\nu^4[\frac{5}{2}-,\mathbf{\frac{7}{2}+},\frac{7}{2}-,\mathbf{\frac{9}{2}+}]\otimes\pi^5[\frac{7}{2}-,\frac{7}{2}+,\frac{9}{2}+,\frac{5}{2}-,\frac{11}{2}-]$	400	457	8505	$+48$	8553	

[a]Configurations: *neutrons* (ν): $\frac{1}{2}-[521]$; $\frac{7}{2}+[633]$; $\frac{5}{2}+[642]$; $\frac{5}{2}-[512]$; $\frac{7}{2}-[514]$; $\frac{9}{2}+[624]$. *protons* (π): $\frac{9}{2}-[514]$; $\frac{7}{2}+[404]$; $\frac{5}{2}+[402]$; $\frac{1}{2}-[541]$; $\frac{11}{2}-[505]$; $\frac{7}{2}-[523]$; $\frac{3}{2}-[532]$; $\frac{1}{2}+[411]$. Boldface indicates Coriolis mixed orbital.

[b]Reference [46].

ciated tentatively with the energetically favored (see Table VII) configuration (iii) and is labeled with $K^\pi=(\frac{21}{2})^-$ in the level scheme.

VII. DISCUSSION

A. *K*-forbidden γ-ray transitions

Electromagnetic transitions for which changes in the K quantum number are larger than the transition multipolarity
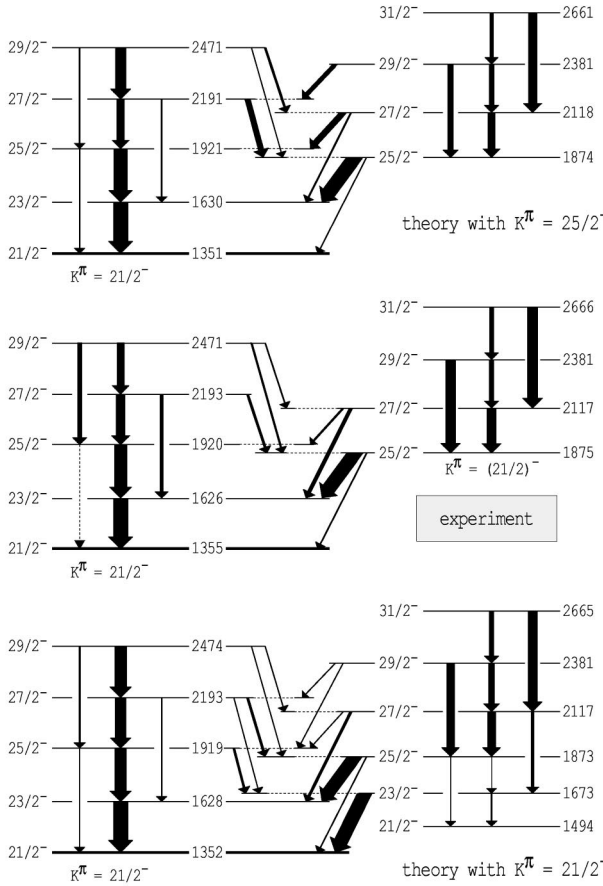
FIG. 21. The experimental relative branching ratios for the $K^\pi=\frac{21}{2}^-$ band at 1355.0 keV and the band above the 1874.9 keV state are compared with the results of band-mixing calculations (see Sec. VI C) assuming $K=\frac{21}{2}$ (bottom panel) or $K=\frac{25}{2}$ (top panel) for the latter band.

(λ) are, in principle, forbidden, although in practice they are observed but hindered. A measure of the amount of retardation is provided by the K hindrance per degree of K forbiddenness f_ν, defined as

$$f_\nu=(T_\gamma/T_W)^{1/\nu}, \qquad (3)$$

where T_γ is the partial γ-ray halflife and and T_W is the Weisskopf single-particle estimate.

In addition to the well-known $K^\pi=\frac{21}{2}^-$ isomer at 1355.0 keV, the present study reveals the presence of several new isomers which decay by K-forbidden transitions, as listed in Table VI with their f_ν values. Note that for $E1$ transitions, the T_W value is multiplied by 10^3 before calculating f_ν to take account of the fact that normal transitions are already usually hindered. The values for transitions from the $K^\pi=\frac{17}{2}^+$ and $\frac{21}{2}^-$ isomers closely correspond with those of $\frac{17}{2}^+$ and $\frac{21}{2}^-$ states in ^{175}Ta [6] which are structurally identical. The 257 and 502 keV transitions (both to the $K^\pi=\frac{17}{2}^+$ band) and the 552 keV transition (to the $K^\pi=\frac{7}{2}^+$ band) depopulating the $K^\pi=\frac{31}{2}^+$ isomer, are anomalously fast, with f_ν values lower than systematics would suggest. For the 257 and 502 keV transitions, this can be attributed at least partly to local mixing with the $\frac{31}{2}^+$ member of the $K^\pi=\frac{17}{2}^+$ band which is within 14 keV. Further, the $K^\pi=\frac{7}{2}^+$ band alignment (see Fig. 14) shows a gain at around $I^\pi=\frac{27}{2}^+$ corresponding to the alignment of $i_{13/2}$ neutrons, which would lead to a mixed K for the higher spin states. This, combined with the mixing of the $\frac{7}{2}^+$ band with $K^\pi=\frac{17}{2}^+$ band (the $\frac{29}{2}^+$ states are within 12 keV), leads to a smaller f_ν value for the 552.2 keV transition which connects the $K^\pi=\frac{31}{2}^+$ isomeric state to the $\frac{27}{2}^+$ member of the $K^\pi=\frac{7}{2}^+$ band. A similar local-mixing situation, leading to small f_ν values, has been reported for the 5-quasiparticle isomer in ^{175}Hf [43].

In addition to the states listed in Table VI, the $K=(\frac{17}{2})$ state at 1476.9 keV (Fig. 2) and the $K^\pi=\frac{19}{2}^-$ state at 1602.7 keV (Fig. 2), also decay by K-forbidden transitions. The f_ν values for the transitions depopulating these two states are in agreement with the systematics.

B. Multiquasiparticle calculations

In our earlier work [4] good agreement was obtained between the experimental energies and those from BCS calculations, with the inclusion of blocking for multiquasiparticle
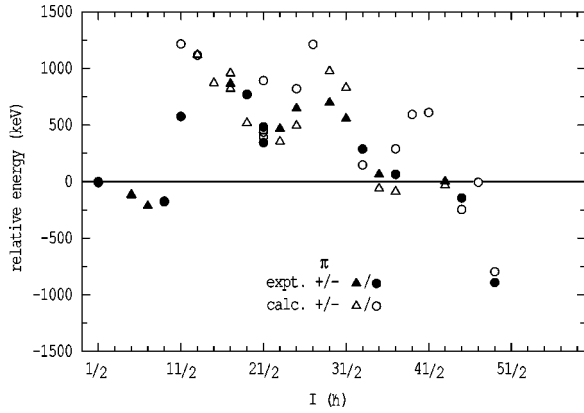
FIG. 22. Comparison between experimental (filled points) and calculated (hollow points) yrast and near-yrast multiquasiparticle states in ^{177}Ta relative to the $\frac{1}{2}^{-}[541]$ band. For the $K^{\pi}=\frac{21}{2}^{-}$ state, two experimental points are shown, one for the 1355.0 keV state and the other at 1467 keV which is the predicted energy from the band-mixing calculation (see Sec. VI C), of the $\frac{21}{2}^{-}$ bandhead associated with the 1874.9 keV band.

states. However, this agreement could be fortuitous due to the inherent limitations [44–46] of the BCS theory, which results in an artificial collapse of pairing for low values of the pairing-force strength, as seen in our previous calculations [4]. These limitations can partly be overcome if the pairing correlations are treated using the Lipkin-Nogami formalism [47]. In this section we present such calculations.

The single-particle energies required as inputs to the calculations, were obtained from the Nilsson model using the deformation parameters given in Sec. V A. The energies of the states close to the Fermi surface were subsequently adjusted to reproduce approximately the experimental one-quasiparticle energies, in ^{177}Ta in the case of protons, and an average of ^{177}Hf and ^{177}W energies in the case of neutrons. Pairing force strengths of $G_{\pi}=20.7/A$ MeV and $G_{\nu}=18.3/A$ MeV were used for the calculations, yielding ground-state pairing gaps of 866 and 742 keV, respectively. Following this procedure, the multiquasiparticle energies were calculated without further adjustment of parameters. These calculations in general agree well with those of Ref. [7], where calculations were performed to obtain a consistent picture of the multiquasiparticle states in a series of Ta isotopes, but the parameters in the present case have been adjusted slightly for ^{177}Ta. As a result, the 7-quasiparticle states, all of which contain a $\frac{9}{2}^{+}[624]$ neutron, are reproduced better in the present calculation and it is likely that in the calculations of Ref. [7], the $\frac{9}{2}^{+}[624]$ level was taken to be too close to the Fermi surface.

The resulting comparison with experiment is presented in Table VII along with the values for the pairing energies for protons and neutrons and the residual interactions [46]. For ease of comparison, the excitation energies relative to the $\frac{1}{2}^{-}[541]$ band members, as a function of spin, are shown in Fig. 22. The calculations, with the inclusion of residual interaction energies, are in good agreement with the excitation energies of the experimentally observed multiquasiparticle

states. It is of note that almost all the states which are predicted to lie in close proximity to the yrast line have been observed.

Even though the overall agreement is good, there are disagreements which need comment. The calculated $\frac{19}{2}^{+}$ state with a configuration $\nu^{2}\{\frac{5}{2}^{-}, \frac{7}{2}^{-}\}\otimes\pi\{\frac{7}{2}^{+}\}$ is predicted to be significantly lower than any corresponding observed state. Experimentally, only a $\frac{19}{2}^{-}$ state (1603 keV) is observed with no plausible candidate for a $\frac{19}{2}^{+}$ state. Considering the component configurations among the neighboring even-even nuclei, a $\nu^{2}\{\frac{5}{2}^{-}, \frac{7}{2}^{-}\}$ configuration forming a 6^{+} state, occurs [9] in ^{178}W at an excitation energy of 1666 keV. Thus the $\frac{19}{2}^{+}$ state formed by the addition of $\pi\{\frac{7}{2}^{+}\}$, which is the ground-state configuration of ^{177}Ta, is expected to have an excitation energy of $\sim$1670 keV. However, it may not compete favorably with the $\frac{19}{2}^{-}$ configuration which has an aligned particle, thus possibly accounting for the $\frac{19}{2}^{+}$ state not being observed. However, it also indicates that the present calculations underpredict the excitation energy of the $\nu^{2}\{\frac{5}{2}^{-}, \frac{7}{2}^{-}\}$ combination. This deduction is also supported by the fact that the $K^{\pi}=\frac{33}{2}^{-}$ state, assigned a $\nu^{2}\{\frac{5}{2}^{-}, \frac{7}{2}^{-}\}\otimes\pi^{3}\{\frac{5}{2}^{+}, \frac{7}{2}^{+}, \frac{9}{2}^{-}\}$ configuration, has an excitation energy higher than predicted, even though the predicted energy for the π^{3} component, resulting in a $\frac{21}{2}^{-}$ state, matches very well with experiment.

The $\frac{25}{2}^{+}$ state at 2098 keV interacts with the $\frac{25}{2}^{+}$ level (1835 keV) of the $\frac{23}{2}^{+}$ band leading to the compression of the first rotational excitation of the latter (see Fig. 3). Since the lower $\frac{25}{2}^{+}$ state is pushed down by $\sim$35 keV due to the interaction, the experimental (upper) $K^{\pi}=\frac{25}{2}^{+}$ state is expected be pushed up by a similar amount. This reduces the discrepancy between the calculated and observed state to $\sim$117 keV. The calculations predict a $\frac{37}{2}^{+}$ configuration to be $\sim$400 keV lower than the $\frac{37}{2}^{-}$ configuration, but the former has not been identified and the latter lies 225 keV below the calculated value (see Table VII). The reason for the $\frac{37}{2}^{+}$ state not being observed could be due to mixing with the closely related structure of $K^{\pi}=\frac{35}{2}^{+}$, which also results in lowering of the $\frac{37}{2}^{+}$ member of the $\frac{35}{2}^{+}$ band as seen experimentally (Fig. 4).

Predicted states with spins higher than $\frac{49}{2}$ are also listed in Table VII. The 9-quasiparticle $K^{\pi}=\frac{67}{2}^{-}$ state, at an excitation energy of 8553 keV, is predicted to be an yrast trap, which is consistent with the expectations of calculations by Åberg [17]. This state could decay either by a low energy ($\sim$30 keV) $M2$ transition to the $\frac{63}{2}^{+}$ state (the $\frac{63}{2}^{+}$ state is expected to be lower in energy than the $\frac{63}{2}^{-}$ state due to the residual interactions) or by an $E3$ transition of $\sim$700 keV to the $\frac{61}{2}^{+}$ state. In either case the transition will be slow, leading to a long lifetime for the $\frac{67}{2}^{-}$ state.

C. Formation of the yrast line

The competition between the intrinsic high-K states and their collective structures in forming the yrast line in the odd-even Ta isotopes is determined primarily by the position of the neutron Fermi surface. For the lighter isotopes like

^{173}Ta and ^{175}Ta, the Fermi surface lies around the $\frac{1}{2}^-[521]$ and $\frac{5}{2}^-[512]$ low-Ω orbitals and thus the high-K configurations with $\frac{7}{2}^+[633]$ and $\frac{9}{2}^+[624]$ neutrons are higher in energy. Consequently, the $\pi^1\{\frac{1}{2}^-[541]\}$ rotational band remains yrast [7] up to very high spins. On the other hand, in the heavier ^{179}Ta isotope the neutron Fermi level lies between the $\frac{7}{2}^-[514]$ and $\frac{9}{2}^+[624]$ orbitals, and the yrast line is formed by high-K multiquasiparticle states and the collective structures associated with their rotation.

In ^{177}Ta, the neutron Fermi surface lies between the $\frac{5}{2}^-[512]$ and $\frac{7}{2}^-[514]$ orbitals, which is approximately in the middle of the $\frac{7}{2}^+[633]$ and $\frac{9}{2}^+[624]$ high-Ω orbitals. Consequently, high-K two- and four-quasineutron configurations occur at low energies and the situation is similar for the one- or three-quasiproton configurations, with the result that many competing multiquasiparticle states can be formed. As illustrated in Fig. 22, the yrast line is formed by the $\frac{1}{2}^-[541]$ band up to $I\sim\frac{35}{2}$, after which high-K states each with configurations involving large-Ω orbitals and their collective rotation become yrast.

Although the three-quasiparticle configurations all lie above the yrast line, the occurrence of many closely related high-K structures gives rise to complex mixing and thus to features in the rotational structures (see Sec. VI), which are not yet fully understood. The five-quasiparticle $K^\pi=\frac{35}{2}^+$ band at 2956.8 keV becomes yrast at $I>\frac{35}{2}$, with further changes occurring at $I=\frac{45}{2}$ and $\frac{49}{2}$, where the $K^\pi=\frac{45}{2}^-$ and the $K^\pi=\frac{49}{2}^-$ states become yrast, respectively. These states decay by transitions minimizing the change in K, to the rotational band members built on high-K bandheads or directly to high-K intrinsic states, thus enabling many quasiparticle states and their rotational bands to be identified.

The least retarded decay path for the $K^\pi=\frac{49}{2}^-$ state is thus to the $K^\pi=\frac{45}{2}^-$ state by a low-energy (86.1 keV), high multipolarity ($E2$) transition leading to its long meanlife. The $\frac{49}{2}^-$ state can thus be identified as a *spin trap*. An almost identical situation arises for the $K^\pi=22^-$ spin-trap [12] in the neighboring ^{176}Hf nucleus with a configuration similar to the $K^\pi=\frac{49}{2}^-$ state ($\frac{49}{2}^-=22^-\otimes\pi^1(\frac{5}{2}^+[402])$), which has a

meanlife of 62 μs and decays to a 20$^-$ state by a 97 keV $E2$ transition.

VIII. CONCLUSIONS

The nucleus ^{177}Ta, with its neutron and proton Fermi surfaces lying close to orbitals with large values of Ω, is ideal for investigating the high-K multiquasiparticle states, their rotational structure and structural changes which occur due to competing configurations. The study reveals a multitude of high-seniority states, some of which are isomeric. Time-correlated γ-ray data were essential in order to identify weakly populated isomeric states and the associated rotational bands.

Configurations for the observed intrinsic states were assigned on the basis of their decay and the properties of their rotational bands. While most of the bands are well understood, the behavior of some of the bands, most notably the one built on the $K^\pi=\frac{21}{2}^-$ 3-quasiparticle isomer, is difficult to explain. Such anomalous behavior is possibly due to mixing with several competing configurations at high spins in ^{177}Ta. Nevertheless, almost all the intrinsic states which are predicted by multiquasiparticle calculations to lie close to the yrast line, have been observed experimentally.

The $K^\pi=\frac{21}{2}^-$ and $\frac{49}{2}^-$ states are very long lived (8.6 ± 0.3 μs and 192 ± 6 μs, respectively) as a result of substantial K hindrance in the former but of spin trapping in the latter. The calculations predict the existence of a $K^\pi=\frac{67}{2}^-$ yrast isomer at an excitation energy of about 8.5 MeV. Experimentally, it is difficult to form such high angular momentum states using stable beams except through low cross-section reactions involving charged particle emission.

ACKNOWLEDGMENTS

[1] A. Bohr and B. R. Mottleson, *Nuclear Structure* (Benjamin, New York, 1975), Vol. II, p. 82.

[2] Y. R. Shimizu, J. D. Garrett, R. A. Broglia, M. Gallardo, and E. Vigezzi, Rev. Mod. Phys. **61**, 131 (1989).

[3] P. M. Walker, G. D. Dracoulis, A. P. Byrne, B. Fabricius, T. Kibédi, A. E. Stuchbery, and N. Rowley, Nucl. Phys. **A568**, 397 (1994).

[4] M. Dasgupta, P. M. Walker, G. D. Dracoulis, A. P. Byrne, P. H. Regan, T. Kibédi, G. J. Lane, and K. C. Yeung, Phys. Lett. B **328**, 16 (1994).

[5] C. S. Purry, P. M. Walker, G. D. Dracoulis, T. Kibédi, S. Bayer, A. M. Bruce, A. P. Byrne, M. Dasgupta, W. Gelletly, F. Kondev, P. H. Regan, and C. Thwaites, Phys. Rev. Lett. **75**, 406 (1995).

[6] F. G. Kondev, G. D. Dracoulis, A. P. Byrne, M. Dasgupta, T. Kibédi, and G. J. Lane, Nucl. Phys. **A601**, 195 (1996).

[7] F. G. Kondev, G. D. Dracoulis, A. P. Byrne, T. Kibédi, and S. Bayer, Nucl. Phys. **A617**, 91 (1997).

[8] C. J. Pearson, P. M. Walker, C. S. Purry, G. D. Dracoulis, S. Bayer, A. P. Byrne, T. Kibédi, and F. G. Kondev, Phys. Rev. Lett. **79**, 605 (1997); (unpublished).

[9] C. S. Purry, P. M. Walker, G. D. Dracoulis, T. Kibédi, F. G. Kondev, S. Bayer, A. M. Bruce, A. P. Byrne, W. Gelletly, P. H. Regan, C. Thwaites, O. Burglin, and N. Rowley, Nucl. Phys. **A632**, 229 (1998).

[10] G. D. Dracoulis, F. G. Kondev, and P. M. Walker, Phys. Lett. B **419**, 7 (1998).

[11] T. E. Ward and P. E. Haustein, Phys. Rev. Lett. **27**, 685 (1971).

[12] T. L. Khoo, F. M. Bernthal, R. G. H. Robertson, and R. A.

Warner, Phys. Rev. Lett. **37**, 823 (1976).

[13] J. Van Klinken, W. Z. Venema, R. V. F. Janssens, and G. T. Emery, Nucl. Phys. **A339**, 189 (1980).

[14] D. Barnéoud, S. André, and C. Foin, Nucl. Phys. **A379**, 205 (1982).

[15] P. Chowdhury, B. Fabricius, C. Cristensen, F. Azgui, A. Bjørnholm, J. Borggreen, A. Holm, J. Pedersen, G. Sletten, M. A. Bentley, D. Howe, A. R. Mokhtar, J. D. Morrisson, J. F. Sharpey-Schafer, P. M. Walker, and R. M. Lieder, Nucl. Phys. **A485**, 136 (1988).

[16] N. L. Gjørup, M. A. Bentley, B. Fabricius, A. Holm, J. F. Sharpey-Schafer, G. Sletten, and P. M. Walker, Z. Phys. A **337**, 353 (1990).

[17] S. Åberg, Nucl. Phys. **A306**, 89 (1978).

[18] D. Barnéoud, C. Foin, A. Baudry, A. Gizon, and J. Valentin, Nucl. Phys. **A154**, 653 (1970).

[19] B. Skånberg, S. A. Hjorth, and H. Ryde, Nucl. Phys. **A154**, 641 (1970).

[20] H. Hübel, R. A. Naumann, and E. H. Spejewski, Phys. Rev. C **4**, 2272 (1971); *ibid.* **5**, 1438(E) (1972).

[21] D. Barnéoud, S. André, and C. Foin, Phys. Lett. **55B**, 443 (1975).

[22] L. Buja-Bijunas and J. C. Waddington, Can. J. Phys. **56**, 872 (1978); F. Dubbers, L. Funke, P. Kemnitz, G. Winter, S. Elfström, Th. Lindbald, and C. G. Lindén, Z. Phys. A **287**, 165 (1978).

[23] E. Browne, Nucl. Data Sheets **68**, 747 (1993), and references therein.

[24] M. A. Riley, D. E. Archer, J. Simpson, T. B. Brown, J. Döring, J. W. Holcomb, G. D. Johns, T. D. Johnson, T. Petters, J. Pfohl, S. L. Tabor, O. N. Tekyi-Mensah, P. C. Womble, and V. A. Wood, Z. Phys. A **346**, 319 (1993).

[25] D. E. Archer, M. A. Riley, T. B. Brown, J. Döring, D. J. Hartley, G. D. Johns, T. D. Johnson, R. A. Kaye, J. Pfohl, S. L. Tabor, J. Simpson, and Yang Sun, Phys. Rev. C **52**, 1326 (1995).

[26] G. D. Dracoulis and A. P. Byrne, Annual Report ANU-P/1052, 115 (1989) (unpublished).

[27] T. Kibédi, G. D. Dracoulis, and A. P. Byrne, Nucl. Instrum. Methods Phys. Res. A **294**, 523 (1990).

[28] S. Bayer, A. P. Byrne, and G. D. Dracoulis, Nucl. Phys. **A591**, 104 (1995).

[29] R. Bengtsson, S. Frauendorf, and F.-R. May, At. Data Nucl. Data Tables **35**, 15 (1986).

[30] T. Bengtsson and I. Ragnarsson, Nucl. Phys. **A436**, 14 (1985).

[31] G. Kaindl, F. Bacon, and A. J. Soinski, Phys. Lett. **46B**, 62 (1973).

[32] Y. Tanaka, R. M. Steffen, E. B. Shera, W. Reuter, M. V. Hoehn, and J. D. Zumbro, Phys. Rev. C **29**, 1830 (1984); **30**, 350 (1984).

[33] E. Hagn and E. Zech, Nucl. Phys. **A369**, 205 (1981).

[34] F. Dönau, Nucl. Phys. **A471**, 469 (1987).

[35] R. Bengtsson and S. Frauendorf, Nucl. Phys. **A327**, 139 (1979).

[36] B. L. Ader and N. N. Perrin, Nucl. Phys. **A197**, 593 (1972).

[37] K. D. Schilling, W. Andrejtscheff, F. Dubbers, and P. Manfrass, Nucl. Phys. **A208**, 417 (1973).

[38] R. B. Firestone, Nucl. Data Sheets **52**, 715 (1987).

[39] E. Browne, Nucl. Data Sheets **58**, 441 (1989).

[40] H. Carlsson, R. A. Bark, L. P. Ekström, A. Nordlund, H. Ryde, G. B. Hagemann, S. J. Freeman, H. J. Jensen, T. Lönnroth, M. J. Piiparinen, H. Schnack-Petersen, F. Ingebretsen, and P. O. Tjøm, Nucl. Phys. **A592**, 89 (1995).

[41] R. B. Firestone, Nucl. Data Sheets **62**, 159 (1991).

[42] C. L. Dors, F. M. Bernthal, T. L. Khoo, C. H. King, J. Borggreen, and G. Sletten, Nucl. Phys. **A314**, 61 (1979).

[43] N. L. Gjørup, P. M. Walker, G. Sletten, M. A. Bentley, B. Fabricius, and J. F. Sharpey-Schafer, Nucl. Phys. **A582**, 369 (1995).

[44] M. Rho and J. O. Rasmussen, Phys. Rev. **135**, B1295 (1964).

[45] H. C. Pradhan, Y. Nogami, and J. Law, Nucl. Phys. **A201**, 357 (1973).

[46] K. Jain, P. M. Walker, and N. Rowley, Phys. Lett. B **322**, 27 (1994).

[47] Y. Nogami, Phys. Rev. **134**, B313 (1964); J. F. Goodfellow and Y. Nogami, Can. J. Phys. **44**, 1321 (1966).